WARSAW UNIVERSITY OF TECHNOLOGY

DISCIPLINE OF AUTOMATIC CONTROL, ELECTRONICS, ELECTRICAL ENGINEERING AND SPACE TECHNOLOGIES

FIELD OF ENGINEERING AND TECHNOLOGY

Ph.D. Thesis

Łukasz Kędzierski, M.Sc.

Rotating Objects Balancing Based on Signal Amplitude and Phase Analysis

Supervisor

Krzysztof Siwek, Ph.D.

Co-supervisor

Radosław Roszczyk, Ph.D.

WARSAW 2023

ABSTRACT

The thesis presents a system that can be used for rotating objects balancing. The system uses the amplitude and phase of the first order signal acquired by either a proximity probe or an accelerometer. Different methods of viewing the analyzed signal, including time domain plots, frequency domain plots, Bode plots and polar plots are presented and their role in the process of balancing is described. The methods used for estimating the magnitude and angular location of the balance weight based on the amplitude and phase of the first order signal are discussed in detail, step by step. Finally the tools used for distributing the estimated balance weight in the available locations around the object being balanced are presented.

Digital signal processing tools necessary for converting the time domain signal into the amplitude and phase of the first order signal, like the Digital Fast Fourier Transform, the conversion of time domain signal to the even-angle domain signal and the order analysis are discussed. The role of each of the digital signal processing methods in the process of rotating objects balancing is described in details, however their mathemical details are omitted on purpose as from the balancing point of view it is important to understand how these tools work but not how they are calculated.

The presented system uses the rotating objects balancing methods that can be divided into two groups: single plane balancing and multi-plane balancing methods. Together a total of two single plane balancing methods, called respectively the vector method and the four-runs method, and one multi plane balancing method, called influence coefficient method, are discussed. Each of these methods is thoroughly described. The results of the balancing scenarios conducted in order to prove the accuracy and reliability of the developed system are presented and commented.

Four software applications have been created in the process of developing the presented balancing system: the *Test Stand Control Application*, the *Order Analysis Application*, the *Single Plane Balancing Application* and the *Multi Plane Balancing Application*. The role of each of the applications in the balancing of the rotating object is discussed, with special emphasis on the controls and indicators available on their front panels.

Keywords: rotating machinery, balancing, order analysis, polar plots, optimization.

STRESZCZENIE

W rozprawie został zaprezentowany system służący do wyważania obiektów wirujących. System wykorzystuje amplitudę oraz fazę sygnału pierwszego rzędu zarejestrowanego przez czujnik zbliżenia lub akcelerometr. Zaprezentowano różne sposoby prezentacji analizowanego sygnału, w tym wykresy w dziedzinie czasu, wykresy w dziedzinie częstotliwości, wykresy Bodego oraz polarne, a następnie omówiono ich rolę w procesie wyważania. Procedura estymacji poziomu niewyważenia oraz jego położenia kątowego na podstawie analizy amplitudy oraz fazy sygnału pierwszego rzędu została opisana szczegółowo, krok po kroku. Zaprezentowano również narzędzia wykorzystywane do dystrybucji masy korekcyjnej w wyważanym obiekcie wirującym.

W celu uzyskania amplitudy oraz fazy sygnału pierwszego rzędu z sygnału w dziedzinie czasu, wykorzystano szereg narzędzi z dyscypliny przetwarzania sygnałów, w tym szybką transformatę Fouriera, transformację sygnału z dziedziny czasu do dziedziny kąta oraz analizę rzędów. Omówiono szczegółowo rolę każdego z tych narzędzi w procesie wyważania obiektów wirujących, pominięto natomiast ich matematyczny aspekt.

Zaprezentowany system wykorzystuje metody wyważania obiektów wirujących, które można podzielić na dwie grupy: techniki wyważania jednopłaszczyznowego oraz techniki wyważania wielopłaszczyznowego. W sumie omówiono dwie metody wyważania jednopłaszczyznowego (technika wektorowa oraz technika czterech uruchomień) oraz jedną metodę wyważania wielopłaszczyznowego (technika współczynników wpływu). Każda z tych metod została szczegółowo omówiona oraz przetestewona, a wyniki wszystkich testów dokładnie przeanalizowane oraz zaprezentowane.

W trakcie opracowywania opisanego systemu do wyważania obiektów wirujących powstały cztery aplikacje programistyczne: *Aplikacja Sterowania Stanowiskiem Testowym*, *Aplikacja Analizy Rzędów*, *Aplikacja Wyważania Jednopłaszczyznowego* oraz *Aplikacja Wyważania Wielopłaszczyznowego*. Zaprezentowano interfejs graficzny każdej z tych aplikacji oraz szczegółowo omówiono ich rolę w procesie wyważania.

Słowa kluczowe: maszyny wirujące, wyważanie, analiza rzędów, wykresy polarne, optymalizacja.

CONTENTS

1. INTRODUCTION 7

1.1 SUBJECT 7
1.2 PURPOSE STATEMENT 8
1.3 THESIS STATEMENT 8
1.4 LITERATURE OVERVIEW 8

2. BALANCING GENERAL OVERVIEW 18

2.1 UNBALANCE 18
2.2 DEVELOPED BALANCING TEST STAND 20
2.3 TEST STAND CONTROL AND DATA ACQUISITION SOFTWARE 30
2.4 ORDER ANALYSIS 34
2.5 PHASE LEAD AND LAG 38
2.6 BODE AND POLAR PLOTS 39
2.7 BALANCE WEIGHT DISTRIBUTION 43
2.8 WEIGHT DISTRIBUTION OPTIMIZATION 50
2.9 MODIFIED DIFFERENTIAL EVOLUTION (MDE) ALGORITHM 53
2.10 ORDER ANALYSIS APPLICATION 59
2.11 COMPLETE BALANCING PROCEDURE 62

3. SINGLE PLANE BALANCING METHODS 64

3.1 VECTOR METHOD 64
3.2 FOUR RUNS METHOD 71
3.3 BALANCING RESULTS COMPARISON 83

4. MULTI PLANE BALANCING METHOD 93

4.1 INTRODUCTION TO THE INFLUENCE COEFFICIENTS METHOD 93
4.2 CALCULATION OF THE TRIM BALANCE WEIGHTS 98
4.3 MULTI PLANE BALANCING SOFTWARE TOOL 100
4.4 BALANCING RESULTS 103
4.5 CONCLUSIONS 151

5. SUMMARY 153

5.1 OVERVIEW 153
5.2 CONDUCTED EXPERIMENTS 156

6. BIBLIOGRAPHY 159

1. Introduction

1.1 Subject

Mechanical faults such as shaft misalignment, mechanical looseness and mass unbalance are the common cause of the vibrations of rotating machinery [1]. Out of all the causes for vibration the mass unbalance is the one that occurs the most often. Considering the increasing number of rotating machinery in the world as well as the increasing rotational speeds of rotating objects in many industries the need for reliable, accurate and easy to use balancing systems is ever growing. The unbalance, when not addressed early enough, can lead to a decrease in the life span of elements like bearings, seals, gears and couplings [2]. The balancing systems are used to attenuate the vibrations caused by the mass unbalance to an acceptable level as it is not possible to balance the rotating objects completely because of the non-uniform density of material, loss of material during the machinery operation, manufacturing faults and many other reasons [1]. The highest vibration in the rotating machinery will always occur at its critical speed, therefore even when the rotor is balanced to a satisfactory level it is never recommended to operate the system at this speed [3]. In this dissertation it will be shown how to balance the rotating object at all of its rotational speeds, even if the critical speed is within this range.

In most of the systems used for balancing purposes the rotor needs to be disassembled from the machine and installed in the bearings of a dedicated balancing machine [4]. However, it is not always possible to disassemble the rotor, therefore in many cases the only solution to the unbalance problem is to perform the balancing of the rotating objects in its own bearings, the so called field balancing [5]. The system developed for the purpose of this dissertation can be used for balancing in the field and furthermore it uses the non-contact methods (when the proximity probes are used). There is a great flexibility in the developed system – the reference angle probe can be any type of TTL or 0/24VDC logic sensor and the rotor unbalance can be measured by either a proximity probe or an accelerometer. When the proximity probe is used the methods used by the system can be considered non-contact methods as all of the proximity sensors available (inductive, capacitive, optical, ultrasound or radio [6]) are non-contact

devices. The described system can be used to balance rotors of all shapes and sizes, even such big and advance rotating machinery as jet engines fans and turbines.

1.2 Purpose statement

The goal of this dissertation is to develop and to deploy an original project solution to the rotating machinery unbalance problem, resulting in a system capable of performing the enhanced rotor balancing in the machine's own bearings. The presented solution includes self developed complete balancing procedure together with trim weight distribution optimization algorithm and was tested using a versatile balancing test stand developed and built by the author.

1.3 Thesis statement

A system based on author's original project, which uses electromagnetic interference mitigation techniques, probes' brackets modal response checks, probes calibration and adjustment, non-contact balancing methods and optimization algorithm for balance weights distribution is capable of providing enhanced rotor balancing results, comparing to existing solutions, while predicting the angle of the unbalance using just a single balancing run.

1.4 Literature overview

The literature covering the balancing of rotating objects is quite extensive. Parkinson [7] reviews rotating machinery balancing techinques for rigid and flexible rotors with in-depth coverage of procedures dedicated for the balancing of high-speed flexible shafts. He reviews over 50 papers on the subject published until 1991. The progress in the field made since then till 1998 is summarized by Foiles, Allaire and Gunter [8] in their comprehensive review of literature concerning rotors balancing. They start by describing the very origins of methods such as modal technique, influence coefficient procedure and both the no-amplitude and no-phase techniques. They also cover the physical concepts of rotating machinery

balancing and describe in great detail the computational algorithms employed in each of the balancing techniques. The most up-to-date review of the rotating objects balancing techniques dates back to 2019 and has been performed by Ibraheem, Ghazaly and Jaber [5]. They review the entire history of the research conducted to study the rotor balancing methods. They cover all the techniques used in modern industry and present the theory used in software algorithms with big focus on the Eigensystem realization algorithm.

The definition of all the terms associated with the balancing of rotating machinery is given by the ISO 21940-2 standard [9]. The unbalance is a condition that exists in a rotor when vibration force or motion is imparted to it and its bearings from centrifugal forces of mass eccentricities [9]. The balancing is a procedure by which the mass distribution of a rotor is examined and, if necessary, corrected to ensure that the residual unbalances are within specified limits. When the correction takes place in just one planet then the method is called single plane balancing and when the correction takes place at 2 or more planes the method is called the mutli plane balancing [9].

Charles Hatch in his book [10] covers all aspects of the rotordynamics field, starting with the fundamentals of vibration, going through different data plots used to view the vibration data and ending with the static and dynamic response of rotor systems. The balancing of rotating machinery is not the main concern of his work, however he discusses topics such as unbalance and rotor response, balancing methodology, locating the heavy spot using a polar plot, selecting the calibration weight and weight splitting to only name a few. The book also covers in great details the malfunctions of rotor systems. A malfunction is described as an operating condition or mechanical problem that, if not treated, may cause a degradation in performance, an unplanned shutdown, or a catastrophic failure [10]. According to the author, the number one cause of most malfunctions is the rotor unbalance, therefore it has to be minimized whenever possible.

When it comes to preventing the malfunctions due to the rotor unbalance Ambur and Rinderknecht proposed an innovative technique of using a self-sensing piezoelectric actuators to detect unbalance in rotating machinery with active bearings [11]. If the unbalance

is detected and immediately corrected the chances of causing a malfunction are mitigated. Ambur and Rinderknecht focused their reseach on rotating machines with active bearings that are equipped with piezoelectric actuators. The authors proposed that since there is an inherent coupling between the mechanical and electrical properties of a piezoelectric material, the piezoelectric actuators can be also used as a virtual sensors. By measuring their voltage and current signals the mechanical deflection can be modelled and hence the unbalance can be detected. Parametric estimation method in frequency domain is used to calculate the magnitude and phase of the unbalance and the hypothesis of localization of faults is used to estimate the location of the unbalance [11].

Another method of predicting the unbalance of rotating machinery was proposed by Yi Yang, Jiaying Wang, Xurong Wang and Yiping Dai [12]. They have focused on geared rotor systems which are especially sensitive to the mass unabalance and therefore require some means of detecting (or predicting, in the best case scenario) the unbalance to prevent malfunctions. The authors developed a general method (proved mathematically) that allows to estimate the unbalance reponse orbit for a geared rotor system. They validated the method using three different geared rotor systems (a spur geared two-rotor shaft, a spur geared multi-shaft and a helical geared multi-shaft) and proved that the numerical results are consistent with the proposed analytical solutions.

Yet another method of vibration response prediction was developed by Zengwei Wang and Ping Zhu [13]. The technique proposed by the authors doesn’t apply solely to rotating machinery and can be used with virtually all mechanical systems. The method is using the in-situ frequency response funtions (FRFs) to predict the operational response of modified mechanical systems. According to authors, knowing the response of the original system and the frequency response functions matrix of the subsystem, the response of the modified system can be calculated using the delta dynamic stiffness matrix. Modifications to the system can include the change in mass, changes in stiffness values of the link between a degree of freedom and the frame, change in the fully rigid link between a degree of freedom and the frame, changes in stiffness values of the link between two degrees of freedom, change in the null link between two degrees of freedom or the change in the fully rigid link between

two degrees of freedom [13]. The authors have validated the proposed method using data generated by finite element simulations.

In order to reduce the risk of rotating system malfunction the unbalance should be minimized. To perform the balancing usually it is required to have access to the amplitude and phase data of the frequency response, however the phase data is not always available (for several different reasons). In such case the balancing can be conducted using only the amplitude data. The first version of this method dates back to 1928 and was proposed by Karelitz [14] who has used three trial weights and four adjustable scales on a common pivot to balance turbine generators. In 1936 Ribary [15] developed a graphical representation of the method that used the response amplitude measured during the initial run followed by three trial runs to balance the rotor. In 1954 Somervaille [16] proposed a four circle method that was a simplification of the graphical technique presented previously by Ribary. The final upgrades to the method has been performed by Jackson [17] who presented both the graphical and mathematical representation of this balancing technique in 1971. The method proposed by Jackson has been called the four-circle method and is commonly used in industry until today.

Several modifications has been proposed for the amplitude-only method over the years. The technique was used only for single plane balancing, however Everett [18] has been able to successfully adapt the method for balancing in two planes. Earlier research by Gunter, Springer and Humphris [19] led to different balancing technique without phase. They used a different approach than the classical four circle method and proposed a modal balancing technique that used three modes and just the amplitude data. More recent research on this branch of balancing techniques has been performed by Ali, Al-Taee and Al-Sarraj [20] who has simplified the graphical representation of the method and proposed an easy to implement software algorithm.

In previous paragraphs the amplitude-only methods has been discussed, however it is also worth mentioning that Foiles and Bently [21] developed a phase-only balancing technique. They proposed both graphical and analytical solutions for rotating machinery balancing. The method developed by them could be used for both single and multiplane balancing.

The greatest advantage of the phase-only technique is that for the single plane balancing it requires only three runs (one base run and two trial runs), where the amplitude-only method requires four runs (one base run and three trial runs). Because of this feature the phase-only technique is sometimes called the three-runs method as distinctive from the amplitude-only technique being called the four-circles method. The effectiveness of the phase-only method is greatly limited when compared to other balancing techniques [8], therefore since the research performed by Foiles and Bently in 1988 it hasn't been developed further.

Perhaps the most widely used balancing method today is the influence coefficient technique developed for a case of a rigid rotor by Everett [22]. Author modelled the unbalance in the system in two planes he called the balance planes (at each balance plane there should be an arbitrary chosen mark representing the phase angle). The balancing is based upon measurements taken in two different planes (called measurement planes) during the base run and at least one calibration run for each balancing plane with a trial weight added. The influence coefficient method takes advantage of the measurements vectors change due to added weights. It enables the estimation of the angular location and magnitude of final weights that should be added to each balancing plane to counter the unbalance. The author conducted over 30 test on different systems to prove the effectiveness of the method.

Actual rotor system mounted on ball bearings was used by Chouskey, Dutt and Modak [23] to conduct experimental studies on finite element model updating that can be efficiently used to predict the unbalance in the rotor. They applied Inverse Eigen Sensitivity Method (IESM) to the state representation of the equations of motion in order to estimate the damping, shaft material damping parameters and bearing stiffness. Authors validated the method by comparing the predicted frequency response of the analytical updated model they developed with the data acquired using a real rotating system. Authors proved that the model obtained using this method can be reliably used to balance a rotor.

Another purely analytical approach to the balancing of rotating machinery was proposed by Ozoegwu, Nwangwu, Uzoh and Ogunoh [24]. In their research they came to a conclusion that unbalance is the main cause of rotor vibration. Therefore they explored the nature

of unbalance, its causes and effects as well as methods that can be implemented for its reduction. Authors derived the analytical equations for both balancing in a single plane and balancing in two planes. The equations are implemented using a software tool that facilitates the balancing process. Authors point out that the extended operation of rotating machinery leads to increasing unbalance. In such cases the task of balancing is often given to the maintenance engineer who can perform the task easily by using their software solution.

One of the attempts to improve the classical influence coefficient method has been conducted by Carvalho, Rende and Dourado [25] based on a fuzzy logic approach. Their research focused on reducing the uncertainties affecting the balancing of rotating machines by adding a preprocessing fuzzy logic stage to the measurement data processing. A fuzzy transformation is applied to the rotor vibration response to define the unbalance fuzzy sets. Then the defuzzification process is used to determine the unbalance condition which can be later introduced in the influence coefficient method. The balancing results obtained with this revised method show improvement over the classical approach which has been proven by authors by both numerical and experimental studies.

Because of the limitations of the least squares optimization techniques there are some industrial applications in which the balancing conducted using the influence coefficient method is not able to sufficiently reduce the vibrations caused by unbalance. Untaroiu, Allaire and Foiles [26] proposed a solution to this problem. In their approach the reasonable constrains on both the magnitude of correction weights and the level of the residual vibrations are first included in the influence coefficient balancing method equations. Then the linear matrix inequality (LMI) is used for these equations. Finally the equations are solved using the numerical algorithms taking advantage of the convex optimization theory. Two numerical balancing examples, both characterized by a set of complicated requirements, have been solved by the authors using the proposed method in order to prove its flexibility and effectiveness.

In the overwhelming majority of the balancing techniques used in industry today the balancing process looks similar in a sense that a base run and one or more calibration runs are required. Xu, Qu and Sun proposed an interesting alternative that does not require

any calibration runs [27]. Authors developed a method in which the optimized correction masses can be calculated using just the measured original vibration response and theoretical unbalance responses. The genetic algorithm proposed by authors is capable of minimizing the residual rotor vibrations at selected balancing speeds and balancing plane locations. The effectiveness of the method was proved by balancing the same rotor twice, first using the classical influence coefficient method and later by using the no-calibration runs method. Both methods reduced the residual rotor unbalance to a camparable levels.

The case of the balancing of highly flexible rotors was researched by Saldarriaga, Steffen, Der Hagopian and Mahfoud [28]. Such kind of rotors exhibit nonlinear behavior which makes the balancing especially difficult using the standard methods. To tackle this challenge the authors proposed an approach in which the rotating system model is identified using a pseudo-random optimization technique (applied through genetic algorithms) and then acted upon using a balancing procedure. The procedure consists of first obtaining the rotor unbalance response of the flexible rotor and then using a finite element model to mimick that response. In this approach the unbalance magnitude and its angular location are the design variables from the optimization point of view and they can be calculated by solving an inverse problem. In order for this technique to work correctly the characteristics of the model have to be adjusted experimentally. The efficiency of the method has been confirmed by authors through series of experiments, however those experiments showed that the method exbibits some limitations.

One of the most popular methods when it comes to the rotor balancing is the modal technique. In modal balancing method it is assumed that the rotating machinery has planar modes of vibration, therefore balancing one mode should not have any effect on the response of all the other modes [8]. The technique works by splitting the principal modes of vibration and then balancing each mode separately. Each of the vibration modes can be used to express the unbalance and additionally the rotor deflection corresponding to each mode can be excited by its corresponding unbalance. When unbalance of each vibration mode is countered by using concentrated correction weights it will lead to the reduction of the deflection, therefore the rotating system will be balanced [29].

The modal balancing technique in the form used commonly in the industry even today was first proposed by Lindsey [30]. He used two factors, a sensitivity factor (which relates to the magnitude of vibration) and a high spot number (which relates to the phase angles) and combined them with static and couple balance weights. When vibration data is acquired at both ends of a machine in one plane it can be used to graphically determine the modal components (first mode and second mode) of the vibration. The modal balancing technique provides good results especially when applied to rotating systems consisting of multiple rotors with long spans. The drawbacks of the method include its poor consideration of the effect that couple weight has on static component of the vibration and the other way around – poor consideration of the effect that static weight has on the couple component of the vibration.

Several attempts have been made to improve the modal balancing technique, with different level of success. A summary of the state of art of modal testing and experimental modal analysis of rotating machinery has been done by Bucher and Ewins [31]. They reviewed the existing modal analysis methods and models focusing on their relevance, advantages and limitations. They also presented some of the new developments that were proposed to counter these limitations. Authors go through several applications of modal testing (including balancing techniques) and provide the experimental results that prove the efficiency of the modal approach.

The modal balancing technique can be applied to a specific type of rotor systems that are otherwise hard to balance. One of such cases has been studied by Han Dong Ju [32]. In his research he focused on applying the modal balancing technique to the specific case of a non-isotropic (not uniform) rotor systems. The author proposed a concept of the dominant balancing mode that can be obtained from the definition of major harmonic of the system unbalance response. According to the author the performance of the balancing using the dominant mode depends on the accuracy of the unbalance modal response. The results of numerical simulations performed using non-isotropic rotor models demonstrate the effectiveness of the method in reducing the vibration response due to unbalance.

Other modification to the modal balancing technique was proposed by Deepthikumar, Sekhar and Srikanthan [33] for the case of rotor systems dealing simultaneously with the unbalance and bow problems. The authors proposed to first identify the distributed unbalance of a long and slender rotor using finite element modelling combined with a polynomial curve. Then the rotor is run at speed below the balancing speed and the vibration responses are measured to enable the estimation of real unbalance eccentricity distributions. Finally the correction weight required to counter both the unbalance and bow of the rotor is computed using the amplification factor at critical speed. The method requires a single balancing run at the critical speed, in contrast to the conventional modal balancing technique that requires multiple balancing runs. A rotating system having both unbalance and bow has been used for the purpose of the method verification.

Another approach consisting of using linear and nonlinear regression to estimate the unbalance was proposed by Nauclér and Söderström [34]. The authors considered a problem with the unknowns in the unbalance parameter estimation entering nonlinearity when subjected to a regression model. They proposed a technique in which this nonlinearity can be transformed to linear estimation procedure having a closed form solution. The authors pointed out that the standard influence coefficient method doesn't take into account the imperfections and distrurbing terms in the rotor model, therefore they proposed a balancing technique which deals with these disturbances. Analytical approach is used to prove the superiority of this new method over the classical influence coefficient technique.

Most of the rotor balancing methods require the system to be rotated in its full speed range in order to acquire the vibration response near the critical speed where the system sensitivity is at its highest. However it is not always possible to run the rotor at the critical speed due to the excessive vibration caused by unbalance. In such cases the balancing technique proposed by Tresser, Dolev and Bucher [35] can be used. Their method requires the rotor system to be subjected to a set of external forces (like parametric excitation or software controlled nonlinear stiffness terms) while rotating at low speed. These forces are chosen specifically to obtain sufficient sensitivity required to estimate the unbalance even when rotating only at low speeds. Authors used both numerical simulations and experimental runs on real rotors to prove the analytical model.

Tiwari and Chakravarthy [36] proposed a method that identifies both the residual unbalance of the rotor as well as the bearing dynamic parameters. The technique presented by the authors takes advantage of the impulse response measurements acquired in flexible rotor-bearing system with multiple degrees of freedom. These measurements are then used by a special algorithm to estimate the residual unbalances at chosen balancing planes and the bearing dynamic parameters (separately for each bearing) dependent on the speed. Both the magnitude and phase information is present in the calculated residual unbalances. Four damping coefficients and four stiffness coefficients are present in the calculated bearing dynamic parameters.

2. Balancing general overview

2.1 Unbalance

Every rotating machine, whether a small compressor that can be found in every-house fridge or a powerful generator turbine, suffers from the same problem which is unbalance. The cause for unbalance might be different in each case (inaccuracies in the manufacturing process, material loss during operation and many others), but no matter the cause, the unbalance will always cause a rotor vibration. Furthermore, it is generally agreed upon that the unbalance is the leading factor causing the unwanted vibration of rotating machinery [37]. It is especially dangerous when the rotor is spinning at the critical speed, when the vibration caused by unbalance can rise to levels several orders of magnitude higher than at the regular speed of operation [38]. The balancing can be described as the process of reducing the rotor vibration caused by the unbalance through adding or removing mass to/from the rotating object. The goal is to distribute the mass of the rotor is such a way that it is even about the centerline of the rotation. Therefore, the balancing is the process of attenuating the inherent vibration caused by unbalance. When properly executed the balancing should reduce the rotor vibration, however there will be always some unbalance left in the system, no matter how precise the balancing process is [39]. Usual approach is to spin the machine through its full speed range while taking the measurements. Having a critical speed in this range is unwanted from the machine operation point of view, however the system has its highest sensitivity in this region which is beneficial for balancing process [35].

The goal of the balancing process is to estimate the magnitude and angular location of the balance weight that will cause the reduction of the unbalance in the rotor. There are many balancing methods used in the industry to achieve this goal, however most common way of balancing, especially on the manufacturing level, is to use a device called a balance machine [40]. In order to use this device the rotor upon which we want to perform the balancing process needs to be disassembled and inserted into the bearings of the balance machine. The bearings are located in the supports which can be adjusted to fit a wide variety of rotor sizes and types. For the purpose of avoiding the resonance in the system, there are vibration dampers installed in the machine [41].

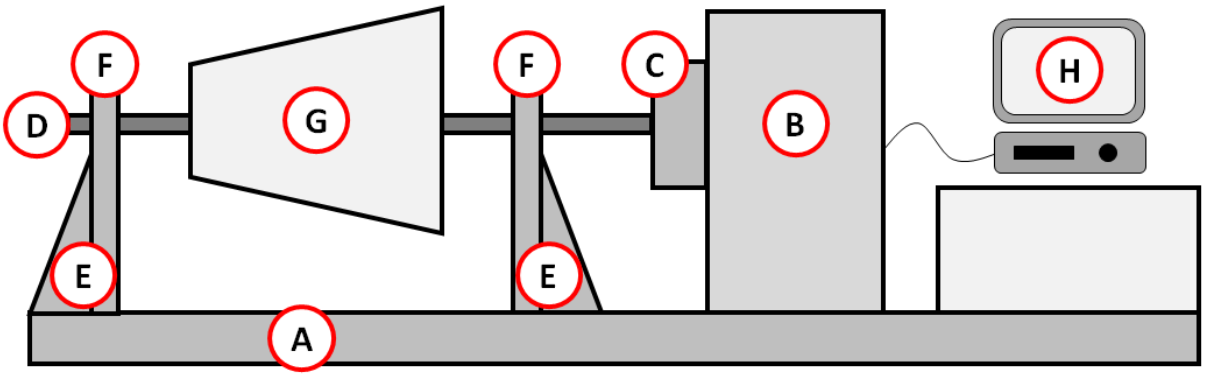

Figure 1 – typical balance machine

Figure 1 shows the construction of a typical balance machine. The machine consists of the following parts:

A) bench – provides the structural basis for the machine,
B) control cabinet – encloses the electrical system, control system and the motor,
C) gearbox – increases the speed,
D) shaft – usually delivered together with the tested rotating object as a single item, however balance machine can have its own shaft for balancing of objects such as discs and other similar items,
E) supports – they are holding the balanced rotating object in the centerline of the gearbox output shaft,
F) sensors – usually accelerometers or strain gages,
G) tested rotating object – the rotor being balanced,
H) PC – provides a human-machine interface.

The balance machines are well-developed devices that can be used successfully for very accurate balancing of rotating machinery. They have several drawbacks though, that greatly reduce the range of their applications. Not every rotor can be disassembled and the balance machine cannot be used for rotating object balancing in its own bearings. They are also very expensive which is an obvious factor limiting their use. The process of balancing while using the balance machine is quite simple. The rotor is spun by the control and drive system while the data is acquired from the sensors installed in both supports. Additionally a tachometer signal is recorded for the angle reference purpose [39]. Each balance machine has its operation manual

which describes the steps necessary to perform the balancing as well as its own software that is used to estimate the magnitude and angular location of the balance weight.

The system described in this dissertation can provide the same quality of balancing as a balance machine when it comes to reducing the vibration caused by the unbalance. The advantage is that hardware necessary for conducting the balancing using this system is both inexpensive and not invasive. To perform the balancing the following sensors are needed:

- one analog proximity sensor when the system uses the four runs method,
- one analog proximity sensor and one tachometer when the system uses the single plane vector method,
- *n* analog proximity sensors (where *n* is the number of planes to balance) and one tachometer when the system uses the multi plane influence coefficient method.

All the probes that are used by the balancing system described in this dissertation are either eddy current, inductive, capacitative or optical probes, therefore they don't need to be coupled to the rotor. Given that there is sufficient room to access the rotor, this system can be therefore used for balancing of any rotor in the field. Additionally this system uses the non-contact balancing procedures which is another one of its greatest advantages.

2.2 **Developed balancing test stand**

A dedicated test stand has been designed and built for the process of development and testing of the balancing system described in this dissertation. The test stand constists of the following elements:

- Besel IE1 SH90-2S – asynchronous induction motor, 3 phase, nominal speed 2820rpm, power 1.5kW; spins the rotor that is being balanced,
- Eaton Electric DC1-127D0FN-A20CE1 – inverter, 1 phase input, 3 phase output, power 1.5kW, frequency control range 0÷500Hz; controls the speed and/or torque of the motor,
- National Instruments cRIO-9063 – programmable automation controller, ARM Cotex-A9 667MHz processor, FPGA Xilinx Zynq-7000, 256MB DRAM, 4 card slot chassis; runs the real-time and FPGA applications, stores the data,

calculates the controls, communicates with the human-machine interface application over the Network Stream protocol,

- National Instruments cRIO-9263 – analog output voltage card, 4 channels, range ±10V, update rate 100kS/s/ch simultaneous; delivers the setpoint signal to the inverter,
- National Instruments cRIO-9215 – analog input voltage card, 4 channels, range ±10V, sampling rate 100 kS/s/ch simultaneous, 16bit; acquires the data from 4 analog proximity probes,
- National Instruments cRIO-9375 – digital input/output card, 32 channels including 16 sinking type inputs and 16 sourcing type outputs, inputs sampling time 7µs, outputs update time 500µs, 0/24VDC logic levels; acquires the signals from the tachometer and the inverter, controls the relays and the inverter (enable and direction signals),
- Panasonic GX-M12A-P-Z – cylindrical inductive proximity sensor, PNP type, normally open; used to detect the notch in the shaft – tachometer,
- Bently Nevada 3300XL – eddy current proximity probe with dedicated transducer, measurement range 200÷3000µm, linear range 400÷2800µm (based on calibration and verification procedures performed), output 0÷10V; measures the displacement of the rotor (4 of these probes were used),
- frame, coupling, supports, bearings, shafts, discs and brackets – mechanical components used to build different configurations of the rotor to balance; 8 steel discs, weighing 1kg each, were used to simulate a variety of rotors,
- dedicated software, including the trim balance weight distribution which uses a self developed optimization algorithm (modified differential evolution).

The differences between the test stand (Figure 2) when the system uses the single plane balancing methods and the test stand (Figure 3 and Figure 4) when the system uses the multi plane influence coefficient method are the following:

- the length of the shaft: 60cm in the case of the single plane methods and 120cm in the case of the multi plane method,
- weight distribution: 8kg in the middle of the shaft in the case of the single plane methods and 8kg equally distributed in 4 spots along the shaft in the case of the multi plane method,
- number of analog proximity probes: only 1 probe in the case of the single plane methods and 4 probes in the case of the multi plane method; the tachometer was used for both single and multi plane methods (in the case of the four runs method the tachometer data has been neglected).

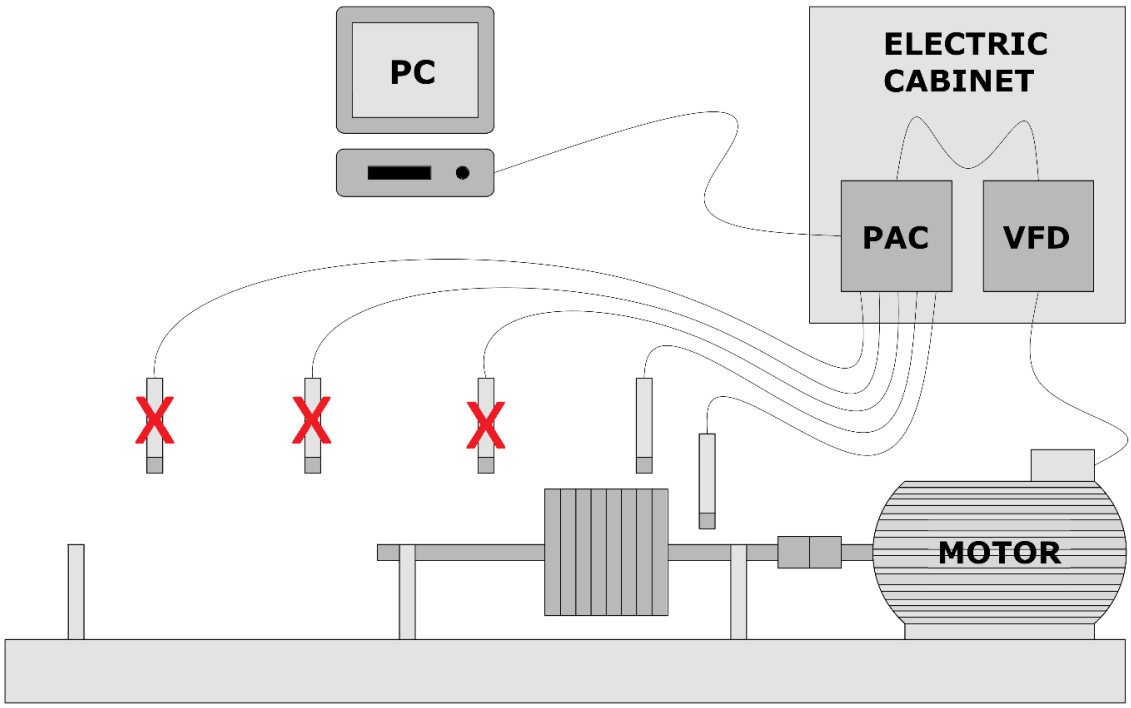

Figure 2 – test stand configuration when the system uses the single plane balancing methods (the crossed-out sensors were installed on the test bench but they were not used for balancing)

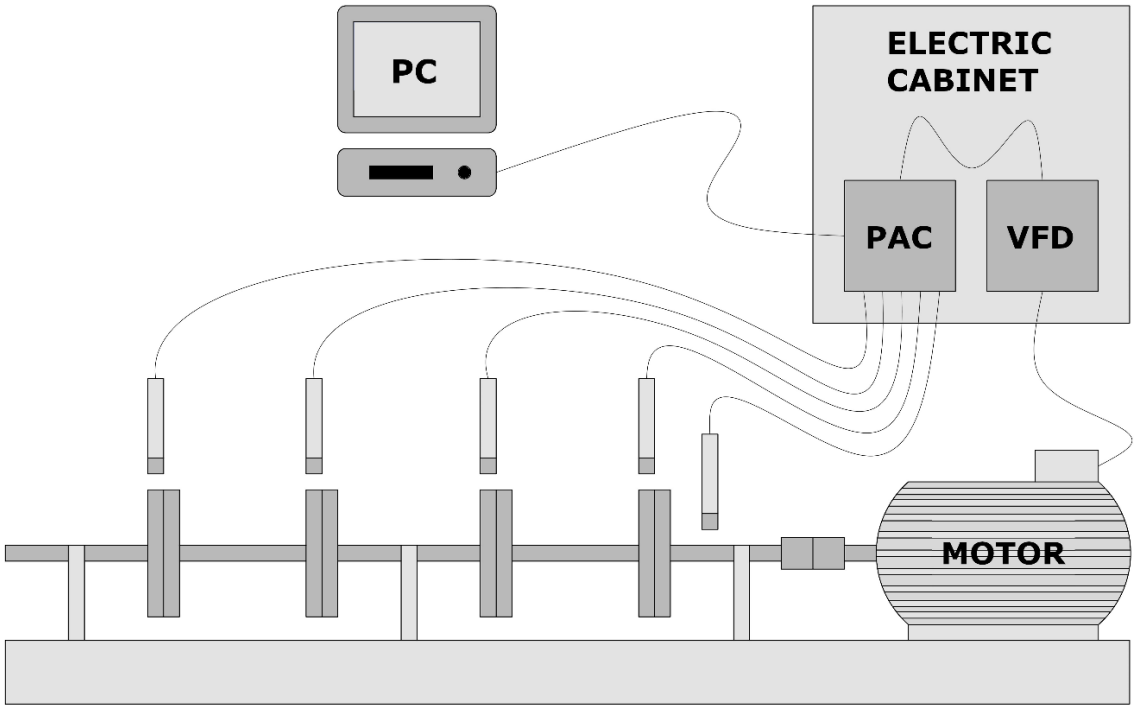

Figure 3 – test stand configuration when the system uses the multi plane influence coefficient method

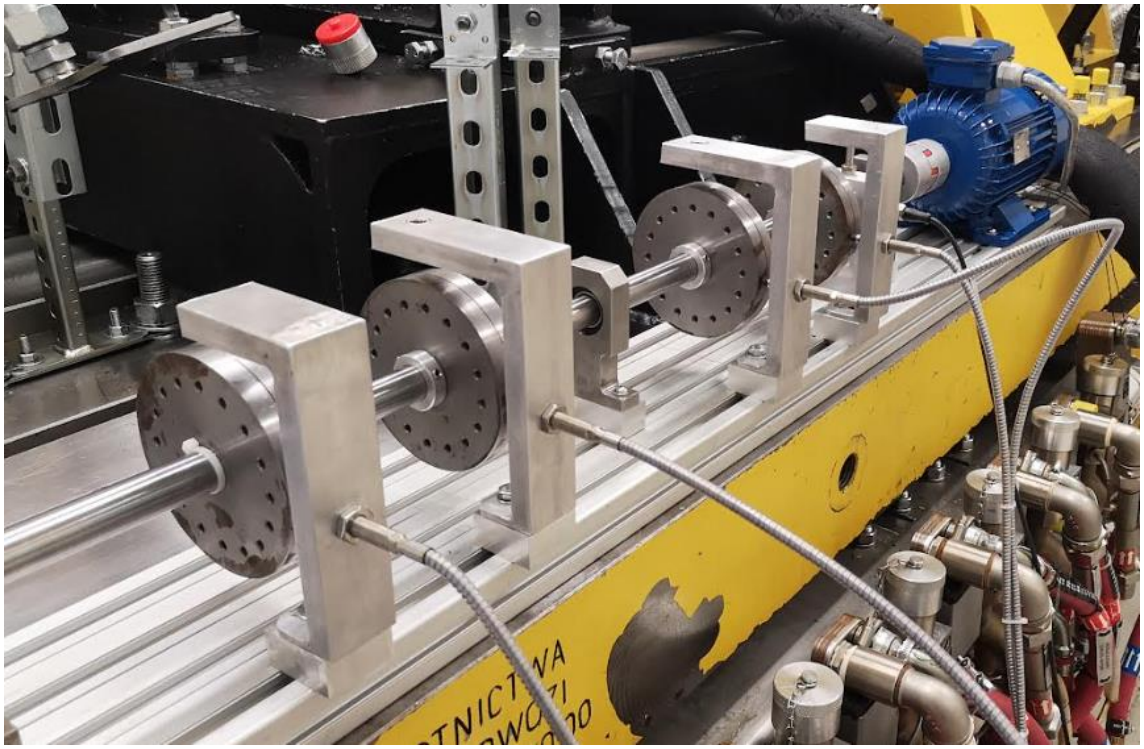

Figure 4 – the developed test stand built on the test bench of the Component Test Laboratory in the Łukasiewicz Research Network – Institute of Aviation, Warsaw (photo by author)

An inductive proximity probe with a PNP output (referred to as PNP proximity probe or tachometer throughout this text) is used to detect a notch in the shaft as the rotor rotates. When 24VDC power source is connected to the PNP output it acts as a sourcing type of output which then can be acquired by a sinking type input [42] of the National Instruments cRIO-9375 card. An Ω shaped bracket is mounted to the base frame of the test stand enclosing the shaft (Figure 5). This bracket is used to hold the proximity sensor over the shaft enabling the detection of the notch as the motor spins. By analyzing the resulting pulse signal in terms of its frequency and time elapsed from the occurance of the last rising edge, the rotational speed of the rotor and its angular position can be calculated at any given time [43]. 3000rpm is the highest rotational speed of the motor, which corresponds to 50Hz, therefore to ensure that the resolution of rotor angular position is not worse than 1°, the sampling rate of the signal should be at least 18kS/s. The update time of the National Instruments cRIO-9375 digital inputs is 7µs, which corresponds to sampling rate close to 140kS/s, therefore the card is more than capable to acquire the tachometer signal with sufficient time resolution. However, to reduce the amount of generated data, the sampling of the tachometer signal has been reduced to 20kS/s, which at the highest rotational speed of the system (3000rpm) corresponds to 400 samples taken every revolution. When the motor is spun at lower speeds the number of samples taken every revolution is getting higher, therefore the angular resolution of the notch detection is also getting better [44].

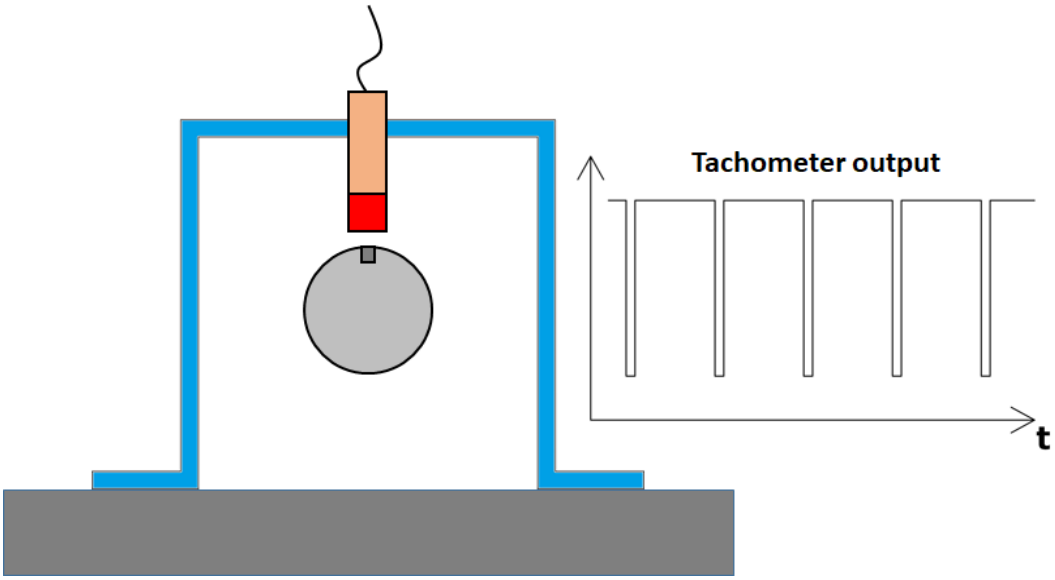

Figure 5 – the tachometer sensor location and output

An eddy current proximity probe (referred to as analog proximity probe throughout this text) is used to detect the displacement of the rotating object being balanced. There are four such sensors used on the test stand. Another Ω shaped bracket is used (one for each sensor) to hold the sensor over the rotor. In the case of the test stand used the rotor consists of different configurations of eight steel wheels (each weighing 1kg). Each steel wheel has a total of sixteen evenly distributed angular locations at which bolts and washers could be added in order to reduce the rotor unbalance (Figure 6). Each sensor has its own conditioning unit which converts the signal measured by the sensor to a 0÷10V output which can be acquired by the National Instruments cRIO-9215 card. The sampling range of each input of the card is 100kS/s at its maximum, however it was reduced to 20kS/s for the same reason as already discussed for the tachometer signal. The Bently Nevada 3300XL proximity probes used have a useful measuring range of 200÷3000µm. A certified height gauge was used to calibrate all the analog proximity sensors using the linear regression method [45]. Through the process of calibration it was established that not the entire measuring range is linear – only the measurements in the range of 400÷2800µm are linear for this particular model of eddy current proximity sensor, therefore the sensors have been calibrated only in this range. The clearance between each of the sensor currently being used (one sensor was used for the single plane balancing methods and all four sensor for the multi plane balancing method) and the rotor was mechanically set to around 1600µm which is a value right in the middle of the linear range [44].

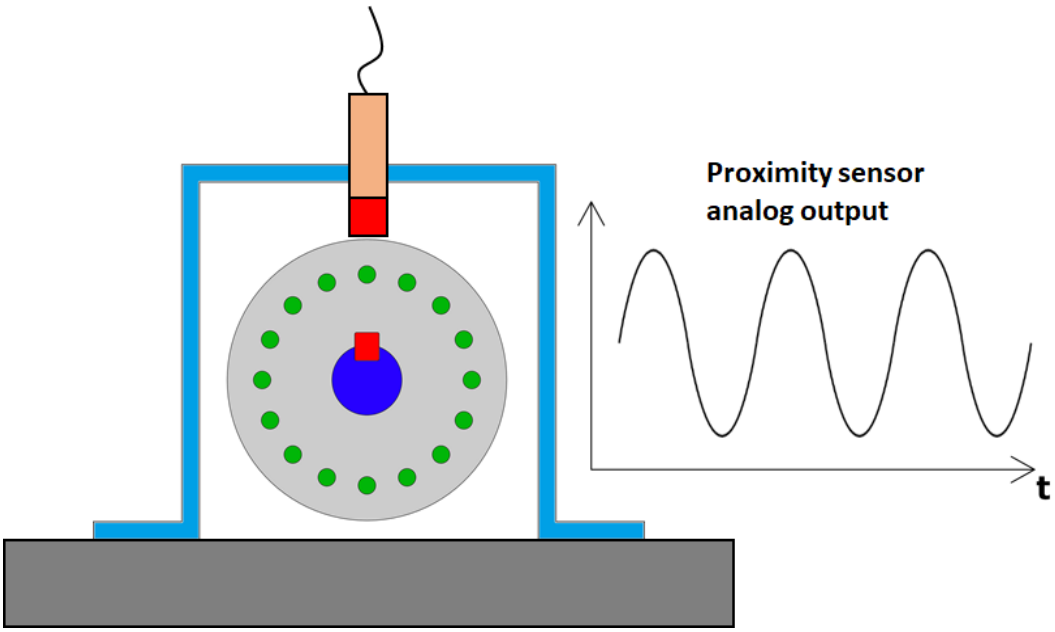

Figure 6 - analog eddy current proximity sensor location and output

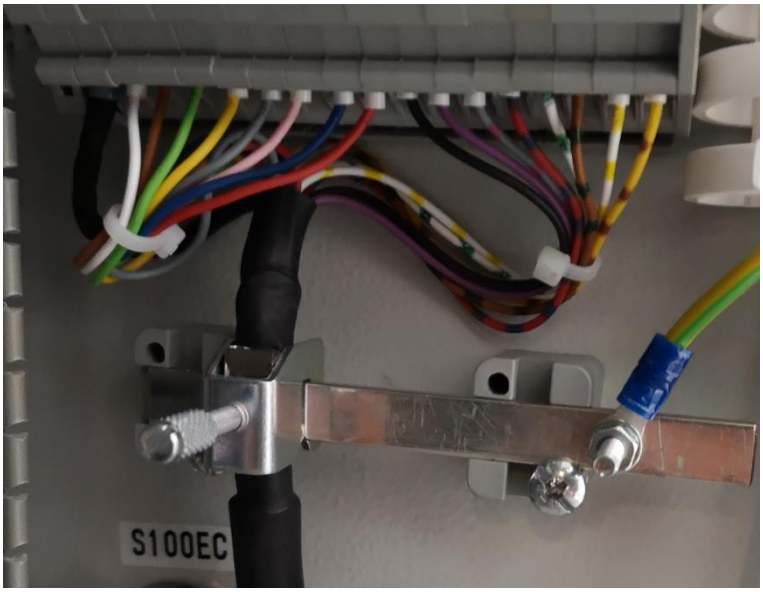

Figure 7 – dedicated 360° terminal block used to terminate the shield (photo by author)

The speed of the motor that spins the test stand's shaft if regulated by an inverter, which generates high electromagnetic interference (EMI). A number of noise mitigating techniques have been implemented in order to reduce the impact of the EMI on the analog proximity probes signals acquired by the system:

- a dedicated radio frequency interference (RFI) filter was installed in the inverted power supply circuit, which reduces the power supply distortion in all other devices (such as DC power supplies) that are connected to the same AC circuits,
- each phase of the motor has been connected using a choke in order to reduce the quick current transients that generate high levels of noise,
- the inverter itself and the AC power supply distribution were installed in a dedicated electrical cabinet having a full steel enclosure acting as a Faraday's cage (to reduce the EMI outside this cabinet),
- all the DC devices (entire data acquisition system) were installed in another dedicated electrical cabinet having a full steel enclosure acting as a Faraday's cage (to reduce the EMI inside the cabinet),
- the ground connections and equipotential bonds have been implemented using a braided wire in order to reduce the skin effect,
- the motor was connected using a double-shielded cable and the shields themselves have been terminated on both ends (motor side and electrical cabinet side),

- the analog proximity probes were connected using a shielded cable with twisted pairs wires and the shields themselves have been terminated only on the electrical cabinet side, according to the good practice rules described by the data acquisition hardware manufacturer [46],
- all the shields connections were implemented using a dedicated 360° (around the cable) terminal blocks (Figure 7).

When the unbalanced rotor spins it causes the test stand's components to vibrate at the frequency of rotation. These vibrations can be neglected in the case of most of the components due to their high mass and high stiffness (for example the test bed on which all other components are mounted). However, the vibration of the brackets used to mount the analog proximity probes needs to be considered due to its impact on the signal acquired by these probes. When the bracket vibrates in the axis coinciding with axis in which the probe is mounted, then the vibration will be added to the proximity signal, which would have a negative impact on the balancing quality. There are two methods of dealing with this problem.

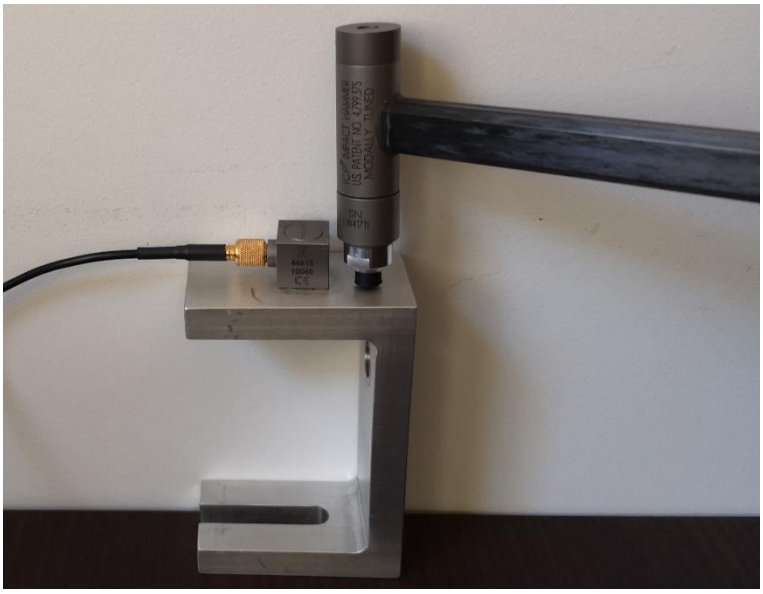

Figure 8 – hammer impact test performed on the structure (photo by author)

First method consists of making sure that the vibration of the bracket is low enough that its impact on the proximity probe signal can be entirely neglected. Modal analysis can be used to perform necessary checking. Modal analysis is a technique that can be used to extract

the dynamic properties of a structure [47], for example its response to forced excitation, such as the rotor vibration. In order to extract the structure's frequency a hammer impact test can be performed. Another test stand designed and build by this dissertation's author is dedicated to this kind of a test. The structure is hit by a special hammer (impact force is measured) in order to excite the structure and in the same time the vibration response is measured (Figure 8). Through analysis of both signals the frequency response can be obtained. Figure 9 shows the frequency response of one of the analog proximity probe's brackets (other brackets have almost similar responses). The analysis of this frequency response shows that in the 0÷500Hz range, the vibration of the bracket is attenuated (values below 0dB), then there is a first mode around 1000Hz with the response amplified by around 18dB. In the frequency range in which the test stand's rotor spins (0÷50Hz) the response is highly attenuated (value below -20dB), therefore a conclusion has been made, that the vibration of the brackets can be neglected. When the impact hammer test shows that the response of the structure in the frequency range in which the system operates is high, then the most sensible thing to do is to redesign the bracket.

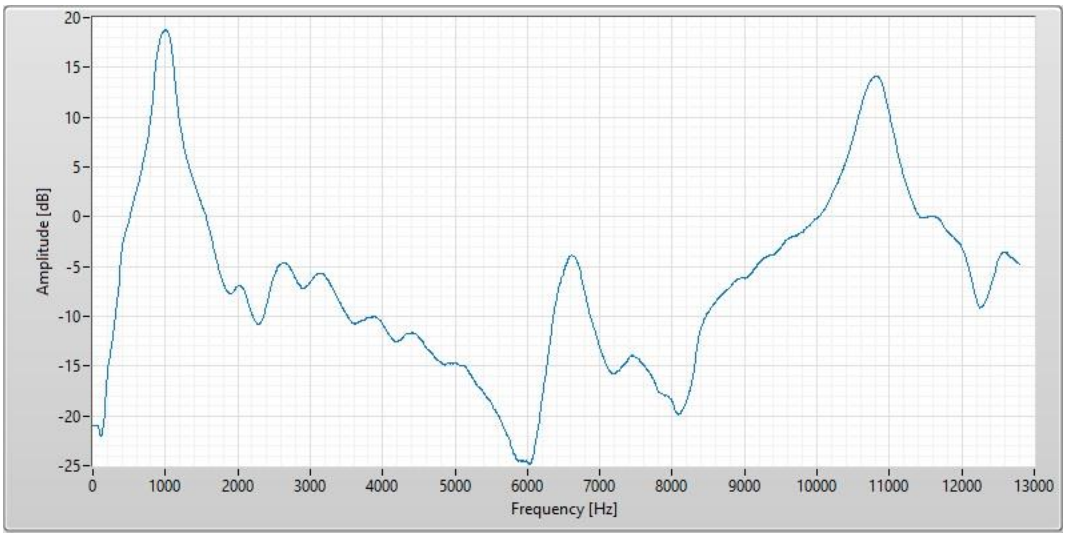

Figure 9 – frequency response of the analog proximity probe's bracket

Second method consists of installing an additional accelerometer in the axis coinciding with the axis in which the analog proximity probe is installed. When the rotor spins the signal acquired by this accelerometer can be used to compensate the brackets vibration component in the proximity probe signal. This technique will be tested as an improvement to the balancing system presented in this dissertation.

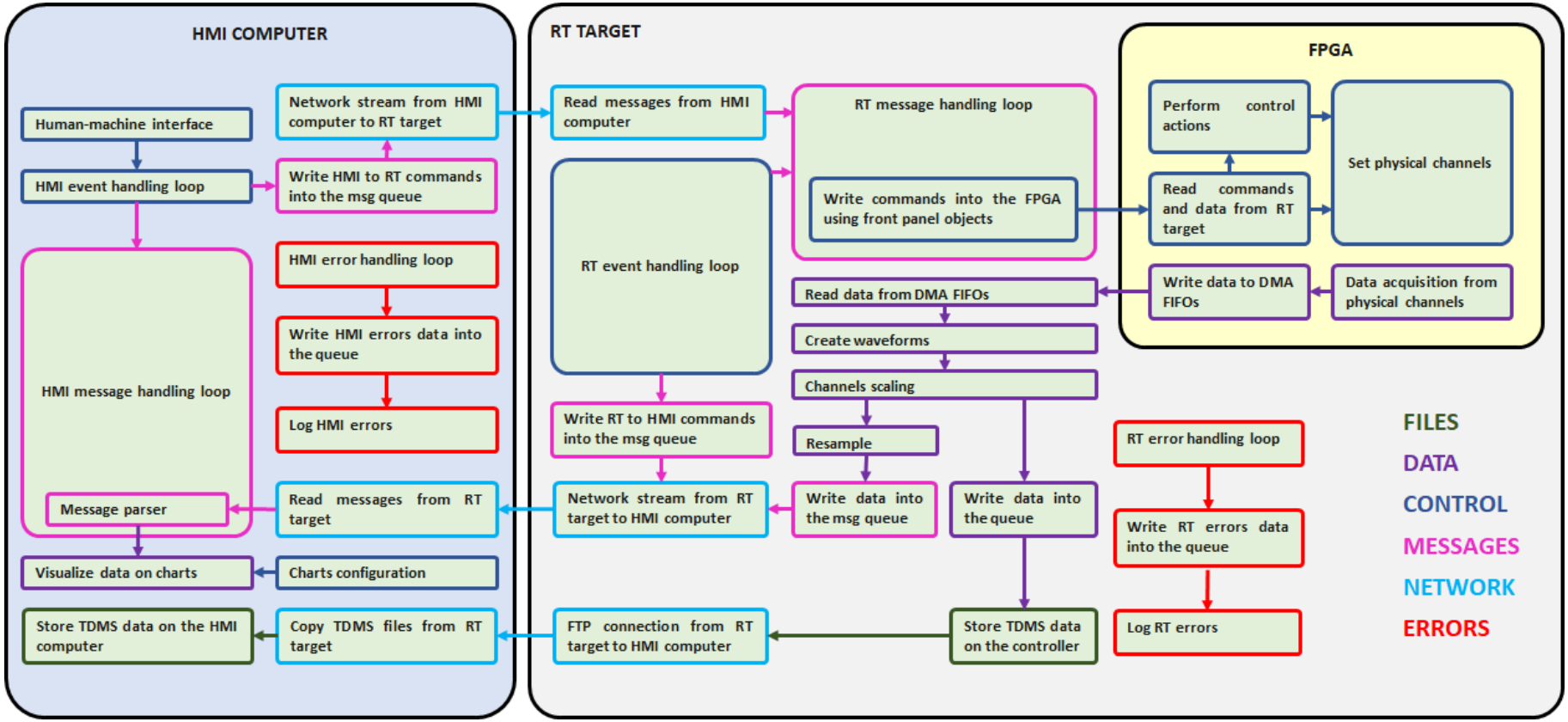

Figure 10 – the structure of the Test Stand Control Application

2.3 Test stand control and data acquisition software

For the purpose of the test stand control and data acquisition a dedicated piece of software, called *Test Stand Control Application*, has been developed. The software consists of FPGA (field programmable gate array) application, real-time operating system application and human-machine interface running on regular Windows system. The structure of the software has been shown on the Figure 10. Through analysis of this structure it can be seen that the FPGA application is a separate piece of software, but it is run and managed by the RT Target (real-time target) application. Additionally, the RT target application running on the National Instruments cRIO controller communicates with the human-machine interface on the PC using the network stream. The network stream is a point-to-point type of communication where the data is being maintained until it is sent or until the communication is disconnected [48], which is perfect for the transmission of critical data such as system current parameters or user control inputs.

The software created benefits greatly from running its critical operations using the FPGA and real-time operating system. The FPGA enables a deterministic execution of operations and extremely high troughput by running the critical and/or intensive tasks which gives the processor more time to perform other operations. The inputs and outputs of the cards are directly connected to the FPGA and therefore tasks such as synchronization, signal processing, triggering and customizable timing can be executed with unparallel performance. The direct connection of the FPGA to inputs and outputs also enables the use of advanced control algorithms by bringing the latency of the control loops to zero [49].

A real-time operating system application has been used to acquire the large amount of data and to perform critical controls and calculation. By using such a system, the software developer can ensure that chosen, important tasks will be deterministic, which means that it will always take an equal amount of time to perform them [50]. The National Instruments cRIO-9063 controller uses an in-house developed real-time system called NI Linux Real-Time. It ensures the deterministic operation of critical tasks, provides proven and stable network stack, is highly robust (the application can recover without any major disruption in the unlikely event

of crashing) and facilitates multitasking for parallel execution of multiple tasks [51]. Given the aforementioned advantages, the NI Linux Real-Time operating system is a perfect tool for the purpose of control and data acquisition and that's why it was chosen.

The major tasks of the developed balancing test stand control and data acquisition software are the following:

- control of the inverter and the motor – speed setpoint, acceleration ramp, decelaration ramp, direction of rotation, inverter disable/enable, motor disable/enable,
- tachometer signal acquisition,
- rotational speed and angular position calculation based on the tachometer signal,
- analog proximity probes data acquisition,
- signal conditioning – scalling and filtering,
- digital signal processing of the data acquired by analog proximity probes,
- data storage (TDMS format),
- communication between human-machine interface and the controller,
- responding to user inputs,
- data viewing on dedicated charts,
- error logging,
- self-monitoring – monitoring of internal loops time, ensuring that the amount of elements in the queues does not exceed the limit, generating and monitoring of the heart beat signal.

If the machine that is being balanced comes with its own control system, then only the data acquisition and monitoring part of the *Test Stand Control Application* can be used and the control capabilities can be switched off. In a case when there is no mechanical element (tooth or notch in the shaft) that could be used to acquire the one pulse per revolution signal, the inductive type of proximity probe can be exchanged for optical type and piece of reflective tape can be put on the shaft. From the perspective of the system both configurations are similar and will work equally well [44].

The *Test Stand Control Application* (Figure 11) consists of the following items:

A) time chart – displays the rotor speed measurements (depending on how many tachometers have been installed) and speed setpoint,
B) time chart channels – toggles on/off the visibility of the channels on the time chart,
C) monitoring info – displays the information about current state of the system,
D) time chart controls – sets the time range of the time charts and toggles on/off its Y axis autoscale,
E) application controls – starts/stops the data acquisition, restarts the master controller and stops the application,
F) tacho parameters – sets the parameters of the tachometer signal,
G) Bode analysis controls – sets the parameters of the order analysis,
H) motor controls – sets the rotor movement direction, starts/stops the inverter and motor, sets the rotor speed and the acceleration/deceleration ramp,
I) FFT chart controls – sets the parameters of the Fast Fourier Transform analysis used to analyze the analog proximity probes signals,
J) FFT chart – displays the frequency chart of the analog proximity probes signals,
K) FFT chart channels – toggles on/off the visibility of the channels on the FFT chart,
L) Bode magnitude plot – displays the chosen order magnitude response of the analog proximity probes signals,
M) Bode magnitude plot channels - toggles on/off the visibility of the channels on the Bode magnitude plot,
N) Bode phase plot – displays the chosen order phase response of the analog proximity probes signals,
O) Bode phase plot channels - toggles on/off the visibility of the channels on the Bode phase plot,
P) polar plot – displays the polar plot of the chosen analog proximity probe signal.

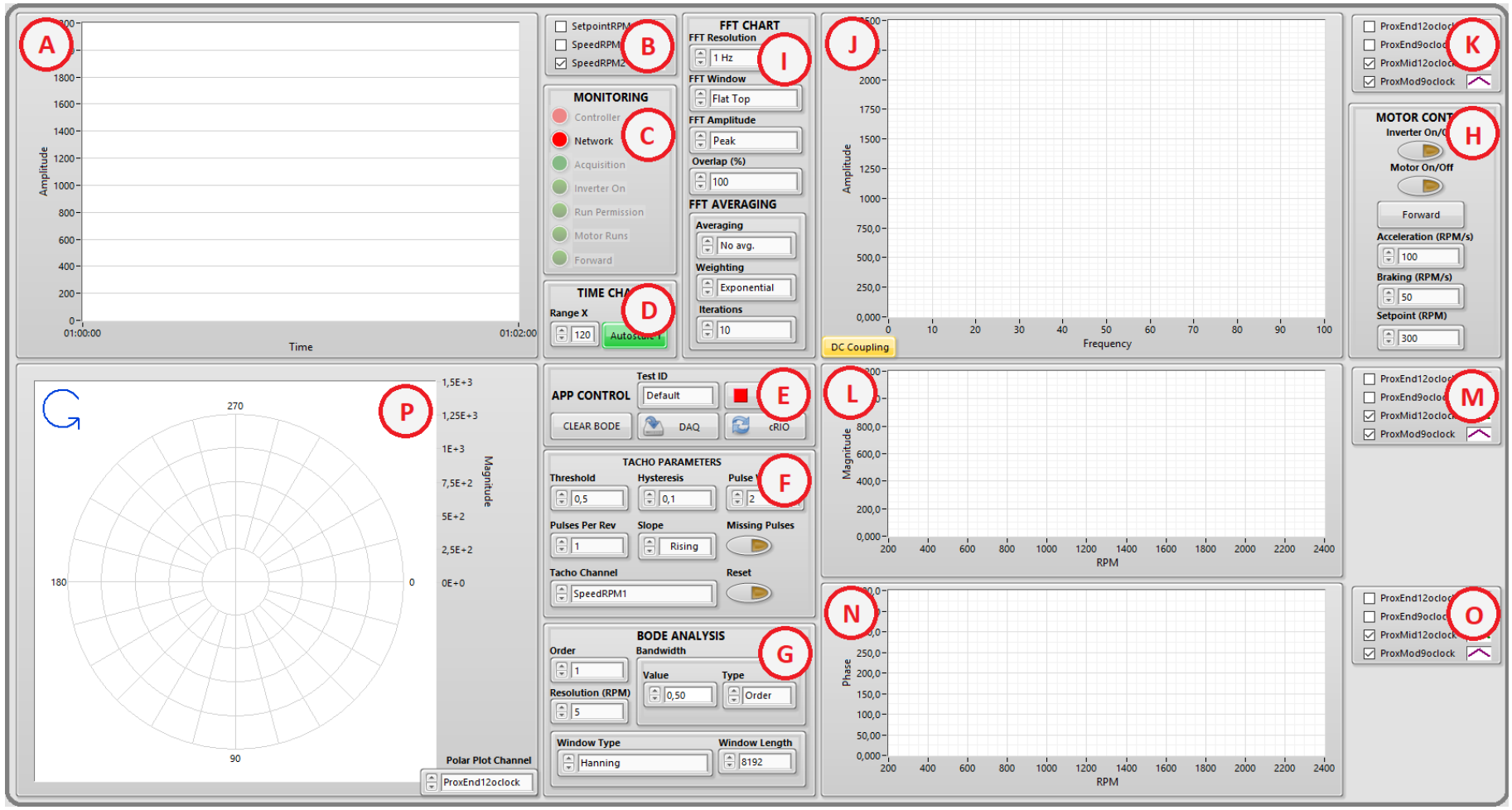

Figure 11 – the front panel of the Test Stand Control Application

2.4 **Order analysis**

Vibration can be measured in three different ways, all of which contain the same amount of information. It could be measured as displacement, speed of vibration or acceleration. When the time waveform of one of them is known the other two can by calculated either by integration or differentiation [52]. The author's goal when developing the balancing system described in this dissertation was to implement non-contact methods, therefore displacement has been chosen as the source of vibration measurement. The displacement is measured by the Bently Nevada 3300XL proximity probes.

When the rotor spins, the unbalance manifests itself as a vibration at the exact frequency at which the system rotates [53]. By calculating the amplitude and phase of this vibration wave at frequency of rotation we can obtain all the information we need to counter the unbalance. The amplitude of the signal corresponds to the magnitude of the unbalance. The phase is a little bit more complicated. If we consider the unbalance as a single heavy spot in the rotating system then the phase is the angular difference between the peak of the vibration signal and a reference point in the rotor [54]. In case of the balancing test stand used there is a notch in the shaft which is monitored by the tachometer to provide the one pulse per revolution signal. The rising edge of the pulse signal is the reference point that could be used to give a physical meaning to the phase of the measured vibration signal [44]. If there's a critical speed in the operating speed range of the system, it might be necessary to properly adjust the calculated phase as the system's response shifts by 180° when going through the resonance [55]:

- when the system spins below the critical speed no phase adjustement is needed – the heavy spot (side of unbalance) flies out,
- when the system spins above the critical speed there's a 180° phase shift – the light spot (side opposite to the unbalance) flies out,
- when the system spins at the critical speed there's a 90° phase shift – the heavy spot leads the geometric center of the rotor.

Given that at the critical speed the system sensitivity is at its highest, to ensure the best balancing accuracy the magnitude and phase of the vibration at the critical speed should be used for calculations. It is therefore important to remember that to properly determine the angular location of the heavy spot representing the unbalance in the rotor, the phase shall be adjusted by 90° [44].

When the balancing is performed the number of analog proximity probes (or any other sensors capable of measuring vibration) should correspond to the number of balancing planes. Balancing plane is a chosen location along the rotation axis of the machine at which we can add correction masses. Ideally, the location of the balancing planes should be specified by rotordynamics engineer, who can determine which planes are most effective. Unfortunately, the usual approach is to choose the balancing planes that are easily available [56]. The balancing consists of several runs (at least two), with and without correction masses, during which the rotor is accelerated to its maximum operating speed while the data acquisition system records the data from tachometer and vibration sensors. The problem is that the unbalance is strictly related to the speed of rotation and when the rotor is being accelerated the speed changes. This means that magnitude and phase of the vibration caused by the unbalance cannot be simply calculated through Fast Fourier Transform [57]. When the FFT is applied to the signal the resulting data is useless in terms of analyzing the unbalance (Figure 12). The amplitude of the signal is constant in the time domain and its frequency is changing. This type of signal is called a chirp signal and it's frequency response calculated using FFT is not a single peak at the desired amplitude but a bell-shaped curve covering a range of frequencies [58].

It is therefore necessary to represent the data in a different form in order to make it more suitable for analyzing the unbalance. This is where a digital signal processing tool called order analysis comes into play. If we want the vibration data corresponding to the unbalance to be periodic even when the speed of the rotor is changing, we need to measure the samples of the signal with equal angle intervals instead of equal time intervals [59]. When signal periodic in time is analyzed, it has a frequency equal to 1Hz when it makes one full oscillation over a 1 second period. Similarly when signal periodic in even-angle domain is analyzed, its order is equal to 1 when it makes one full oscillation over 1 revolution of the rotor. By applying the Fast Fourier Transform to the even-angle domain signal the amplitude

and phase of each order can be calculated. When the speed of the system changes the order spectrum will remain useful as opposite to the frequency spectrum [60]. The amplitude and phase of the first order of the vibration signal are directly related to the unbalance what makes the order analysis an ideal tool for obtaining useful data in terms of balancing.

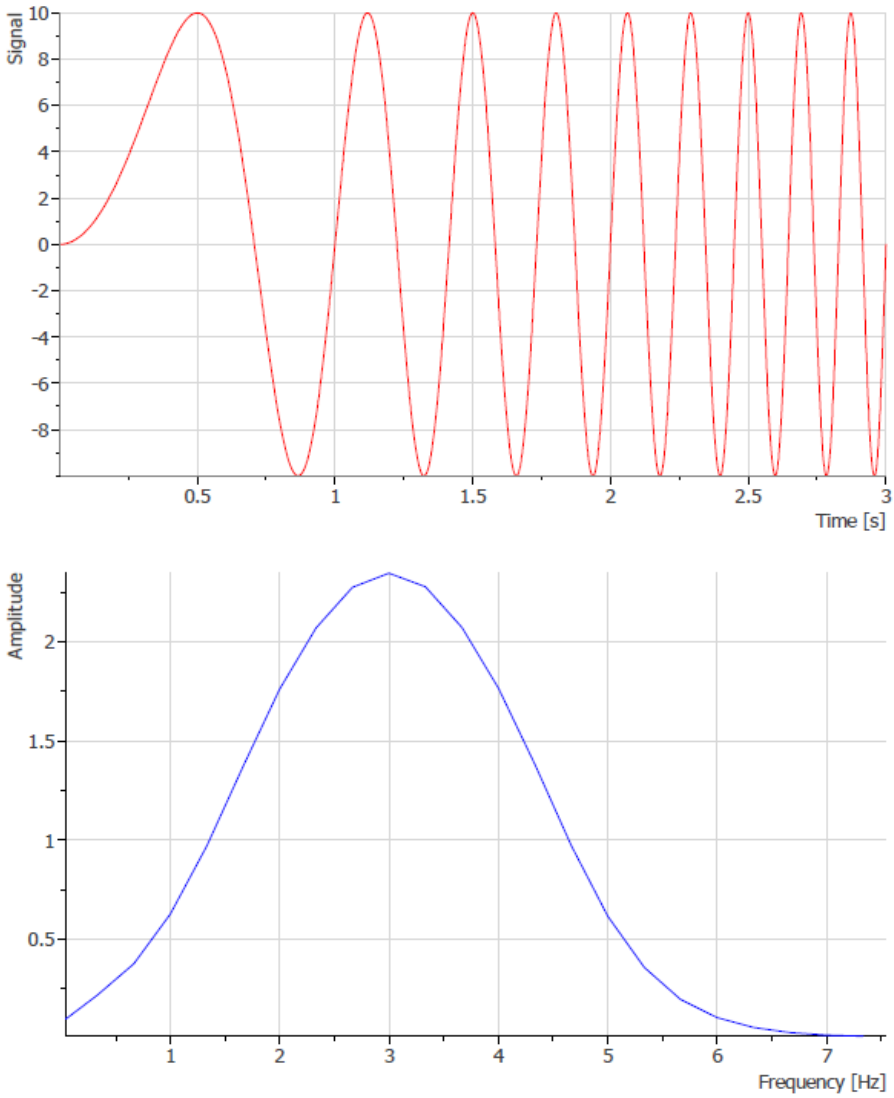

Figure 12 - time domain signal and its frequency response when the rotor is accelerated

To convert the signal into the even-angle domain (also called the angular domain [61]) the recorded vibration signal first needs to be segmented into smaller portions of data, each containing the signal acquired during exactly one revolution of the rotor. The beginning of each new rotor revolution is marked by the rising edge of the tachometer signal, therefore this step can be easily performed. Next step is to resample the data in each segment

to the required number of angular locations (usually 360 for 1° signal resolution or 720 for 0.5° signal resolution). It is assumed that the speed during one single revolution of the rotor does not change. This is a simplification but the speed change during just one revolution is negligible and has virtually no effect on the final result of the order analysis. Finally the FFT is applied to the resampled signal and the order spectrum is obtained [62]. Figure 12 showed a signal of constant amplitude with increasing frequency and its frequency spectrum. Figure 13 shows the same signal converted to the angular domain and its order spectrum. It is obvious that data presented in this form is more useful for balancing purposes.

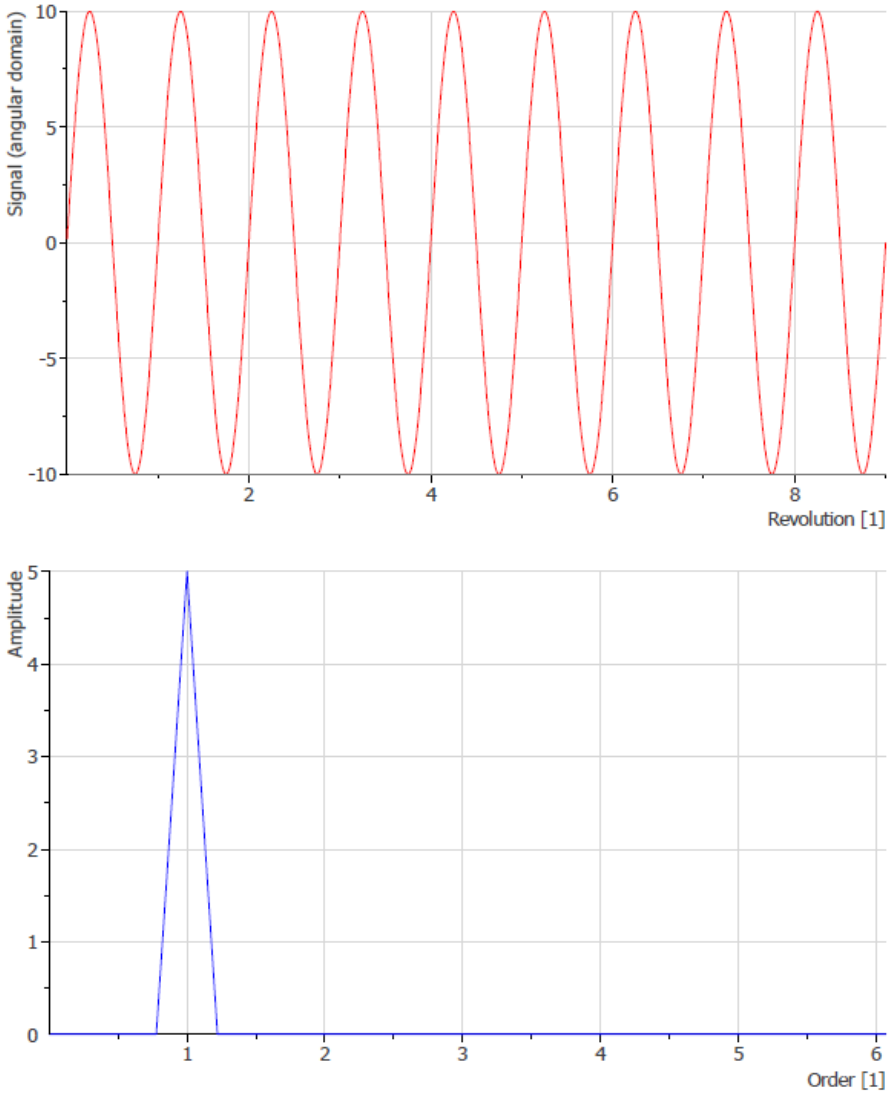

Figure 13 - even angle signal and order response of a sine wave with frequency increasing linearly in the time domain [44]

2.5 **Phase lead and lag**

For the purpose of the balancing system described in this dissertation the phase is defined as a relative shift between two periodic signals of the same frequency. When the signals are analyzed in the time domain then the phase is measured in seconds. Again, it's not a very useful information for the purpose of analyzing the vibration caused by the unbalance. When the signals are analyzed in the angular domain though, the phase can be measured as an angle (unit can be either degree or radian as long as it is used consistently). If we consider the rising edge of the tachometer signal to be the zero degree angle reference point then the phase is the relative angle difference between the peak of the first order vibration signal and this point [63]. This is a key information because as it was already stated the unbalance can be characterized by the magnitude and phase of the first order vibration signal and defining the phase as relative angular shift to a known angular position gives it a physical meaning [60].

Phase can be measured in two ways, either as phase lead or phase lag (also called respectively phase advance and phase delay). It is a common problem that the two phase conventions are mistakenly used in calculations as the same variable when in fact they are fundamentally different. Figure 14 shows an example illustrating the fundamental difference between phase lead and lag. The red box represents the notch in the shaft and the blue dot represents the unbalance as a single heave spot in the rotor. In the given example the rotor spins in the counter-clockwise direction. During the rotation, the vibration signal can be considered in two ways [44]:

- the vibration signal is leading the reference point – the positive peak of the sine waveform happens earlier in time than the rising edge of the tachometer signal,
- the vibration signal is lagging behind the reference point – the positive peak of the sine waveform happens later in time than the rising edge of the tachometer.

The balancing system described in this dissertation uses the phase lag. There is no advantage in using one convention over the other. The only important thing to remember is that once the phase convention is chosen, it shall be used throughout all of the calculations.

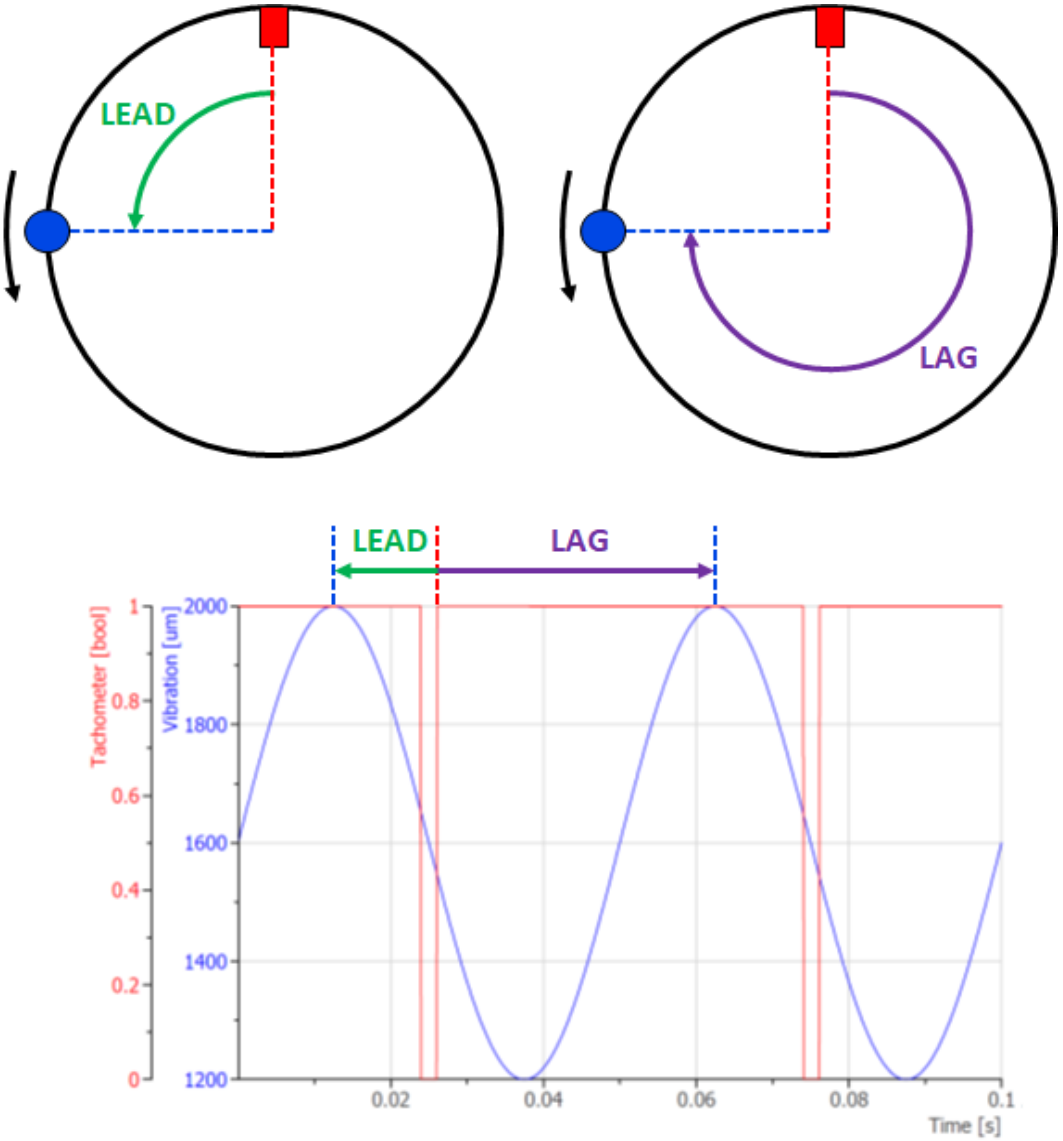

Figure 14 - phase lead versus phase lag comparison

2.6 **Bode and polar plots**

It has been already stated that by analyzing the vibration and tachometer data, the unbalance magnitude and phase can be estimated. The trick to extracting this information is to use the right digital signal processing tools and then view the data in the most representative form. Figure 15 shows the time domain raw data acquired by the analog proximity probe when the rotor was decelerated starting from 3000rpm down to 500rpm. The data has been displayed on a regular time chart. It is safe to say that when viewed in this form, no useful information can be extracted regarding the unbalance in the system.

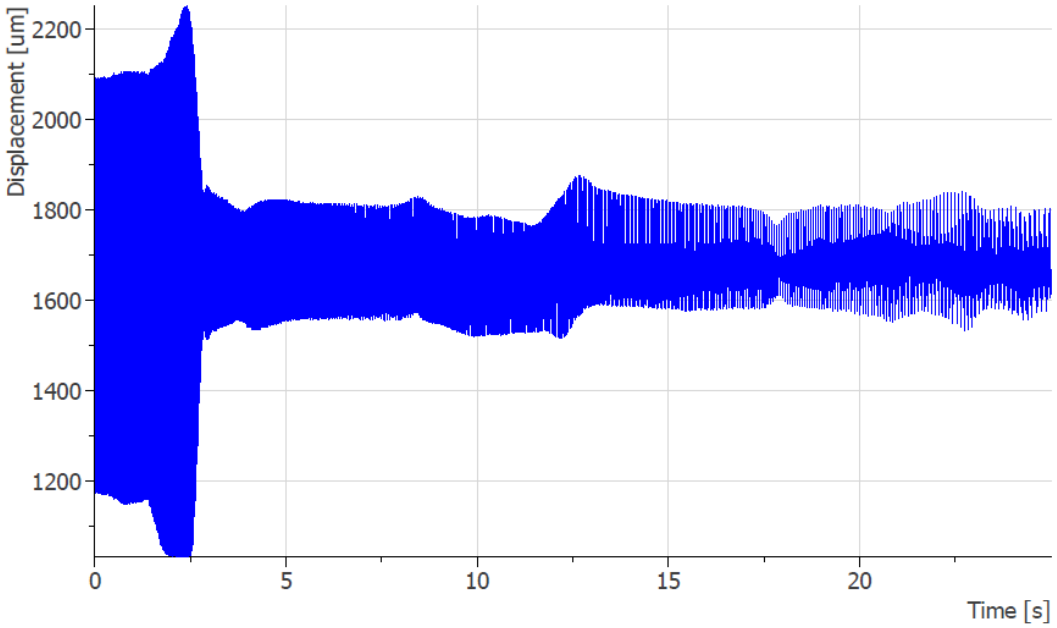

Figure 15 – example of data acquired by the proximity probe during rotor deceleration

Figure 16 shows the same data, plotted together with the tachometer signal, in great close-up (only around 60ms od data is displayed). Some useful information can be extracted from this plot, for example the amplitude of vibration at this particular moment or the time shift between the peak of the vibration waveform and the rising edge of the tachometer signal. However, by processing the data further even more information can be gathered.

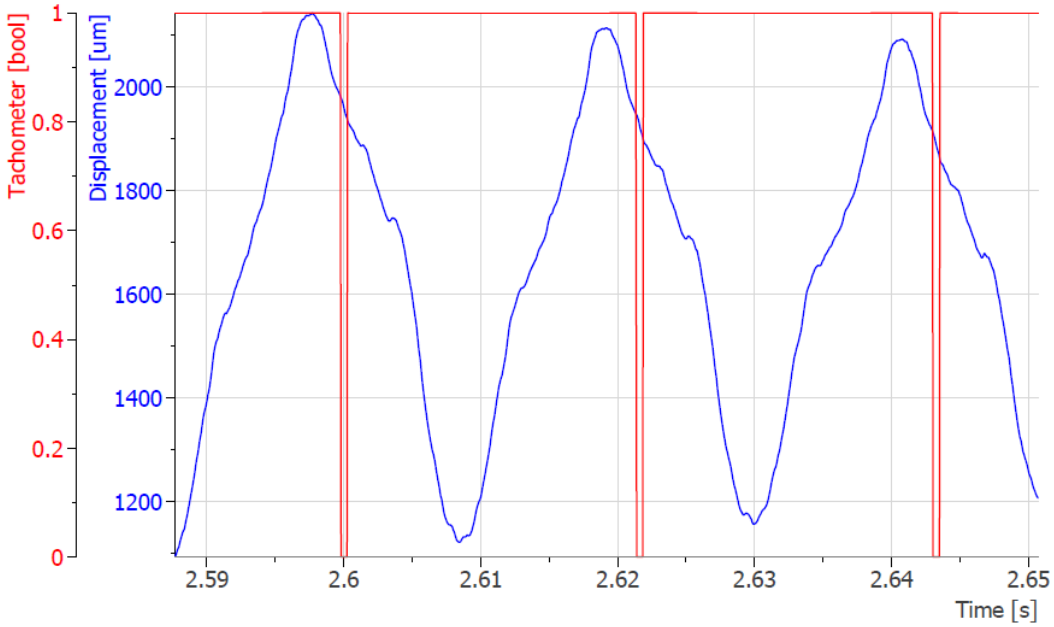

Figure 16 – example of displacement (vibration) data plotted together with the tachometer signal

To convert data from the time domain into the angular domain, it first needs to be segmented. Each segment contains data acquired during exactly one revolution of the rotor. Because the rotational speed change between two adjacent data segments is negligible the samples taken with fixed time interval can be considered to be also taken with fixed angle interval. At this point the resolution of the order tracking can be enhanced by up-sampling the data [64]. Data in each segment can be characterized by the time of its first sample or by the current rotational speed. Therefore, when FFT is taken of each segment the resulting amplitudes and phases can be plotted on a chart with time or speed on the horizontal axis [60]. This kind of plot is called a Bode plot and is a very useful tool commonly used in rotordynamics to analyze the dynamic behavior of the system. Figure 17 shows the signal from Figure 15 on the Bode plot when time is used on the horizontal axis.

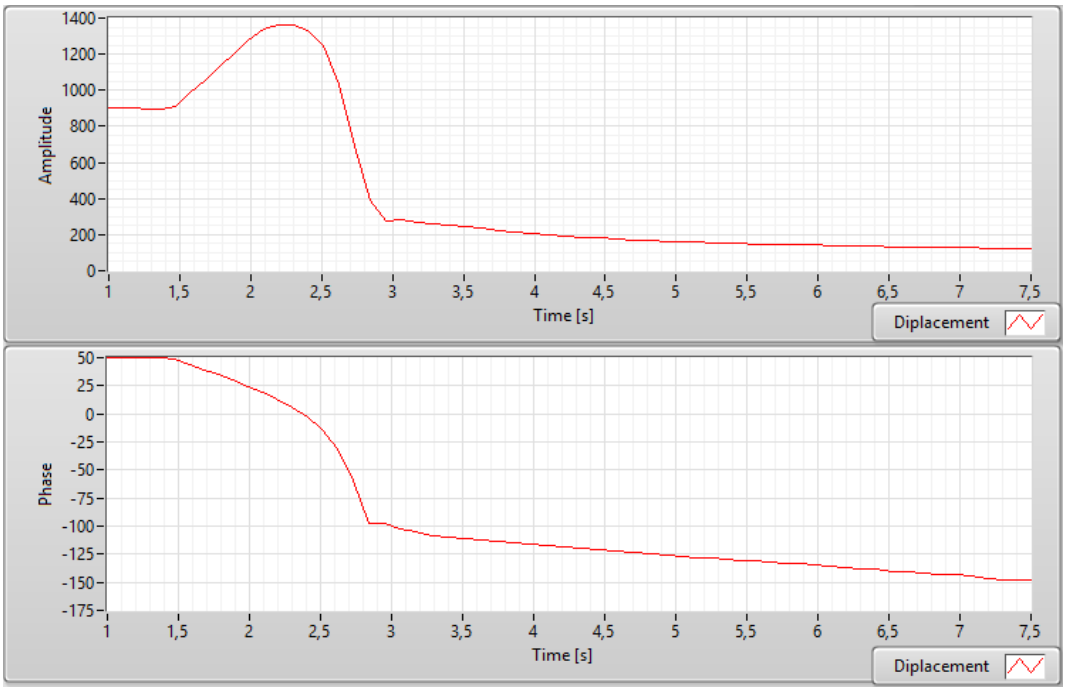

Figure 17 - example of a Bode plot (time on horizontal axis)

The changing amplitude and phase can be observed, however this is still not the full information that could characterize the unbalance in the rotor. When analyzing the Bode plot the most important identifier of the unbalance in the machine is the pattern of amplitude and phase plotted in the function of speed [65]. Figure 18 shows one such plot of the same data discussed with regard to previous plots. By analyzing the data displayed in this format, it can be concluded that the amplitude of vibration associated with unbalance is slowly rising with the speed right to the point when the resonance is encountered. In the close proximity

of the critical speed the amplitude is sharply increasing and reaches its peak approximately at 2850rpm. Then it starts to quickly roll-off. There is also a roughly 180° phase shift when the system goes through the resonance. This is exactly the information needed for the purpose of balancing.

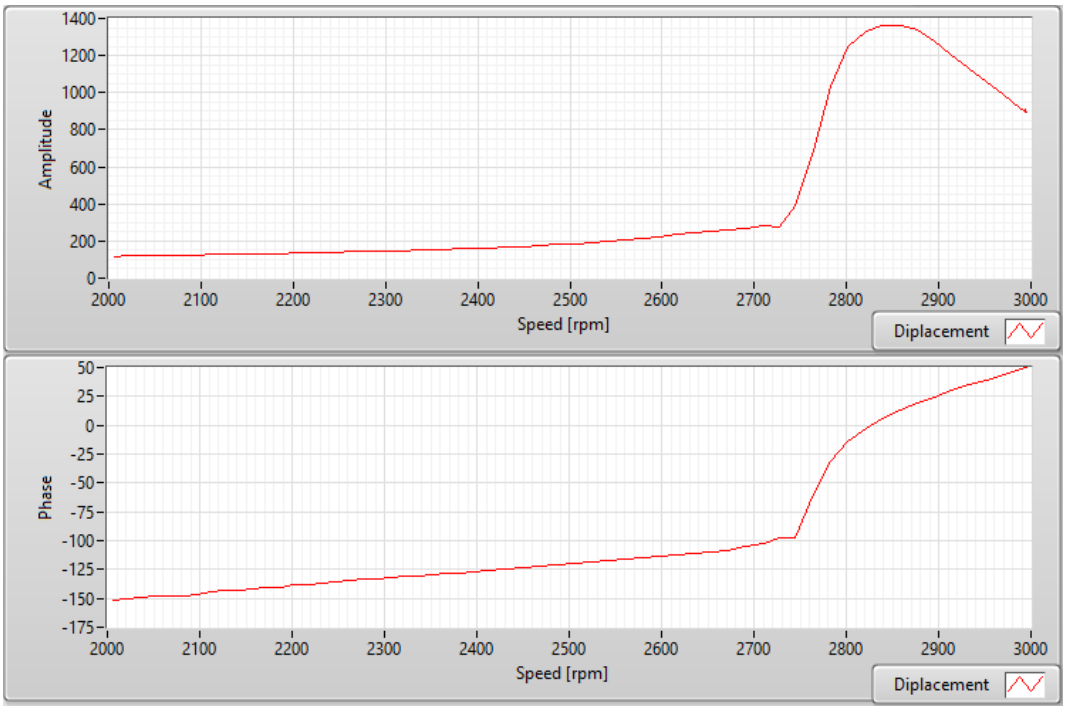

Figure 18 – example of a Bode plot (speed on horizontal axis)

There is one more type of plot that is very useful for the unbalance analysis – the polar plot. On the Bode plot the amplitude and phase can be best analyzed with respect to speed or time. On the other hand, the polar plot is a better tool when the amplitude is analyzed with respect to phase [44]. Example of a polar plot can be seen on Figure 19 which shows the data from Figure 18 displayed in polar coordinates. The distance from the center of the plot represents the amplitude and the angular location represents the phase. Additionally the speed can be tracked by following the blue dots on the plot. The point furthest away from the center of the polar plot is representing the vibration at the critical speed. By shifting this point by 90°, the location of the unbalance in the rotor can be very easily found using the polar plot.

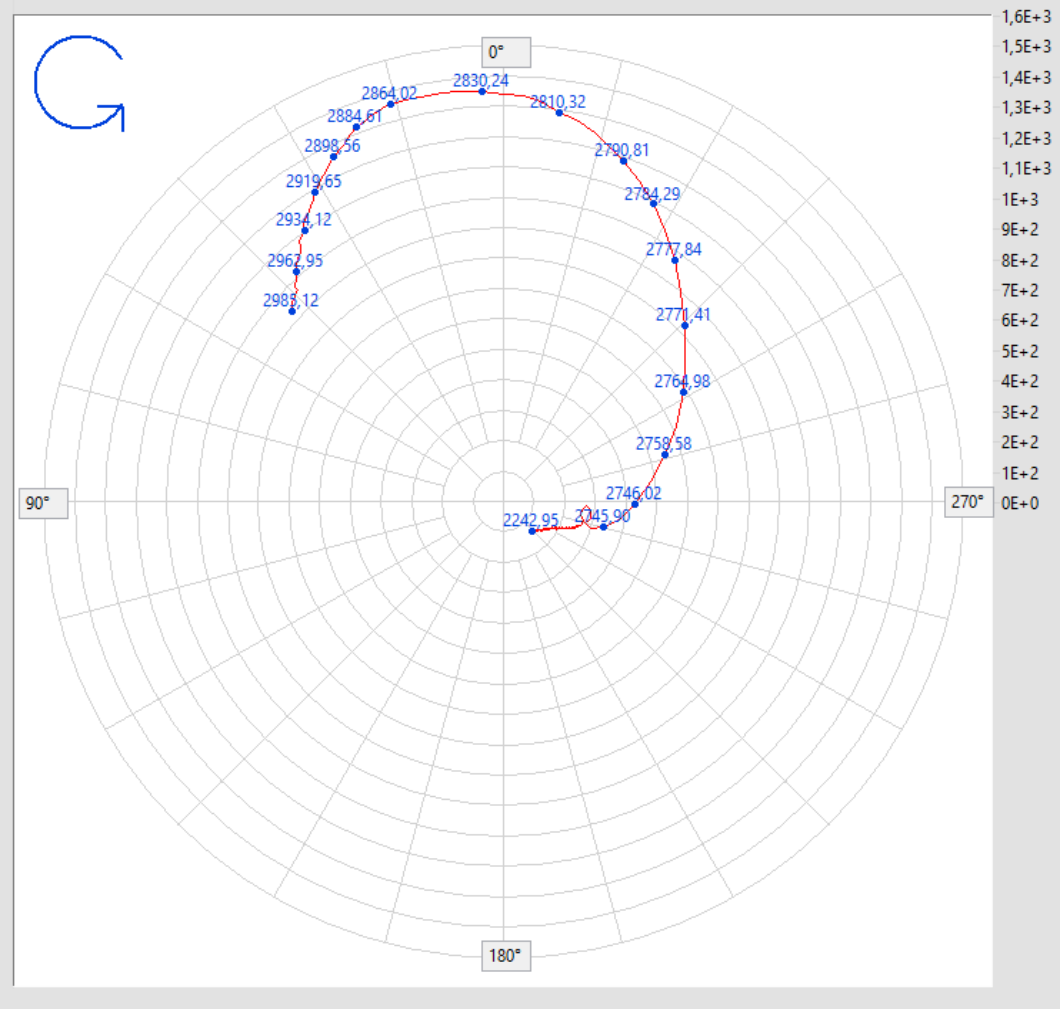

Figure 19 – example of a polar plot

2.7 **Balance weight distribution**

The goal of conducting the balancing using the developed system is to estimate the magnitude and angular location of balance weight that will counter the unbalance. Once these two values are found the resulting balance weight can be added to the rotor in several ways [66]:

- by removing of equal amount of weight to calculated balance weight from the side opposite to its calculated angular location – this has an obvious disadvantage of being one-time activity, which cannot be simply undone,
- by taking the exact amount of moldable material equal to the the calculated balance weight and glueing it to the inside of the rotor (see Figure 20) – this approach is only possible for specific type of rotors which contain a hollow section where

the moldable material can be inserted and secured by the centrifugal force when the rotor is spinning,

- by inserting bolts and washers into the angular locations made specifically for balancing purposes – these are usually threaded holes evenly distributed around the rotor at specified radius.

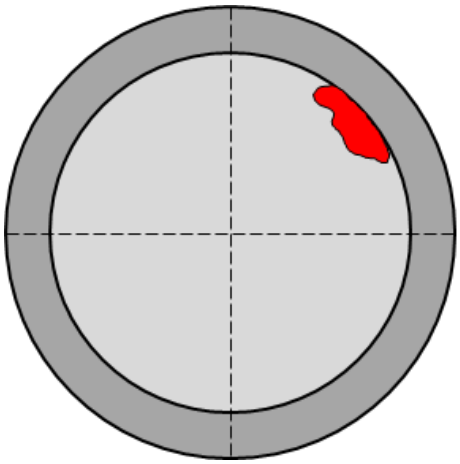

Figure 20 – using moldable material to install the correction balance weight

The system described in this dissertation uses the last approach. Figure 6 shows one of the steel discs used to simulate different types of rotors. Each disc has sixteen evenly distributed angular locations at radius equal to 45mm. When the magnitude and angular location of the balance weight is estimated, the calculated angle will almost never exactly match the location of the threaded hole in the disc and the calculated weight will almost never exactly match either one of the available configurations of combined bolts and washers weight. Therefore it is necessary to use several angular locations to distribute the available bolts and washers in a way that will match the estimation as close as possible.

The balancing test stand build to research the performance of the developed balancing system had the following items available for correction weights: bolts weighing 4.5g each, small washers weighing 0.8g each and big washers weighing 3.0g each. Due to the length of the threaded part of the bolt, it was possible to install max 4 washers at one angular location. Table 1 shows the available configurations of the unbalance correction weights that could

be used. When it comes to the correction weights the usual approach is to specify their magnitude by multiplying the weight and the radius at which they are installed [11]. This is due to the fact that the bolt weighing 5g installed at 100mm radius will have the same effect on the unbalance as the bolt weighing 10g installed at 50mm radius. In the industry the commonly used units of correction weights are g-mm, lb-in and g-in. It is not a coincidence that these are also the units used to quantify the unbalance [67].

Table 1 – available configurations of unbalance correction weights

No	Configuration	Radius	Weight	Radius x Weight
1	1 bolt	45 mm	4.5 g	202.5 g-mm
2	1 bolt, 1 small washer	45 mm	5.3 g	238.5 g-mm
3	1 bolt, 2 small washers	45 mm	6.1 g	274.5 g-mm
4	1 bolt, 3 small washers	45 mm	6.9 g	310.5 g-mm
5	1 bolt, 1 big washer	45 mm	7.5 g	337.5 g-mm
6	1 bolt, 1 big washer, 1 small washer	45 mm	8.3 g	373.5 g-mm
7	1 bolt, 1 big washer, 2 small washers	45 mm	9.1 g	409.5 g-mm
8	1 bolt, 1 big washer, 3 small washers	45 mm	9.9 g	445.5 g-mm
9	1 bolt, 2 big washers	45 mm	10.5 g	472,5 g-mm
10	1 bolt, 2 big washers, 1 small washer	45 mm	11.3 g	508.5 g-mm
11	1 bolt, 2 big washers, 2 small washers	45 mm	12.1 g	544.5 g-mm
12	1 bolt, 3 big washers	45 mm	13.5 g	607.5 g-mm
13	1 bolt, 3 big washers, 1 small washer	45 mm	14.3 g	643.5 g-mm

Each of the software applications used by the developed balancing system has a section built-in that performs the distribution of the available unbalance correction weights in the available angular locations (Figure 21). User can try different weight distributions manually and observe the current weight distribution vector on a polar plot (red arrow). There is also a second vector displayed on the polar plot showing how much the current weight distribution differs from the calculated one (blue arrow). The software is however capable of performing the unbalance correction weights distribution automatically, which is a recommended approach as it is both faster and more precise. First the available configurations of the unbalance correction masses should be loaded from a spreadsheet file. Then user needs to specify the maximum number of angular locations in which the weights can be inserted. By clicking the start button the algorithm tries every possible distribution fulfilling the specified parameters and finds the one that is the closest match. There is a progress bar showing how much time it will take to finish the search. Additionally the best match found

so far is being shown. If at any time of the search the user decides the best distribution found until this moment is good enough, the search can be stopped.

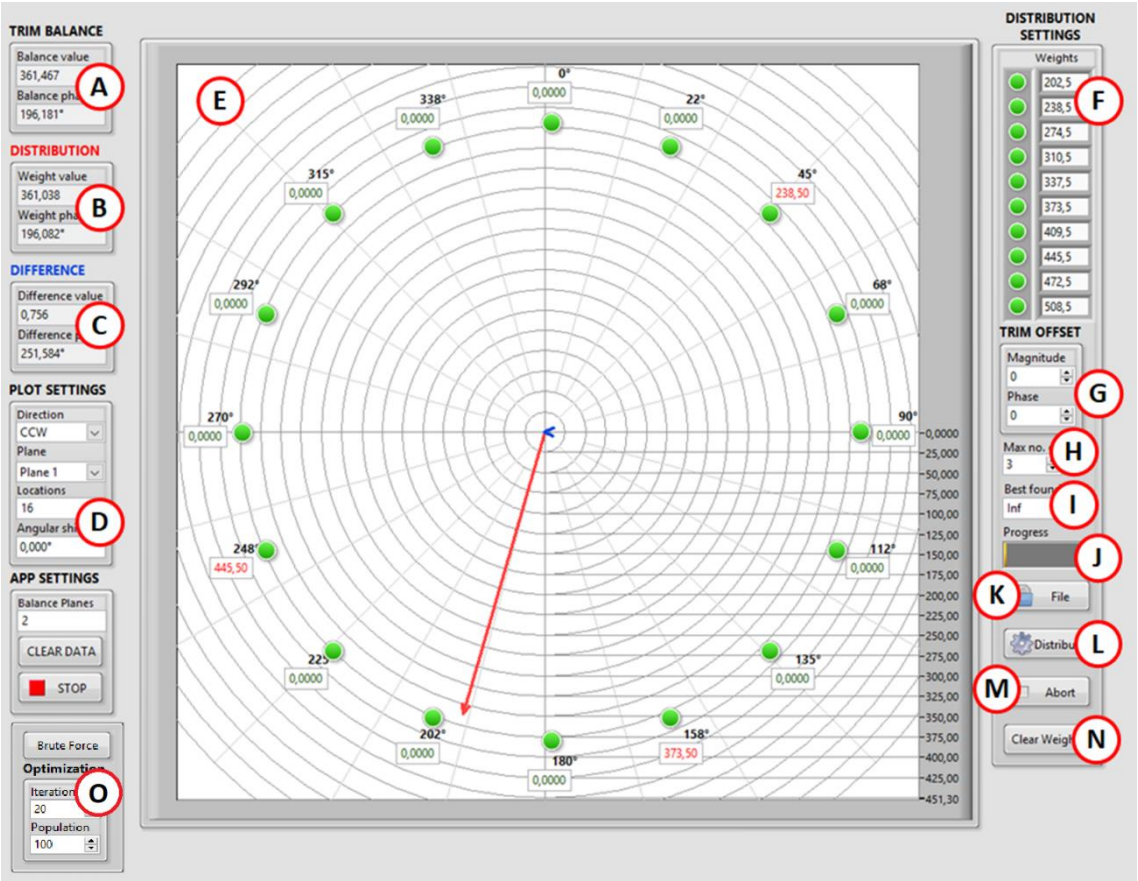

Figure 21 – unbalance correction weight distribution software

The weight distribution section of the software (Figure 21) contains the following items:

A) trim balance cluster – contains the calculated magnitude and phase of the unbalance correction weight,

B) distribution cluster – contains the magnitude and phase of the balance weights currently distributed on the polar plot (red arrow on the polar plot is a graphical representation of the data in this cluster),

C) difference cluster – contains the magnitude and phase of difference between current balance weight distribution and the calculated one (blue arrow on the polar plot is a graphical representation of the data in this cluster),

D) plot settings – sets the direction of rotation (CCW or CW), currently analyzed balance plane (available only for multi-plane method), number of evenly distributed angular locations around the polar plot and the angular shift of the first angular location

on the polar plot (in case the notch detected by the tachometer for angle reference purpose is not aligned with any of the angular locations for inserting balance weights),

E) polar plot – displays the data in a graphical form, let's the user manually input the magnitude of the balance weight in the desired angular locations and allows the user to disable (by clicking on the green LEDs) some of the angular locations for the automatic distribution of the unbalance correction weights,
F) weights list – displays the list of balance weights loaded from the spreadsheet file and allows the user to disable (by clicking on the the green LEDs) weight configurations that are not possible to use for automatic distribution,
G) trim offset cluster – sets the magnitude and phase of the combined balance weights that are already installed in the rotor,
H) maximum number of distribution locations control – sets the maximum number of angular locations that are allowed for automatic distribution of balance weight,
I) best match indicator – displays the best match found by the automatic distribution algorithm,
J) progress bar – displays the progress of the automatic distribution process,
K) load balance weight configurations button – opens a dialog window allowing to load the spreadsheet file containing the configurations of available unbalance correction weights,
L) start automatic distribution button – starts the execution of the automatic balance weight distribution algorithm,
M) abort automatic distribution button – stops the execution of the automatic balance weight distribution algorithm (the best match found till the moment the button was pressed will be recorded),
N) clear weights button – sets all the values of the balance weights on the polar plot to zero,
O) distribution algorithm settings – the button toggles the distribution algorithm between brute force and global optimization (the number of iterations and population size can only be set for the global optimization approach to weight distribution).

Trying every possible combination of balance weights in every possible angular location is called a brute force approach and obiously is not the best solution to the problem [68]. To calculate the number of all the combinations that should be tested while using the brute force solution, the equation (1) for variations with repetitions (elements can be used multiple times, order of elements does matter) can be used [69].

(1) $\bar{V}_n^k = n^k$

where:

n – number of unique available unbalance correction weights

k – number of available angular locations

Let us consider the number of solutions to try when dealing with the test stand used for researching the performance of the developed balancing system. Table 1 lists all available configurations of the unbalance correction weights – there are thirteen of them, however we can also decide to not insert any weights (balance weight equal to zero) in particular angular location which increases the number of unique available unbalance correction weights to fourteen (n=14). There are sixteen angular locations available at each steel disc for balancing purpose (k=16). Applying the equation (1) to these number gives us approximately 2.2×10^{18} solutions to test. This is a problem that even the fastest supercomputers available would have a hard time solving. Things start to look much better if we reduce the number of angular locations that could be tried at once (for example we tell the algorithm that out of the sixteen angular locations available it can use maximally three at the time, whether it is location no. 1, 2 and 3 or 14, 15 and 16). To find the number of solutions to try in this new scenario we need to split the problem [69]:

- first we need to calculate the number $\bar{C}_n^m$ of available combinations of balance weights (combinations with repetitions – there are n total available configurations of balance weights, we need to use them at m different angular locations, each configuration of balance weights can be used more than once) – equation (2),
- second we need to calculate the number V_k^m of available combinations of angular locations (variations without repetitions – there are k total angular locations, only m of them can be used at once, each angular location cannot be used more than once) – equation (3),
- third we need to calculate the number $C_{n,m,k}$ of total solutions to try (multiply the number of balance weight combinations $\bar{C}_n^m$ by the number of combinations of angular locations V_k^m they can be inserted in) – equation (4).

(2) $\bar{C}_n^m = \frac{(m+n-1)!}{m!(n-1)!}$

(3) $V_k^m = \frac{k!}{(k-m)!}$

(4) $C_{n,m,k} = \bar{C}_n^m \cdot V_k^m$

where:

n – number of total available configurations of unbalance correction weights

k – number of all angular locations

m – maximum number of angular locations that could be used at once

Table 2 shows how the number of solutions to try changes due to the maximum number of permitted angular locations (total number of unbalance weight configurations n=14, total number of angular locations k=16, maximum number of permitted angular locations m=1÷5). When m≤3 the best match is found in a matter of seconds, when m=4 it takes around a minute and when m=5 it takes around 30 minutes (computer with Intel i7 2.9GHz processor and 8GB of RAM).

Table 2 – total number of solutions to try and resulting balance weight change due to the maximum number of angular locations available at once

Max	Combinations	Balance weight distribution					
		Desired		Best found		Error	
		Mag.	Phase	Mag.	Phase	Mag.	Phase
1	224	361.5	196.1	373.5	202.5	42.3	92.9
2	25 200	361.5	196.1	358.1	195.5	5.6	248.1
3	1 881 600	361.5	196.1	361.0	196.1	0.8	251.6
4	103 958 400	361.5	196.1	361.8	196.1	0.4	342.7
5	4 491 002 880	361.5	196.1	361.5	196.2	0.1	5.9

Table 2 also shows how the best match found changes due to the maximum number of permitted angular locations (the error column displays the difference between the resulting balance weight distribution and the desired one). Significant changes can only be observed until m=3 and further increase in the number of permitted angular locations has a little impact on the distribution error. In the numerous tests conducted while reasearching the performance of the developed balancing system it has been established that m=3 is a sweet spot

when it comes to both the precision of balance weight distribution and the computational time required to find the best match [44].

2.8 Weight distribution optimization

The balance weight distribution algorithm described in the previous chapter uses the brute force approach to the problem, which means that every possible solution is tried before the final result can be obtained. While the brute force algorithm guarantees that the global minimum of the function will always be found, the computational time required to arrive at the solution is often not acceptable. To reduce the computations required in order to find the global minimum of the analyzed function we can use optimization tools. Currently there is a broad range of mathematical optimization techniques dedicated to solving problems that are limited in size, for example Simplex algorithm, integer programming and gradient methods, to only name a few [70]. However, these tools are not best suited to the weight distribution problem being analyzed because as both the number of possible weights combinations and the number of angular locations available for weights installation increase the required computational time increases exponentially.

All of the aforementioned optimization techniques are deterministic in their nature, meaning that their focus is to find the global solution to the problem [71]. Given the machining imperfections leading to inaccuracies in the angular locations intended for balance weights installation as well as the deviations in weights of the bolts and washers used for balancing purpose, there will always be some error in the balance weight distribution. Because this error can get quite significant, finding the global solution of the weight distribution problem is not necessary and "a good enough" result is sufficient. This is a perfect situation to use one of the heuristic optimization methods. The word heuristic itself means a technique that is not guaranteed to give the best possible solution, but rather a result that is satisfactory given the requirements. When using a heuristic optimization tool there is no guarantee that the method will converge to an optimal solution, however a good quality result to complicated problems can be found in a satisfying amount of time [72]. All heuristic methods use a trial and error approach to tackle a complex problem that cannot be otherwise solved in a reasonable amount

of time. The general idea of this kind of algorithm is to have an optimization tool that is both practical and efficient, while capable of producing results of sufficient quality.

Each heuristic optimization method can be characterized by two parameters, intensification and diversification, that are competing each other. On the one hand algorithms with high intensification are trying to focus the search for a best solution to a local area in which a good result has already been found. This means that if global minimum is in this region it will be found quicker, however it may also cause the algorithm to get stuck on a limited area of the data plane while the global solution is located somewhere else. On the other hand algorithms with high diversification are more focused on the exploration of the entire search space, which avoids the situation when the method is trapped in a local region, however it also means that it converges on the solution much slower [72]. The right balance between intensification and diversification is a crucial aspect to the implementation of a heuristic method and while one combination of these two parameters will work perfectly for a specific problem it may behave poorly when used for a different problem.

There are many different heuristic optimization methods available today and some of the most popular among them are [73]:

- genetic algorithm (GA) – this algorithm is based upon genetic processes of biological organisms and the concept that over many generations, populations that evolve naturally will do so according to the rule that only the fittest will survive [74]; the method starts by modeling of an initial population and initialization of parameters, then the algorithm employs operators like mutation and crossover on best suited individuals in the last generation to produce the new generation,
- particle swarm optimization (PSO) – this algorithm is based upon observations of a behavior of bird flocks [75]; the method starts by assigning an initial position and velocity to each element (particle); when a given element finds a new best solution other particles move in its direction by applying a change to their velocity vector,
- differential evolution (DE) – this algorithm starts with a set of uniformly random candidates for solution to the problem, then in every next iteration it mutates

the base vectors (representing secondary parents) with scaled differences of the distinct individuals from the current population [76]; DE requires only three parameters (the scale factor, the crossover probability and the population size) to be varied in order to tune the method to the problem being tackled, which makes it a great tool in a practical point of view; among other heuristic optimization techniques, DE stands out as a very simple algorithm that nevertheless is capable of producing great results,

- group search optimization (GSO) – this algorithm is inspired by behavior of animal living in groups, especially their searching techniques [77]; the method is based on the assumption that the members of the population search either for joining or finding opportunities; by extension of this concept searching mechanisms such as animal scanning techniques can be implemented to solve continuous optimization problems,
- cuckoo search (CS) – this algorithm adapts the breeding and egg laying of the cuckoo bird; the cuckoos lay eggs in other birds nests and employ a number of strategies to increase the probability of their eggs hatching and their offspring receiving food from the host bird [78]; in CS method every egg in the nest can be thought of as a solution to the problem; a cuckoo egg can be introduced to the nest (new, potentially better solution) which replaces one of the eggs that are already in the nest (old, worse solutions); there are three rules that govern the CS algorithm; first, only one egg can be introduced by each cuckoo in a nest that is chosen randomly; second, the next generations consists only of the best nests with eggs of high quality (good solutions); third, the number of nests is fixed and the cuckoo egg can be discovered by the host and thrown out with a set probability (0÷100%).

The list above describes only the most popular of the heuristic methods, however there are many more, such as grey wolf optimization (GWO), harmony search (HS) algorithm, bee colony optimization (BCO), invasive weed optimization (IWO), teaching learning based optimization (TLBO), firefly algorithm (FA), krill herd (KH) algorithm, line-up competition algorithm (LCA), exchange market algorithm (EMA) and civilized swarm optimization (CSO), to only name a few [73]. Out of all the aforementioned heuristic optimization techniques, the differential evolution (DE) has been chosen due to its simplicity and the fact that it is a good

fit for problems with multiple variables. Given that there are **k** total angular locations at which trim weights can be installed and only **m** of them can be used at once, the function we are trying to optimize has **2m** variables and can be represented as $\mathbf{f(x_1, x_2, \ldots, x_m, y_1, y_2, \ldots, y_m)}$. Each of the **x** variables represents an index of the angular location (integers in the range **1÷k**, $\mathbf{x_1 \neq x_2 \neq \ldots \neq x_m}$). There are also **n** available configurations of trim weights and each of the **y** variables represents an index of the trim weight configuration (integers in the range **1÷n**). The trim weight specified by index $\mathbf{y_1}$ shall be installed in angular location specified by index $\mathbf{x_1}$, then the trim weight specified by index $\mathbf{y_2}$ shall be installed in angular location specified by index $\mathbf{x_2}$, and so on. Finally the vector of combined trim balance weights is calculated. The goal of all the balancing system that is discussed in this dissertation is to calculate the vector of the rotor unbalance (specified by its magnitude and phase) and then shift it by 180° to obtain the vector of the unbalance correction weight. We want to make the vector of combined trim balance weights to be as close to the vector of the unbalance correction weight as possible. Therefore the aim of the optimization algorithm is to minimize the magnitude of the vector sum that is the result of adding the vector of combined trim balance weights and the vector of rotor unbalance.

2.9 **Modified differential evolution (MDE) algorithm**

A built-in LabView global optimization software tool [79], which implements the differential evolution (DE) technique, was used as the basis. Figure 22 shows the algorithm of this global optimization software tool. A modified differential evolution (MDE) technique, that is specifically tailored to the problem being solved, was proposed by the author. The goal of the search is to find the angular locations that provide the best distribution of the balance weight. The standard DE algorithm forces the results to fit into the specified range of values, in this case to the 0÷360° range. This is not the best approach to the problem being solved, because when the algorithm moves the results below 0° or above 360° they shouldn't be coerced to the closest value within the range, but instead the angle should be wrapped around. The MDE algorithm has been introduced that performs this additional action (when the angle of the results goes below 0° it is wrapped around to below 360° and when it goes above 360° it is wrapped around to above 0°). Furthermore, the MDE deals with the situation when the new candidates for the best solution include angular locations that are not unique (it's not possible to place

a trim weight in a single angular location more than once). The new candidates for the angular locations form an array (new candidates array). The array containing all the available angular locations (available locations array) is also used by the algorithm. The MDE starts the candidates evaluation step by checking if all elements in the new candidates array are unique – if true, then the candidates evaluation step is finished, if false then further actions are required. First MDE removes all the elements from the available locations array that are also present in the new candidates array – the available locations array can now be called remaining locations array. Then the MDE moves the first element from the new candidates array to a fresh array (unique candidates array). In the next step, the MDE moves the next element from the new candidates array to the unique candidates array – if the candidate that has been moved is already present in the unique candidates array, then the closest angular location is chosen from the remaining locations array (if there are 2 angular locations equally close to the repeated candidate, then the one in the clockwise direction is chosen) and written to the unique candidates array instead (it is also deleted from the remaining locations array). This step is repeated until all the elements from the new candidates array are moved to the unique candidates array.

In the process of the DE algorithm tuning in attempt to tackle the problem of finding the best weight distribution, the scale factor was finally set to 10 and the crossover probability to 50%. There are two parameters left that can be set by the user in the *Unbalance Correction Weight Distribution Software* (Figure 21), the population size and the number of algorithm iterations. Table 3 shows the results of balance weights distribution conducted using brute force algorithm and the MDE method for **n=10** and **k=16**. The aim of the search was to find the weights distribution closest to 260.955gmm at 318.215°. When the brute force algorithm was used only one test was conducted for each value of **m**. The table shows the results (the error between the required distribution and the one found by the algorithm) and the execution time of the search. The tests were not conducted for **m>5** because of exponentially increasing execution time. When using the differential evolution method the value of **m**, the iterations number and population size were varied. For each different set of these parameters 30 test were conducted to calculate the mean result and mean execution time. The table also shows the best result found out of all 30.

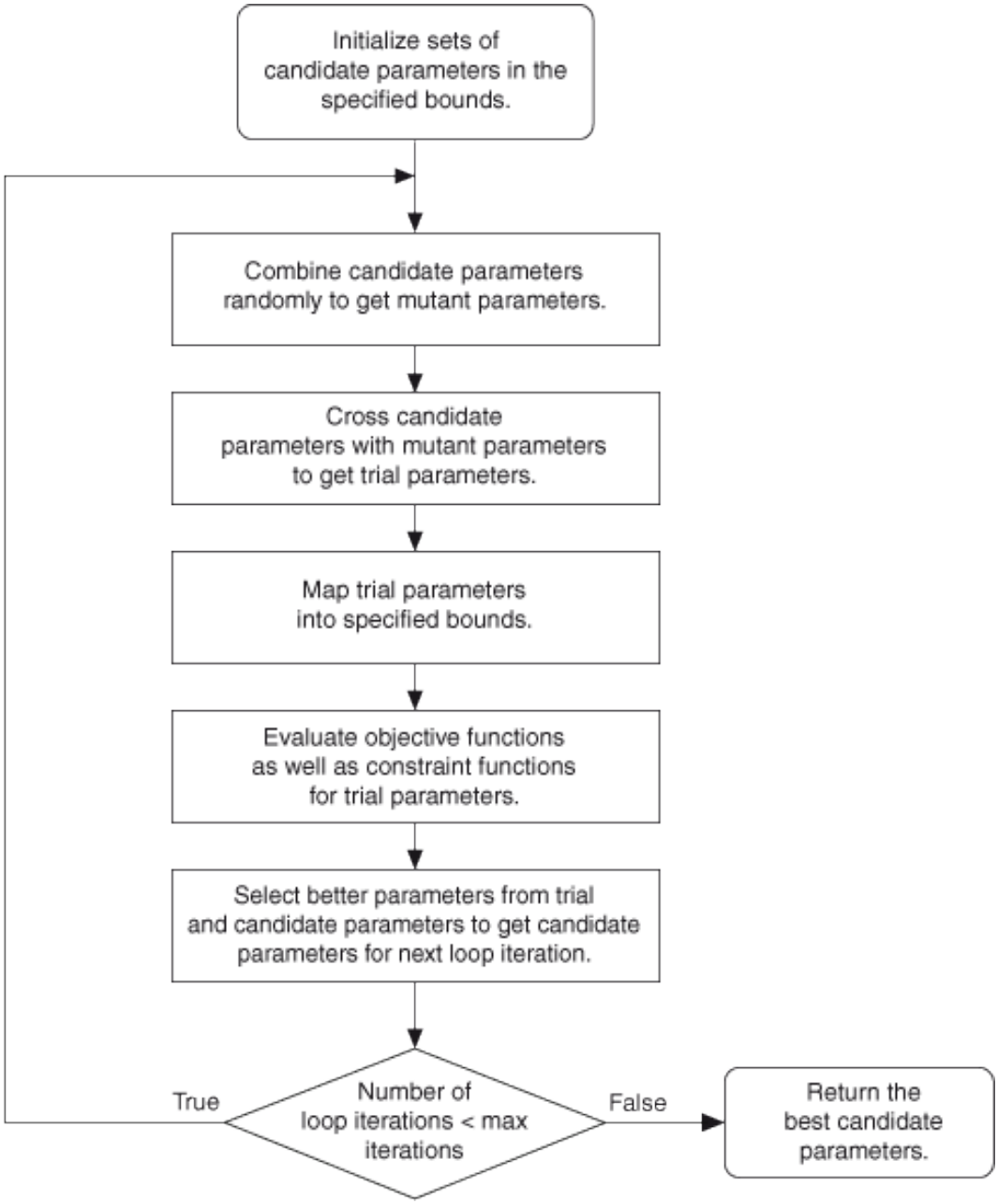

Figure 22 – the global optimization algorithm implementing the differential evolution [79]

The results of the brute force algorithm can serve as a benchmark for the differential evolution method because when using the brute force approach the global minimum is guaranteed to be found. When **m=1** and **m=2** the optimization algorithm always finds the optimal solution. When **m=3** the global minimum is found very often but not always. Only when using the higher values of iterations number and population size, the algorithm finds the optimal solution every time. However, the mean execution time required was at least 9s when the brute force algorithm finds the same solution in just 1s. When **m=4** for all tested

configurations of the optimization parameters the global minimum is found at least once but there is no configuration that had 100% success rate. When **m=5** only one of the MDE configurations tested were capable of providing the optimal solution at least once. No reference is available for **m>5**, however by observing the mean result and mean execution time it can be seen that increasing **m** has little impact on the obtained results quality and the time it takes to calculate the solution. Both the number of iterations and population size influence the differential evolution method in the same manner – the higher the value of the parameter, the better the results at the cost of increased execution time. Even though the brute force algorithm guarantees to find the optimal solution, this approach can be entirely neglected as the results are only marginally better than those provided by the differential evolution method and the execution time of the brute force algorithm scales exponentially with increasing value of **m**. The same goes for optimization parameters – setting the number of iteration and population size to high values that cause the execution time to rise over couple of seconds have very little impact on the final result.

Both standard DE and MDE algorithms have been extensively tested to compare the differences in their results. Table 4 provides details of one of these tests. For each combination of both standard DE and MDE algorithms parameters (number of iterations and population size) 30 simulations have been performed. The results presented in the table show the mean weight distribution error, separate for standard DE and MDE algorithms. The MDE algorithm showed a better performance for each combination of the algorithm parameters. The average gain of the MDE over standard DE algorithm was 9.7% in the presented test (the results for m=1÷3 has been neglected because both algorithms were capable of finding the optimum solution each time, therefore there was no gain to be made).

Table 3 – comparison of weight distribution error while using brute force and modified differential evolution (MDE) algorithms. For each combination of MDE algorithm parameters (number of iterations and population size) 30 simulations have been performed – the presented results show the mean weight distribution error, best result of all simulations and the average simulation time. Bold text indicates best results for given combination. There were 16 total available angular locations (k=16), each column of the table represent different number of those locations that can be used at once (m).

Required weight distribution	260.955 @ 318.215°										**Diff. evol. algorithm iterations**	**Diff. evol. algorithm population**
Max locations to use **m**	1	2	3	4	5	6	7	8	9	10		
All possible distributions	160	13200	739200	$3.1 \cdot 10^{7}$	$1.1 \cdot 10^{9}$	$2.9 \cdot 10^{10}$	$6.6 \cdot 10^{11}$	$1.3 \cdot 10^{13}$	$2.0 \cdot 10^{14}$	$2.7 \cdot 10^{15}$		
Brute force - result	20,221	5.535	0.948	0.184	**0,015**	untested	untested	untested	untested	untested		
Brute force – execut. time	19ms	27ms	1s	45s	28min	~hours	~days	~weeks	~months	~years		
MDE - mean result	20.221	5.535	1.481	**1.286**	1.827	2.174	2.536	2.892	3.350	3.485	5	50
MDE - best result	20.221	5.535	0.948	0.184	0.167	0.608	0.217	0.549	**0.112**	0.431		
MDE – execution time	578ms	599ms	637ms	678ms	720ms	761ms	794ms	838ms	886ms	901ms		
MDE - mean result	20.221	5.535	0.987	**0.557**	0.762	0.888	0.950	1.444	1.647	1.766	5	200
MDE - best result	20.221	5.535	0.948	0.184	**0.018**	0.047	0.186	0.305	0.374	0.397		
MDE – execution time	2s	2s	2s	2s	3s	3s	3s	3s	3s	3s		
MDE - mean result	20.221	5.535	0.948	**0.320**	0.349	0.412	0.579	0.619	0.639	0.711	5	1000
MDE - best result	20.221	5.535	0.948	0.184	0.186	**0.047**	0.140	0.165	0.216	0.134		
MDE – execution time	9s	10s	11s	11s	12s	13s	14s	15s	15s	16s		
MDE - mean result	20.221	5.535	1.061	**0.672**	0.684	0.944	1.203	1.306	1.496	1.551	20	50
MDE - best result	20.221	5.535	0.948	0.184	0.167	**0.103**	0.280	0.235	0.215	0.188		
MDE – execution time	2s	2s	2s	2s	3s	3s	3s	3s	3s	3s		
MDE - mean result	20.221	5.535	0.948	0.420	**0.405**	0.508	0.576	0.668	0.701	0.727	20	200
MDE - best result	20.221	5.535	0.948	0.184	0.138	0.167	0.087	0.127	0.116	**0.078**		
MDE – execution time	8s	8s	9s	9s	10s	11s	12s	12s	13s	13s		
MDE - mean result	20.221	5.535	0.948	**0.388**	0.401	0.427	0.501	0.523	0.611	0.695	100	50
MDE - best result	20.221	5.535	0.948	0.184	0.085	**0.047**	0.138	0.056	0.183	0.199		
MDE – execution time	10s	11s	11s	12s	13s	14s	15s	15s	16s	17s		
MDE - mean result	20.221	5.535	0.948	0.202	**0.179**	0.214	0.248	0.299	0.313	0.320	100	200
MDE - best result	20.221	5.535	0.948	0.184	0.015	0.014	**0.011**	0.078	0.056	0.041		
MDE – execution time	38s	41s	44s	47s	50s	54s	57s	61s	63s	67s		

Table 4 - comparison of weight distribution error while using standard DE and modified differential evolution (MDE) algorithms. For each combination of both standard DE and MDE algorithms parameters (number of iterations and population size) 30 simulations have been performed – the presented results show the mean weight distribution error (separate for standard DE and MDE algorithms) and MDE algorithm gain over the standard DE algorithm. There were 16 total available angular locations (k=16), each column of the table represent different number of those locations that can be used at once (m)

Required weight distribution	260.955 @ 318.215°										**Diff. evol. algorithm iterations**	**Diff. evol. algorithm population**
Max locations to use **m**	1	2	3	4	5	6	7	8	9	10		
All possible distributions	160	13200	739200	$3.1 \cdot 10^{7}$	$1.1 \cdot 10^{9}$	$2.9 \cdot 10^{10}$	$6.6 \cdot 10^{11}$	$1.3 \cdot 10^{13}$	$2.0 \cdot 10^{14}$	$2.7 \cdot 10^{15}$		
Brute force - result	20.221	5.535	0.948	0.184	0,015	untested	untested	untested	untested	untested		
Standard DE - mean result	20.221	5.535	1.674	1.667	1.987	2.489	2.789	3.170	3.562	3.573	5	50
MDE - mean result	20.221	5.535	1.481	1.286	1.827	2.174	2.536	2.892	3.350	3.485		
MDE - gain	0.0%	0.0%	11.5%	22.9%	8.1%	12.7%	9.1%	8.8%	6.0%	2.5%		
Standard DE - mean result	20.221	5.535	1.009	0.654	0.776	0.897	1.009	1.533	1.710	1.874	5	200
MDE - mean result	20.221	5.535	0.987	0.557	0.762	0.888	0.950	1.444	1.647	1.766		
MDE - gain	0.0%	0.0%	2.2%	14.8%	1.8%	1.0%	5.8%	5.8%	3.7%	5.8%		
Standard DE - mean result	20.221	5.535	0.948	0.337	0.365	0.444	0.644	0.726	0.652	0.739	5	1000
MDE - mean result	20.221	5.535	0.948	0.320	0.349	0.412	0.579	0.619	0.639	0.711		
MDE - gain	0.0%	0.0%	0.0%	5.0%	4.4%	7.2%	10.1%	14.7%	2.0%	3.8%		
Standard DE - mean result	20.221	5.535	1.171	0.725	1.070	1.192	1.322	1.366	1.845	1.576	20	50
MDE - mean result	20.221	5.535	1.061	0.672	0.684	0.944	1.203	1.306	1.496	1.551		
MDE - gain	0.0%	0.0%	9.4%	7.3%	36.1%	20.8%	9.0%	4.4%	18.9%	1.6%		
Standard DE - mean result	20.221	5.535	0.967	0.460	0.485	0.566	0.629	0.732	0.717	0.905	20	200
MDE - mean result	20.221	5.535	0.948	0.420	0.405	0.508	0.576	0.668	0.701	0.727		
MDE - gain	0.0%	0.0%	2.0%	8.7%	16.5%	10.2%	8.4%	8.7%	2.2%	19.7%		
Standard DE - mean result	20.221	5.535	0.967	0.413	0.434	0.591	0.597	0.536	0.668	0.729	100	50
MDE - mean result	20.221	5.535	0.948	0.388	0.401	0.427	0.501	0.523	0.611	0.695		
MDE - gain	0.0%	0.0%	2.0%	6.1%	7.6%	27.7%	16.1%	2.4%	8.5%	4.7%		
Standard DE - mean result	20.221	5.535	0.948	0.230	0.189	0.234	0.265	0.319	0.362	0.419	100	200
MDE - mean result	20.221	5.535	0.948	0.202	0.179	0.214	0.248	0.299	0.313	0.320		
MDE - gain	0.0%	0.0%	0.0%	12.2%	5.3%	8.5%	6.4%	6.3%	13.5%	23.6%		

2.10 **Order analysis application**

The developed balancing system requires the analysis of the proximity signals acquired during the test runs. The goal of this analysis is to find the first order magnitude and phase of the analog proximity probe (or probes, depending on the balancing method used by the system). The only exception is when the balancing system uses the four runs method when the phase information is not required. To automate this step a special purpose software tool has been created – the *Order Analysis Application*. Figure 23 shows the front panel of this application. This software tool enables the user to perform the necessary order analysis by simply loading the TDMS file containing the data acquired during the test run and providing the necessary parameters (tacho signal parameters, order of interest, order bandwidth, speed range, analysis resolution and direction of rotor movement). Then by clicking the *Bode Analysis* button, the analysis is performed and the results are viewed on Bode and polar plots. The *Order Analysis Application* (Figure 23) consists of the following items:

A) Bode analysis channels – chooses the channel (from within the loaded TDMS file) on which the Bode analysis shall be performed,
B) tacho parameters – chooses the channel containing the tacho signal and sets the parameters of the tachometer signal,
C) control buttons – loads the TDMS file, views the chosen channel on the time chart, loads the tacho signal, checks whether the provided tacho signal and parameters are correct, performs the Bode analysis,
D) Bode analysis controls – sets the parameters of the Bode analysis,
E) report cluster – chooses multiple channels to perform Bode analysis,
F) time chart – displays the chosen channel as a function of time,
G) Bode magnitude plot – displays the magnitude of the order analysis performed on the chosen channel using the provided parameters; the X axis can be either speed, time or frequency, depending on the user choice,
H) Bode phase plot – displays the phase of the order analysis performed on the chosen channel using the provided parameters; the X axis can be either speed, time or frequency, depending on the user choice,
I) polar plot – displays the polar plot of the order analysis performed on the chosen channel using the provided parameters.

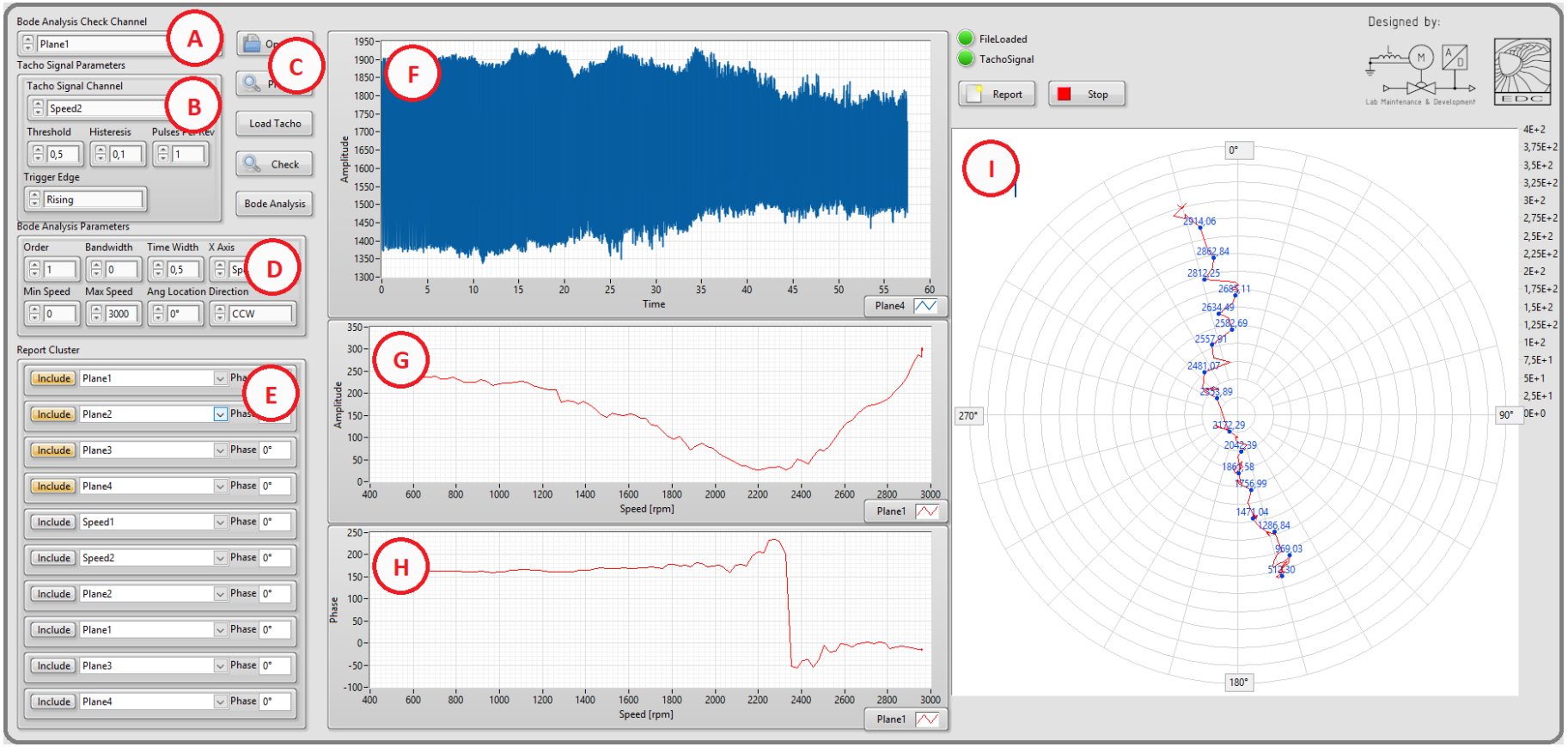

Figure 23 – the front panel of the Order Analysis Application

The *Tacho Signal Parameters* and *Bode Analysis Parameters* clusters consist of the following controls:

A) tacho signal channel control – sets the channel containing the tachometer signal,
B) threshold control – sets the value of the signal edge detection (value of transition between low and high states); the balancing test stand uses PNP proximity probe which has only 2 states (low state equals 0 and high state equals 1), therefore the threshold should be set to 0.5,
C) hysteresis control – sets the value of transition hysteresis (when digital probe is used to acquire tachometer signal it could be set to zero, however when analog probe is used the hysteresis should be set to amplitude above the signal's noise level),
D) pulses per revolution control – sets the number of pulses in the tachometer signal acquired during each rotor revolution; there is a single notch in the shaft used in the balancing test stand, therefore the pulses per revolution should be set to 1,
E) trigger edge control – toggles the zero degree angle reference point between the rising and falling edge of the tachometer signal; it should be taken into account that there is an angular difference between falling and rising edge due to the size of the notch,
F) order control – sets the number of the order that should be analyzed; the unbalance manifests itself as the first order vibration, therefore this control should be set to 1,
G) bandwidth control – sets the range of the order analysis (increasing this value will cause a broader range of orders to be analyzed); the unbalance is associated with exactly the first order therefore the bandwidth should be set to 0,
H) time width control – sets the time range of order analysis required to calculate a single point on the Bode and polar plots; if the rotational speed was held constant during data acquisition then this value can be set to 1s or more, however it should be decreased when data acquired during rotor run-up or coast down is analyzed,
I) X axis variable control – toggles the X axis variable between time and speed; it is recommended to use speed on the X axis when balancing data is being analyzed,
J) minimal speed control – sets the lower end value of the rotational speed range for which the order analysis shall be performed,
K) maximal speed control – sets the higher end value of the rotational speed range for which the order analysis shall be performed,
L) angular location control – sets the angular shift between physical circumferential location of the tachometer probe and vibration (analog proximity) probe,

M) direction control – sets the direction of rotation (must be consistent with the recorded data).

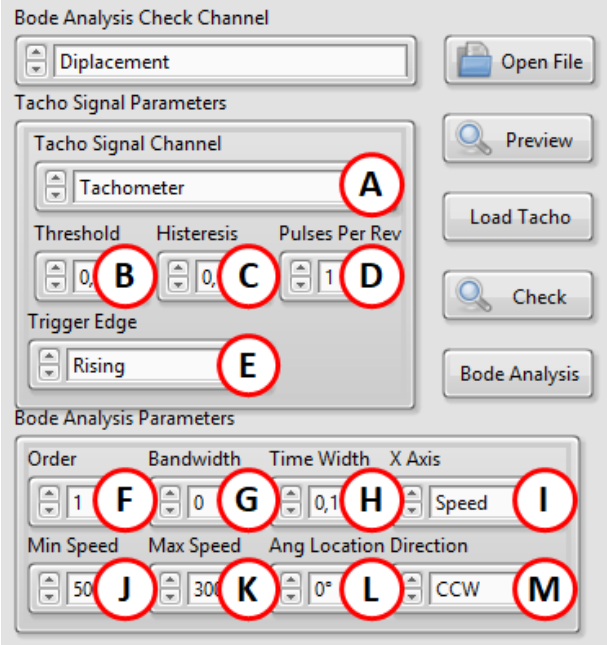

Figure 24 – order analysis parameters

2.11 **Complete balancing procedure**

To provide the optimum balancing results the developed balancing system is using a step by step procedure which helps the system's user to prepare the rotating machine for balancing, then to perform the balancing itself and finally to distribute the trim balance weight in an optimum configuration. The preparation stage of the procedure consists of the analog proximity probes calibration, signals noise check, brackets impact test and the probes installation and adjustment. The balancing should be performed using any of the methods described in this dissertation – it is highly recommended to install the calibration weights at an angle that was estimated to reduce the unbalance. Finally, the trim weights distribution should be performed using the modified differential evolution (MDE) technique. Figure 25 shows all these steps in the form of a flowchart. By following the described complete balancing procedure, an optimum balancing results are going to be obtained.

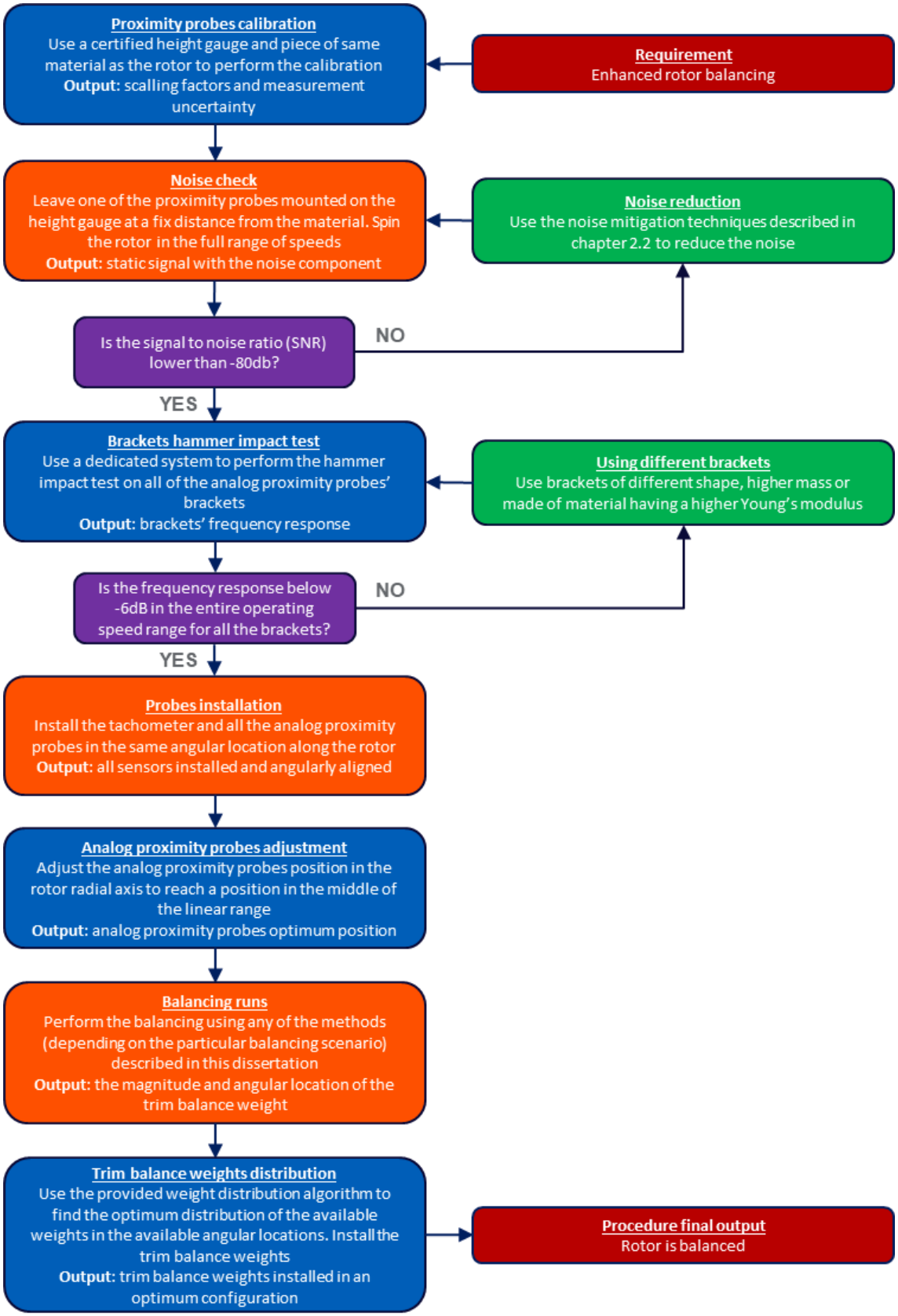

Figure 25 – complete balancing procedure flowchart

3. Single plane balancing methods

3.1 Vector method

Figure 2 shows the test stand configuratoion when the developed balancing system uses the vector method. All kinds of steel discs configurations were used to simulate different rotors, however only when all of the discs were installed (total mass of the rotor, without the shaft, equal to 8kg) the critical speed of the system could be encountered within the operating speed range of the motor (0÷3000rpm, critical speed at approximately 2850rpm). The vector method needs only two probes to work – the tachometer and one analog proximity probe. To conduct the balancing using the vector method it is required to perform the following steps [80]:

- step no. 1 – perform the base run of the machine; accelerate the rotor up to its maximum operating speed while acquiring the data from proximity probes (tachometer signal and rotor displacement),
- step no. 2 – use the *Order Analysis Application* to analyze the Bode and polar plots; choose the rotational speed at which the balancing will be performed and record the amplitude and phase of the vibration caused by unbalance at this speed,
- step no. 3 – install the calibration weight,
- step no. 4 – perform the calibration run; again accelerate the rotor up to its maximum operating speed while acquiring the data,
- step no. 5 – use the *Order Analysis Application* to analyze the calibration run data; record the amplitude and phase of the vibration caused by unbalance at previously chosen speed,
- step no. 6 – calculate the trim balance weight by setting the recorded magnitudes and phases in the corresponding controls in the *Single Plane Balancing Application*,
- step no. 7 – perform the confirmation run; again accelerate the rotor up to its maximum operating speed while acquiring the data,
- step no. 8 – use the *Order Analysis Application* to analyze the confirmation run data; if the vibration caused by unbalance is below the required limit then the balancing can be finished; to further decrease the vibration next iteration of the method can be performed.

Step no. 1 consists of performing the base run. The goal of this step is to acquire vibration data of the system's initial unbalanced state. The rotor should be accelerated to its maximum operating speed. The data acquired during the run-up will be used to prepare Bode and polar plots. It is highly recommended to use low acceleration ramp during all the balancing runs and to carefully observe the first order vibration amplitude during the rotor run-up. If at any point the amplitude exceeds a predefined red limit, the abort button should be clicked to immediately disengaged the motor. In such case the system should be first balanced at lower rotational speed before proceeding to balancing at the speed of operation.

Step no. 2 consists of using the *Order Analysis Application* (see chapter 2.10) to analyze the base run data. The data acquired during the run is stored in TDMS file and can be loaded in the application. Once the file is successfully opened, the *Tacho Signal Parameters* cluster becomes active and user can set the required parameters (Figure 24). When all the tachometer parameters are set, the *Load Tacho* button should be pressed. If the signal and parameters are correct, the plot of rotational speed calculated from the tachometer signal will be displayed and the *Bode Analysis Parameters* cluster will become active. The parameters of the order analysis should be then set. Finally the *Bode Analysis* button should be pressed. The vibration data associated with the unbalance can be then analyzed. If the presence of critical speed can be observed on the Bode plot, then the balancing should be performed for this speed as the system is most sensitive at the resonance. If no critical speed is found then the balancing should be performed for the highest operational speed of the system. The amplitude and phase of the first order vibration at the chosen balancing speed should be recorded before proceeding to the next step.

Step no. 3 consists of the calibration balance weight installation in the rotor. The magnitude of the calibration weight should be chosen carefully – if too heavy trial weight is added it could lead to excessive rotor vibration, especially at the critical speed, and as a consequence to system destruction. At this point the weight unit should be chosen. The unbalance is specified as the product of mass and eccentricity (commonly used units include g-mm, lb-in or even a combination of metric and imperial units g-in [67]) and therefore it is recommended to use the same convention and same units to characterize the balance weights. However, virtually any unit capable of meaningfully specifying the magnitude of weight can be used as long

as it is used consistently throughout all the calculations. The author has chosen g-mm as the unit used in the system and in all the calculations. Analysis of the polar plot in step no. 2 can help in the estimation of the angular location at which adding the calibration weight should decrease the vibration amplitude. As discussed in chapter 2.4, when the unbalance is considered as a single heavy spot in the rotor then before the critical speed is reached the heavy spot will fly out while spinning. The phase of the first order vibration should therefore be a rough estimation of the unbalance angular location. However, when proximity probe is used to measure the vibration it is necessary to apply a 180° phase shift to the angular location read on the plot. This is due to the fact, that order analysis calculates the phase as the angular shift between the reference signal and the positive peak of the sine wave and rotor is considered to be at its maximum displacement position when it is closest to the proximity probe so when the signal acquired by the probe is at its minimum. To decrease the vibration caused by the unbalance it is necessary to add the trial weight opposite to the angular location of the unbalance, therefore it is necessary to apply another 180° phase shift. The total phase shift is a full 360° which means that the angular location of trial weight that should theoretically decrease the vibration caused by the unbalance can be observed on the Bode or polar plot as the phase of the first order vibration at any speed below the critical frequency [44]. From the balancing system point of view, it is not required that adding the trial weight should decrease the vibration, however it is dictated by the common sense.

Step no. 4 consists of performing the calibration run. The procedure is similar as with the base run discussed in step no. 1. The data acquired during the calibration run will provide the information concerning the first order vibration change due to the inserted trial weight.

Step no. 5 consists of using the *Order Analysis Application* to analyze the calibration run data. The newly acquired data stored in TDMS file shall be loaded. The tachometer and order analysis parameters that were set when base run data has been analyzed should be used once more without any changes. When order analysis is performed and the Bode and polar plots are displayed the amplitude and phase of the first order vibration at the previously chosen balancing speed should be recorded before proceeding to the next step. When balancing is performed at the critical speed and its value has changed when compared to the base run,

then the amplitude and phase of the first order vibration should be recorded at the new position of the critical speed.

Step no. 6 consists of using the *Single Plane Balancing Application* to calculate the magnitude and phase of the final balance weight. The application uses the following equations to calculate the trim balance [4]:

(5) $\vec{V}_{\Delta} = \vec{V}_{CAL} - \vec{V}_{INIT}$

(6) $\vec{S} = \frac{\vec{V}_{\Delta}}{\vec{W}_{CAL}}$

(7) $\vec{W}_B = -\frac{\vec{V}_{INIT}}{\vec{S}}$

where:

$\vec{V}_{\mathrm{INIT}}$ – magnitude and phase (vector) of the first order vibration acquired during the base run

$\vec{V}_{\mathrm{CAL}}$ – magnitude and phase (vector) of the first order vibration acquired during the calibration run

$\vec{V}_{\Delta}$ – magnitude and phase (vector) of the first order vibration difference between the calibration and base runs

$\vec{S}$ – magnitude and phase (vector) of the sensitivity

$\vec{W}_{CAL}$ – magnitude and phase (vector) of the chosen calibration weight

$\vec{W}_B$ – magnitude and phase (vector) of the final balance weight

Figure 38 shows this approach graphically. The $\vec{V}_{\Delta}$ is a vector of the initial system response change due to the addition of the calibration weight. Having this vector calculated, we can then proceed to derive the system's sensitivity vector $\vec{S}$ which can be used to estimate the change in the reponse of the system due to any balance weight. Finally the trim balance weight is estimated by applying the calculated sensitivity to the vector opposite to the initial system's response $\vec{V}_{\mathrm{INIT}}$. Using this approach we get the final balance weight $\vec{W}_B$ which should cause the system's response change such that it will cancel out the initial response [81].

The calculation is performed automatically by the software application within the developed balancing system. It contains all the controls and functionality that are necessary to perform the balancing using both the vector method and the four runs method, therefore it has been named the *Single Plane Balancing Application.* Figure 26 shows the front panel of this application when it is configured for balancing using the vector method. The final balance weight is calculated using the first order vibration amplitudes and phases recorded at the balancing speed during the base run and the calibration run in addition to the magnitude and phase of the calibration weight. The user needs to set these values in the corresponding fields of the *Calculation Data* cluster. The resulting final balance weight is displayed in the *Trim Balance* cluster (the result updates every time any value in the *Calculation Data* cluster is changed). There is also a compass plot in the application which displays the vectors representing the first order vibration recorded during base and calibration runs as well as the vectors representing the calibration and trim balance weights.

Step no. 7 of the method consists of removing the calibration weight from the rotor, installing the calculated trim balance and then performing the confirmation run. The data acquired during the confirmation run will provide the information concerning the first order vibration change due to the inserted final balance weight.

Step no. 8 consists of using the *Order Analysis Application* to analyze the confirmation run data. The confirmation run TDMS file should be loaded. The tachometer and order analysis parameters should remain unchanged. If the resulting first order vibration amplitude is below a predefined required level then the balancing is considered successful and can be finished. On the other hand, if the vibration amplitude is still too high, then the balancing can be performed again. When second iteration of the method is being conducted, the trim weight inserted in the rotor before the confirmation run should remain in the system. The data recorded during the confirmation run of the first iteration can be used as the base run data in the second iteration. When second iteration is performed both calibration and final balance weights should be added on top of the trim balance already installed in the rotor.

The *Single Plane Balancing Application*, while the balancing system is configured to use the vector method (Figure 26) consists of the following items:

A) vector method data – lets the user input the magnitude and phase of the order analysis performed during each of the balancing runs,
B) method switch – switches the application between the vector method and the four runs method,
C) vector plot – displays the order analysis data of all the balancing runs in a vector form,
D) vector plot legend – assigns colors to each vector on the plot,
E) weight plot settings – sets the rotation direction, number of possible weight locations and angle offset,
F) weights data – indicates the magnitude and phase of the calculated trim weight, the current weight distribution and difference between the two,
G) weights plot – displays all the information about the weight distribution but can be also used to manually input the balance weights and to observe changes in weight distribution,
H) possible weights – lists all the possible balance weights loaded from a file,
I) trim offset control – can be used to input the calculated trim balance from a previous balancing,
J) weight distribution settings – set the maximum number of allowed weight locations, load possible balance weights from a file, perform automatic balance weights distribution, abort the automatic distribution, clear all the data from weights plot, stop the application.

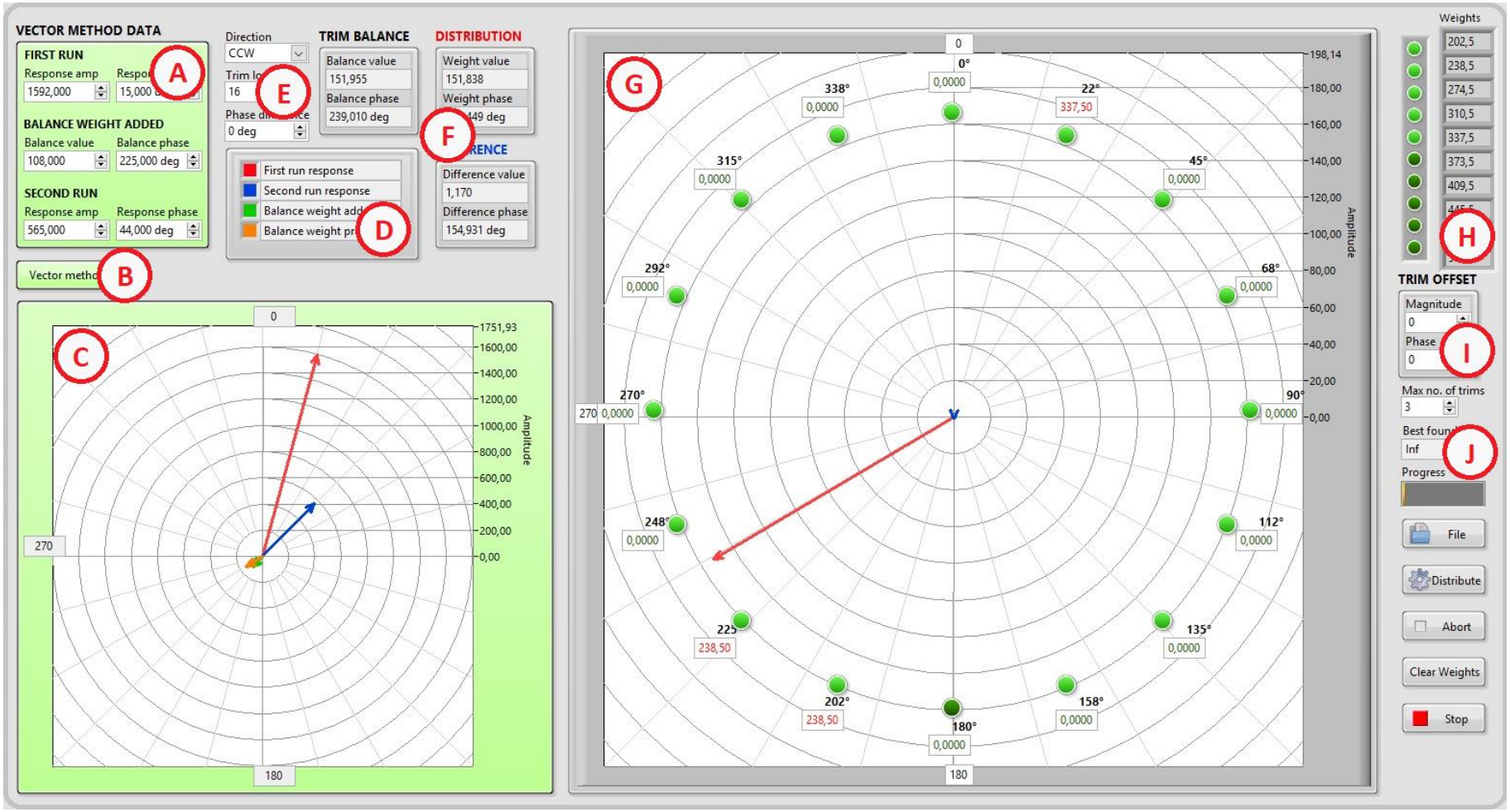

Figure 26 – the front panel of the Single Plane Balancing Application while the balancing system is configured to use the vector method

3.2 Four runs method

Another method dedicated to single plane balancing, called the four runs method, can be used by the developed balancing system when it is not possible to use the PNP proximity sensor (also reffered to as the tachometer sensor). The reason for the unavailability of the tachometer signal may differ depending on the rotating object that is being balanced. The most common reason is that it's simply not possible to access the rotor at any other location than the balancing plane itself making it impossible to find a suitable location for the tachometer sensor installation. The PNP proximity sensor also needs a single notch or a single tooth in the rotor to work properly and such a notch or tooth is not always available. In those cases only the analog proximity probe can be used and there's not enough data to perform the balancing using the vector method which needs the tachomter signal. Here is where the four runs method comes in. The strongest advantage of this method is that it needs only the analog proximity data (or any other type of signal representing the vibration) for its operation [82]. However, as will be shown, it is much less accurate than the vector method, therefore it shall only be used by the developed balancing system in situations when the balancing using the vector method cannot be performed. Figure 27 shows the test stand configuration when the developed balancing system uses the four runs method (the PNP proximity sensor is marked with a red cross, indicating that it's not used for the purpose of balancing).

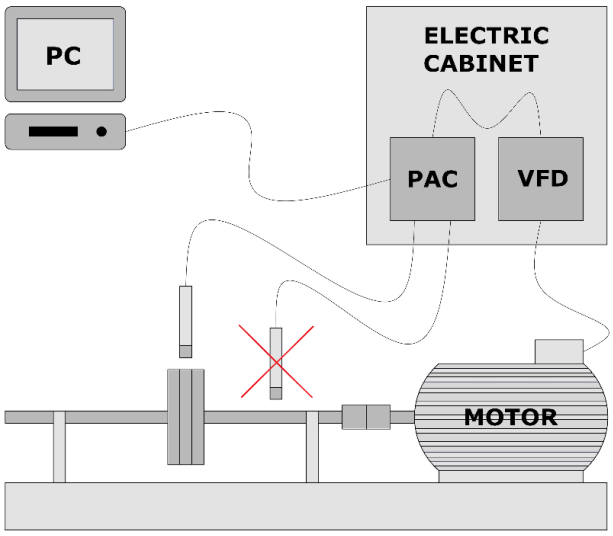

Figure 27 - test stand configuration when the balancing system uses the four runs method

The method, as suggested by its very name, consists of performing four balancing runs [20] at the rotor operation speed:

- first run – no weights installed; this is the run performed to establish the initial vibration of the rotating object,
- second run – calibration weight installed at arbitrary 0° angle; this is the run performed to establish the rotating object response to additional weight at 0° angle,
- third run – calibration weight installed at arbitrary 120° angle; this is the run performed to establish the rotating object response to additional weight at 120° angle,
- fourth run – calibration weight installed at arbitrary 240° angle; this is the run performed to establish the rotating object response to additional weight at 240° angle.

The magnitude of the calibration weights added at runs two, three and four should be kept the same. The vibration amplitude (expressed in terms of the proximity signal peak-to-peak value) shall be recorded for all the runs. This can be done by recording the peak-to-peak value of the FFT signal at the frequency of rotation or by analyzing the Bode plot of the recorded data. The balance weight is then calculated using the calibration weight magnitude and all four vibration amplitudes. Effectively, the method also requires a fifth run that should be performed in order to check the effectiveness of the balancing. If the vibration reduction is not satisfactory then data acquired during this fifth run can be used as the input (amplitude of the initial vibration) for the next iteration of the balancing.

To calculate the magnitude and phase of the balance weight the system response to trial weights added at runs two, three and four shall be thoroughly followed using a compass plot [20]. The compass plot is a special type of graph that looks very similar to a polar plot and which displays data in a form of vectors that emanate from its origin. A single vector can be plotted either by providing its radius and angle or the coordinates (usually as a single complex number) of its arrow tip [83]. The compass plot consists of four quadrants: first quadrant covers the 0÷90° range, second quadrant the 90÷180° range, third quadrant the 180÷270° range and fourth quadrant the 270÷360° range. The four runs method

will be described by following the vectors distribution on the compass plot. All the amplitudes and phases of the system vibration response were specifically chosen to fit into the first quadrant of the compass plot. This was strictly done to make the math easier to follow, however all the following considerations and equations apply as well to systems which have their response vectors in all four quadrants.

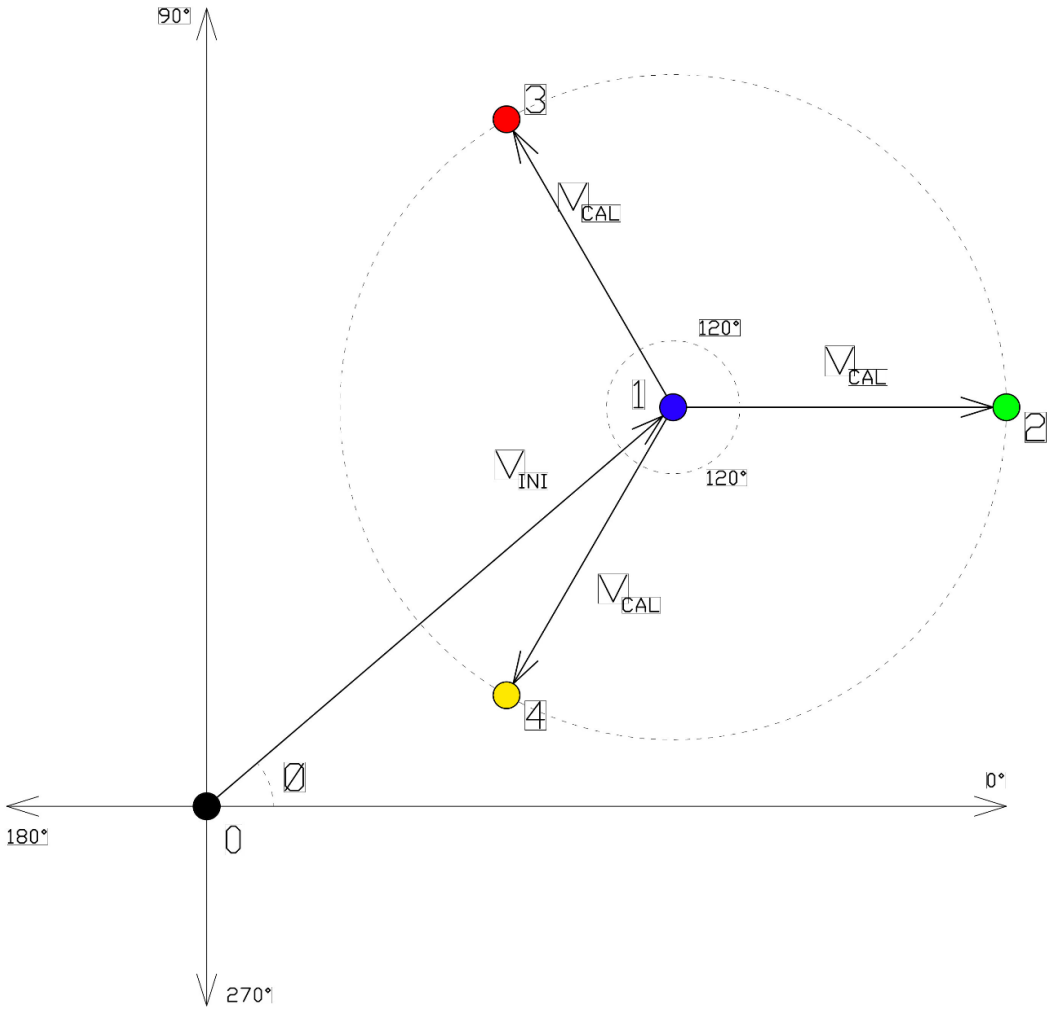

Figure 28 – initial vibration and its change due to the added calibration weights

Let's start by considering the initial system response V_{INI} and its change V_{CAL} due to addition of the calibration weight at different angles. Figure 28 shows the initial vibration V_{INI} at unknown angle φ (run 1 - blue), change V_{CAL} of the initial vibration due to the calibration weight added at 0° angle (run 2 – green), change V_{CAL} of the initial vibration due to the calibration weight added at 120° angle (run 3 – red) and change V_{CAL}

of the initial vibration due to the calibration weight added at 240° angle (run 4 – yellow). The calibration weight added at runs two, three and four has the same magnitude, therefore it generates exactly the same change V_{CAL} in the system's response but at different angles.

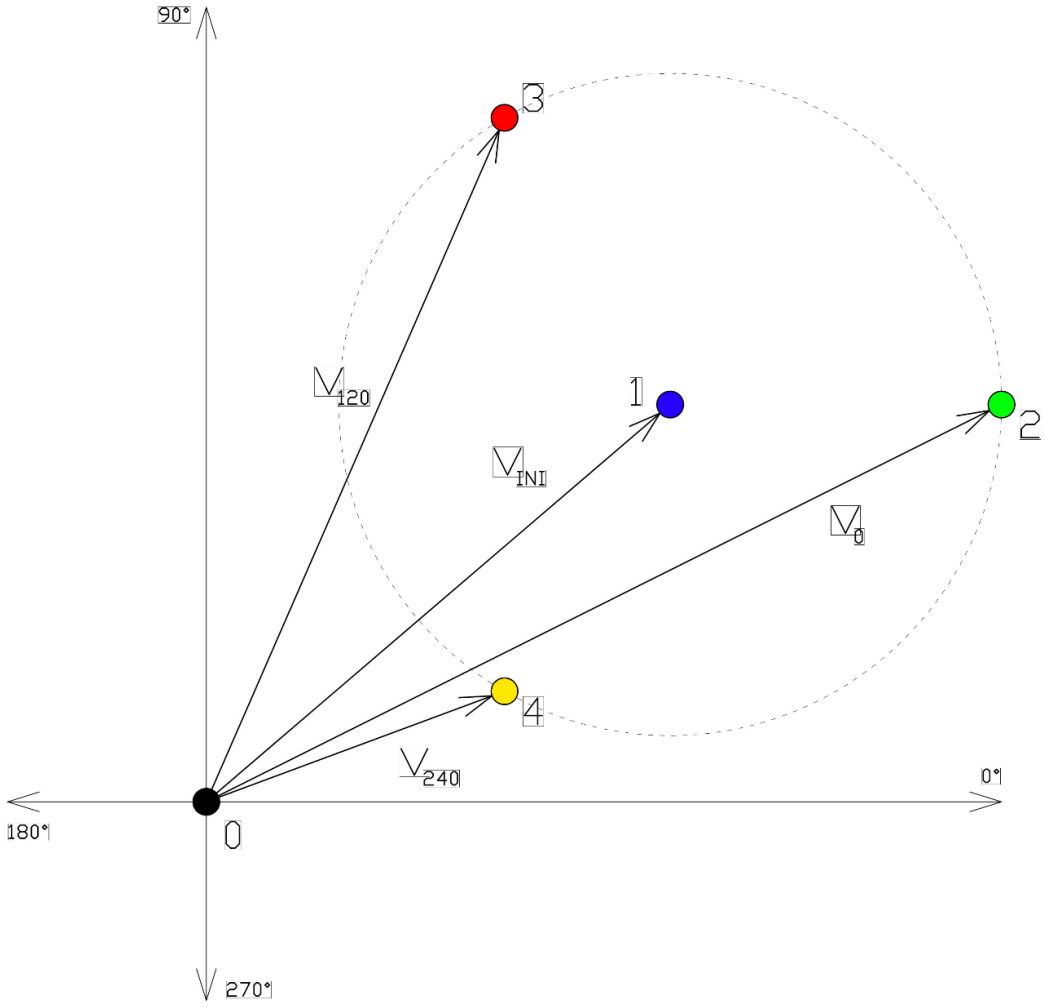

Figure 29 – vector of the initial vibration (V_{INI}) and vectors of the vibrations recorded during runs two (V_0), three (V_{120}) and four (V_{240})

The response of the system at runs two (calibration weight at 0° angle), three (calibration weight at 120° angle) and four (calibration weight at 240° angle) can be shown on the compass plot by drawing vectors connecting the origin point of the plot with the points created by adding the vector of initial response V_{INI} and the vector V_{CAL} of change due to addition of the calibration weight at corresponding angle. Figure 29 shows the vectors of the vibrations recorded during all four runs on the compass plot.

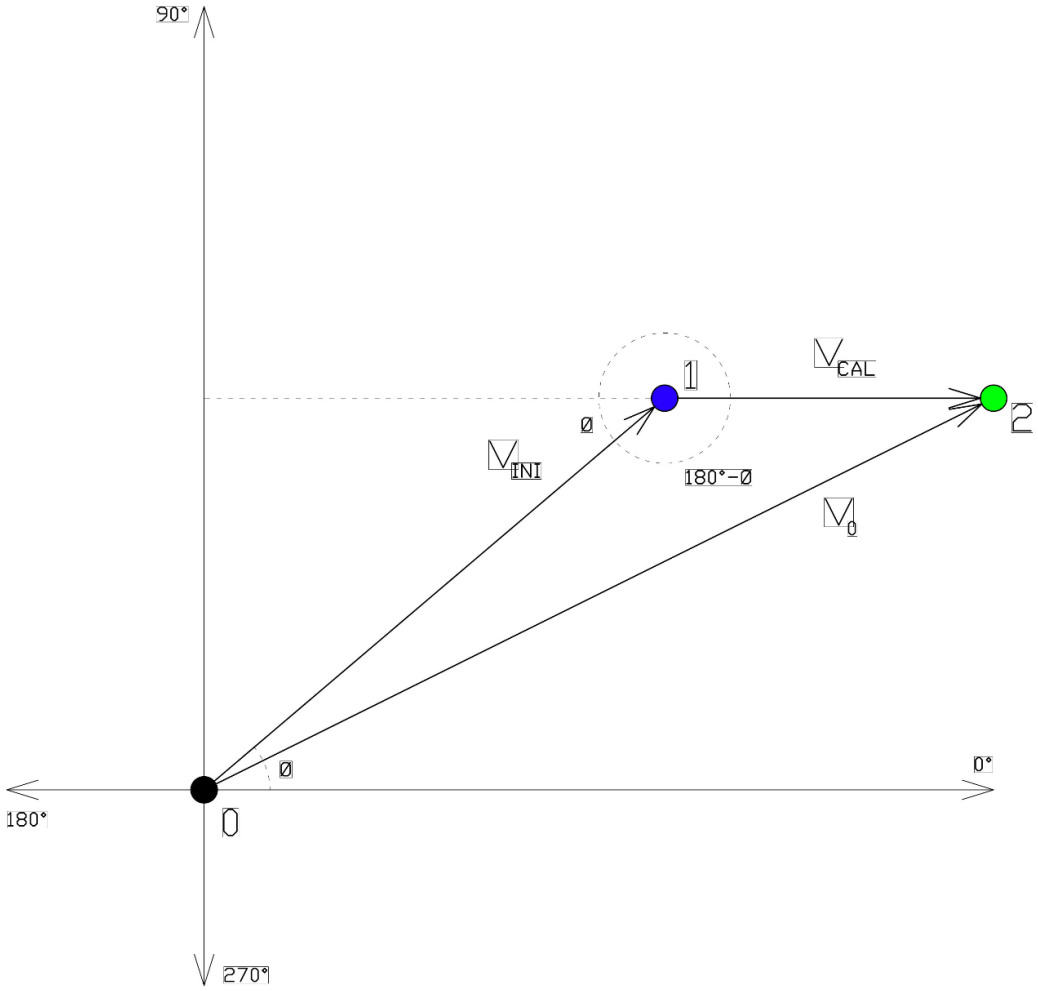

Figure 30 – vector plot of second run response (calibration weight added at 0° angle)

By combining the data shown on both compass plots (Figure 28 and Figure 29) the magnitude of the change V_{CAL} vector can be calculated. First let us consider a triangle Δ012 created by vectors V_{INI}, V_{CAL} (response change due to calibration weight added at 0° angle) and V_0. Figure 30 shows the compass plot of the second run response. Using the cosine law [84] we can calculate the vector V_0 magnitude in terms of the V_{INI} vector phase φ and the magnitudes of vectors V_{INI} and V_{CAL}:

(8) $$V_0^2 = V_{INI}^2 + V_{CAL}^2 - 2 \cdot V_{INI} \cdot V_{CAL} \cdot \cos(180° - \varphi) \rightarrow$$

$$V_0^2 = V_{INI}^2 + V_{CAL}^2 + 2 \cdot V_{INI} \cdot V_{CAL} \cdot \cos \varphi$$

Then let us consider a triangle Δ013 created by vectors V_{INI}, V_{CAL} (response change due to calibration weight added at 120° angle) and V_{120}. Figure 31 shows the compass plot of the third run response. Using the cosine law we can calculate the vector V_{120} magnitude in terms of the V_{INI} vector phase φ and the magnitudes of vectors V_{INI} and V_{CAL}:

(9) $$V_{120}^2 = V_{INI}^2 + V_{CAL}^2 - 2 \cdot V_{INI} \cdot V_{CAL} \cdot \cos(60° + \varphi) \rightarrow$$

$$V_{120}^2 = V_{INI}^2 + V_{CAL}^2 - 2 \cdot V_{INI} \cdot V_{CAL} \cdot (\cos 60° \cdot \cos \varphi - \sin 60° \cdot \sin \varphi) \rightarrow$$

$$V_{120}^2 = V_{INI}^2 + V_{CAL}^2 - 2 \cdot V_{INI} \cdot V_{CAL} \cdot \left(\frac{\cos \varphi}{2} - \frac{\sqrt{3} \cdot \sin \varphi}{2}\right) \rightarrow$$

$$V_{120}^2 = V_{INI}^2 + V_{CAL}^2 - V_{INI} \cdot V_{CAL} \cdot (\cos \varphi - \sqrt{3} \cdot \sin \varphi)$$

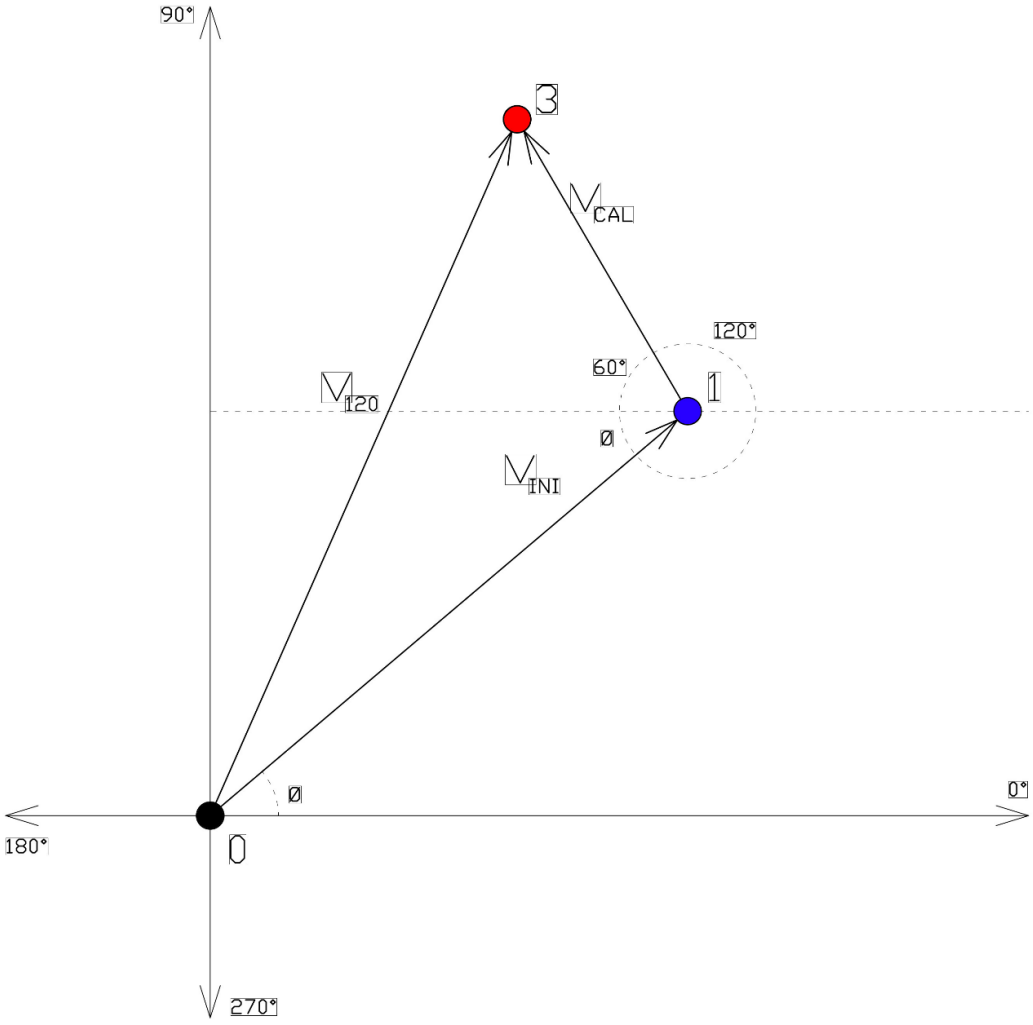

Figure 31 - vector plot of third run response (calibration weight added at 120° angle)

Last let us consider a triangle Δ014 created by vectors V_{INI}, V_{CAL} (response change due to calibration weight added at 240° angle) and V_{240}. Figure 32 shows the compass plot of the third run response. Using the cosine law we can calculate the vector V_{240} magnitude in terms of the V_{INI} vector phase φ and the magnitudes of vectors V_{INI} and V_{CAL}:

(10) $$V_{240}^2 = V_{INI}^2 + V_{CAL}^2 - 2 \cdot V_{INI} \cdot V_{CAL} \cdot \cos(60° - \varphi) \rightarrow$$

$$V_{240}^2 = V_{INI}^2 + V_{CAL}^2 - 2 \cdot V_{INI} \cdot V_{CAL} \cdot (\cos 60° \cdot \cos \varphi + \sin 60° \cdot \sin \varphi) \rightarrow$$

$$V_{240}^2 = V_{INI}^2 + V_{CAL}^2 - 2 \cdot V_{INI} \cdot V_{CAL} \cdot \left(\frac{\cos \varphi}{2} + \frac{\sqrt{3} \cdot \sin \varphi}{2}\right) \rightarrow$$

$$V_{240}^2 = V_{INI}^2 + V_{CAL}^2 - V_{INI} \cdot V_{CAL} \cdot \left(\cos \varphi + \sqrt{3} \cdot \sin \varphi\right)$$

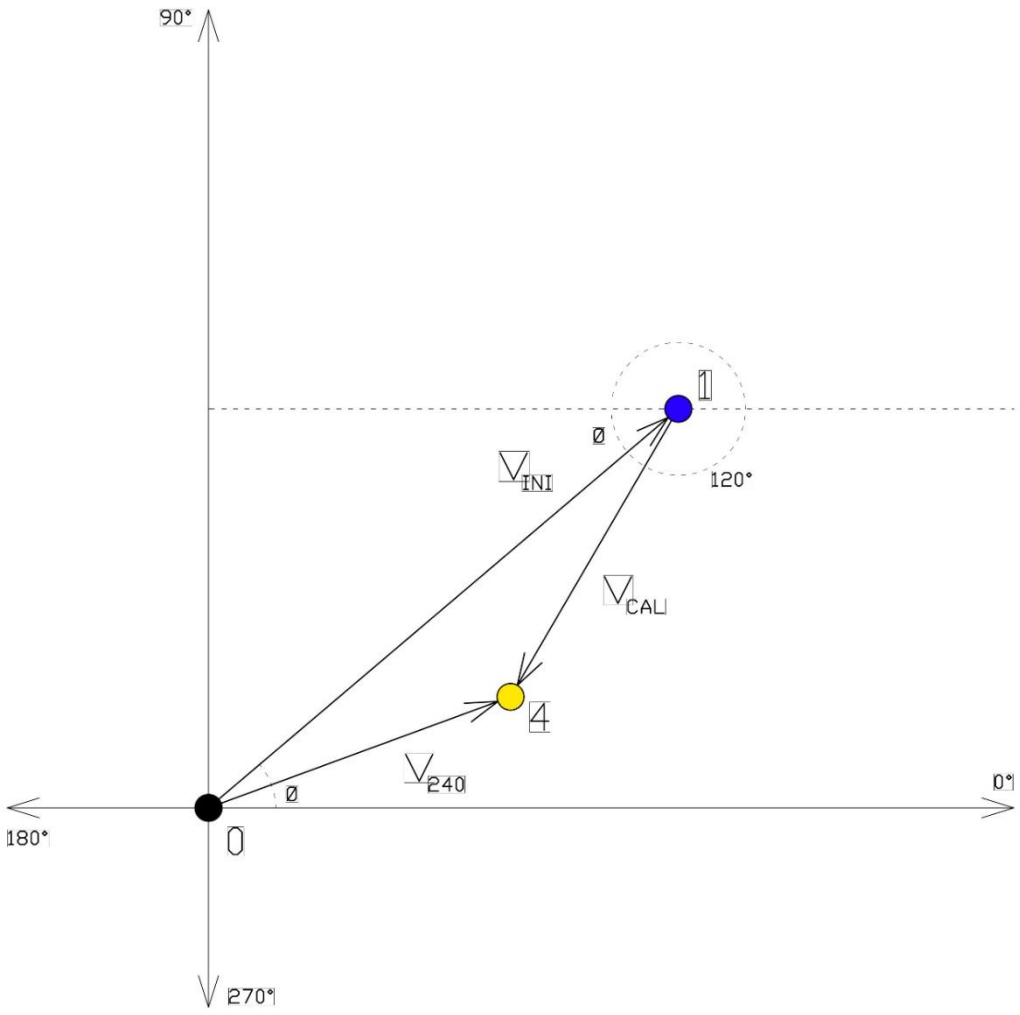

Figure 32 - vector plot of third run response (calibration weight added at 240° angle)

By adding the equations (8), (9) and (10) the magnitude of the change vector V_{CAL} can be calculated in terms of the known values of the vectors V_{INI}, V_0, V_{120} and V_{240} magnitudes:

(11) $V_0^2 + V_{120}^2 + V_{240}^2 = 3V_{INI}^2 + 3V_{CAL}^2 + V_{INI}V_{CAL}\left(2\cos\varphi - \cos\varphi + \sqrt{3}\sin\varphi - \cos\varphi - \sqrt{3}\sin\varphi\right) \rightarrow$

$V_0^2 + V_{120}^2 + V_{240}^2 = 3 \cdot V_{INI}^2 + 3 \cdot V_{CAL}^2 \rightarrow$

$3 \cdot V_{CAL}^2 = V_0^2 + V_{120}^2 + V_{240}^2 - 3 \cdot V_{INI}^2 \rightarrow$

$$V_{CAL} = \sqrt{\frac{V_0^2 + V_{120}^2 + V_{240}^2 - 3 \cdot V_{INI}^2}{3}}$$

From this point forward the magnitude of the change vector V_{CAL} is a known value. To calculate (14) the unknown phase φ of the initial response vector V_{INI} we need to calculate its sine and cosine values first. The sine of the phase φ can be calculated (12) by subtracting equation (10) from equation (9). The cosine of the phase φ can be calculated (13) by rearranging equation (8).

(12) $V_{120}^2 - V_{240}^2 = -V_{INI} \cdot V_{CAL} \cdot \left(\cos\varphi - \sqrt{3} \cdot \sin\varphi - \cos\varphi + \sqrt{3} \cdot \sin\varphi\right) \rightarrow$

$V_{120}^2 - V_{240}^2 = 2\sqrt{3} \cdot \sin\varphi \cdot V_{INI} \cdot V_{CAL} \rightarrow$

$$\sin\varphi = \frac{V_{120}^2 - V_{240}^2}{2\sqrt{3} \cdot V_{INI} \cdot V_{CAL}}$$

(13) $V_0^2 = V_{INI}^2 + V_{CAL}^2 + 2 \cdot V_{INI} \cdot V_{CAL} \cdot \cos\varphi \rightarrow$

$2 \cdot V_{INI} \cdot V_{CAL} \cdot \cos\varphi = V_0^2 - V_{INI}^2 - V_{CAL}^2 \rightarrow$

$$\cos\varphi = \frac{V_0^2 - V_{INI}^2 - V_{CAL}^2}{2 \cdot V_{INI} \cdot V_{CAL}}$$

(14) $$\tan\varphi = \frac{\sin\varphi}{\cos\varphi} = \frac{V_{120}^2 - V_{240}^2}{2\sqrt{3}\cdot V_{INI}\cdot V_{CAL}} \cdot \frac{2\cdot V_{INI}\cdot V_{CAL}}{V_0^2 - V_{INI}^2 - V_{CAL}^2} = \frac{V_{120}^2 - V_{240}^2}{\sqrt{3}\cdot\left(V_0^2 - V_{INI}^2 - V_{CAL}^2\right)} \rightarrow$$

$$\varphi = \tan^{-1}\left(\frac{V_{120}^2 - V_{240}^2}{\sqrt{3}\cdot\left(V_0^2 - V_{INI}^2 - V_{CAL}^2\right)}\right)$$

The final balance weight shall be installed at angular location oposite to the calculated phase of the initial vibration V_{INI}. The last uknown is the magnitude W_{BAL} of the final balance weight, however it can be easily calculated using the equation (15), where W_{CAL} is the magnitude of the calibration weight used during runs two, three and four.

(15) $$W_{BAL} = \frac{V_{INI}}{V_{CAL}} \cdot W_{CAL}$$

There's one very interesting property of the four runs balancing method – as opposed to the mathematical solution presented above, it can also be solved graphically. Figure 33 shows the graphical solution of the problem using just the magnitudes of the vibrations recorded during all four runs. However, using this approach will only provide one uknown of the system, that is the angular location of the final balance weight, which means that it is still necessary to use equations (11) and (15) to calculate the magnitude of the final balance weight. The graphical approach to the method consists of five steps [85]:

- draw a circle of radius equal to the magnitude of the initial vibration V_{INI}, centered in the origin of the compass plot (run 1 – blue point) – this is the starting circle,
- draw a circle of radius equal to the magnitude of the second run (calibration weight added at 0° angle) vibration V_0, centered in the point located at 0° angle on the starting circle circumference (run 2 – green point) – this is the 0° angle circle,
- draw a circle of radius equal to the magnitude of the third run (calibration weight added at 120° angle) vibration V_{120}, centered in the point located at 120° angle on the starting circle circumference (run 3 – red point) – this is the 120° angle circle,
- draw a circle of radius equal to the magnitude of the fourth run (calibration weight added at 240° angle) vibration V_{240}, centered in the point located at 240° angle

on the starting circle circumference (run 4 – yellow point) – this is the 240° angle circle,

- mark the point created by the intersection of the 0° angle, 120° angle and 240° angle circles (BAL – purple point); the angle of this point is the angular location of the final balance weight; vector V_{INI} has been drawn on the Figure 33 for reference purpose – it can be seen that the intersection point has an exactly opposite angle to this vector proving the validity of the four runs method graphical solution.

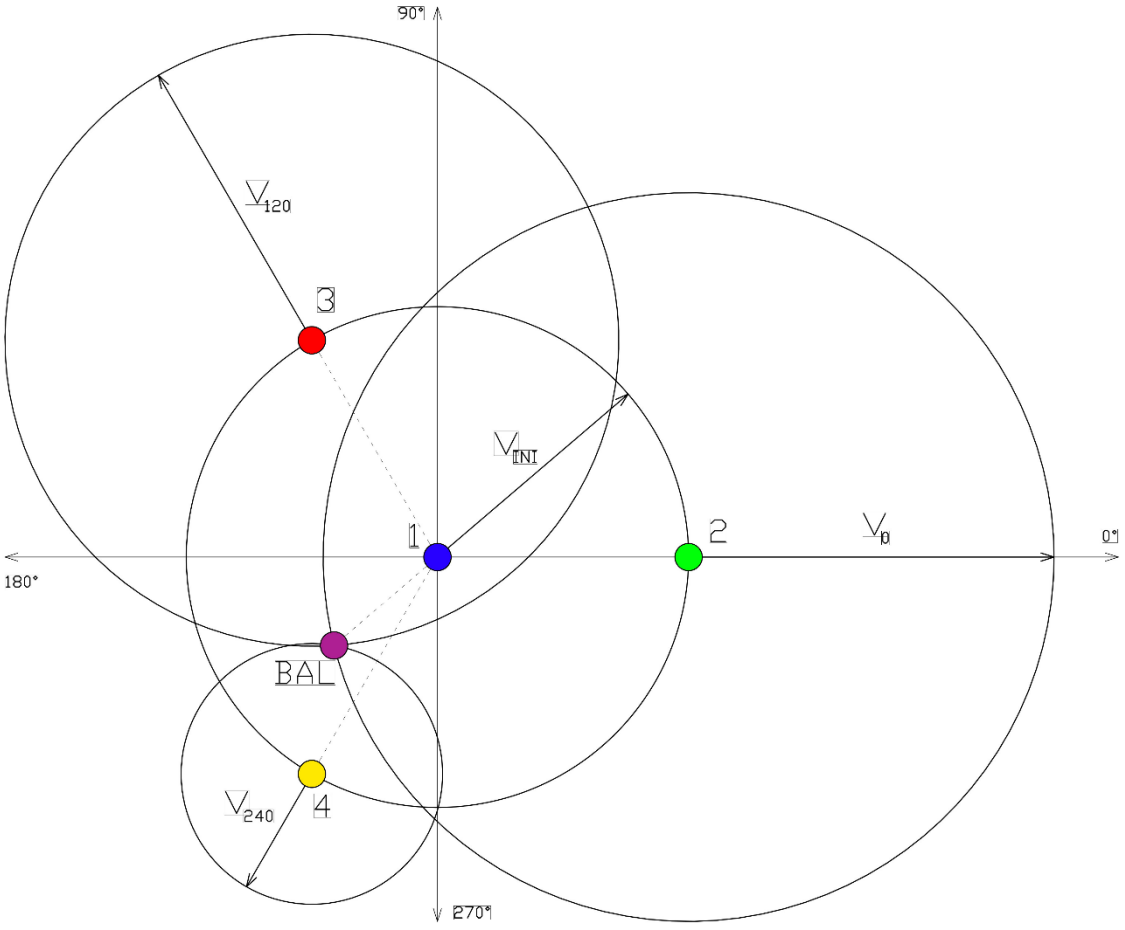

Figure 33 – graphical solution of the four runs method

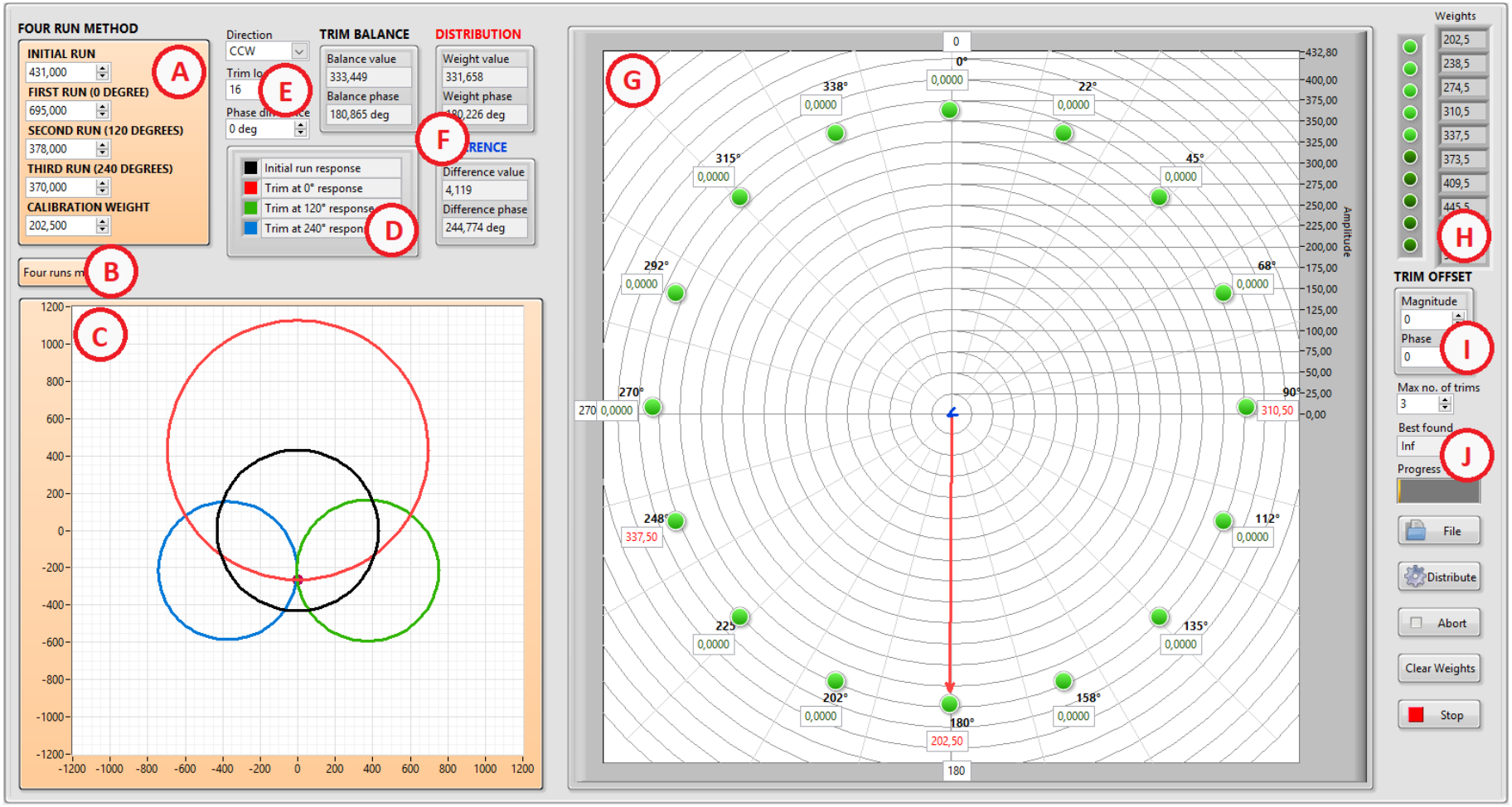

Figure 34 - the front panel of the Single Plane Balancing Application while the balancing system is configured to use the four runs method

The *Single Plane Balancing Application* described in the chapter concerning the vector method (3.1) is also capable of performing the balancing using the four runs method. The *Single Plane Balancing Application*, while the balancing system is configured to use the four runs method (Figure 34) consists of the following items:

A) four runs method data – lets the user input the magnitude of the calibration weight and the magnitudes of the vibration recorded during all four runs,
B) method switch – switches the application between the vector method and the four runs method,
C) XY plot – displays the circles associated with each of the four runs as described for the graphical solution of the method; the final balance weight point visible on the plot is however calculated using the mathematical approach; this combination was chosen on purpose – it is more informative for the user to see the solution provided by the graphical approach to the four runs method but on the other hand it is more accurate to calculate the actual solution using the mathematical approach; the data visible on the XY plot is therefore the combination of the best features provided by these two different approaches,
D) XY plot legend – assigns colors to each circle on the plot,
E) weight plot settings – sets the rotation direction, number of possible weight locations and angle offset,
F) weights data – indicates the magnitude and phase of the calculated final balance weight, the current weight distribution and difference between the two,
G) weights plot – displays all the information about the weight distribution but can be also used to manually input the balance weights and to observe changes in weight distribution,
H) possible weights – lists all possible balance weights loaded from a file,
I) trim offset control – can be used to input the calculated balance weight from a previous balancing,
J) weight distribution settings – lets the user set the maximum number of allowed weight locations, load possible balance weights from a file, perform automatic balance weights distribution, abort the automatic distribution, clear all the data from weights plot and stop the application.

3.3 **Balancing results comparison**

Figure 2 shows the test stand configuration when the balancing system was used to compare the results of both single plane balancing methods. Eight steel wheels, each weighing 1kg, were mounted in the center of a 60cm long steel shaft. Both ends of the shaft were supported by stiff bearings. The resonance speed of the system was around 2850rpm. Balancing was performed for several different operation speeds of the rotor as well as for several different initial calibration weights.

Table 5 shows the balancing results obtained when the balancing system was configured to use the vector method. The following conclusions can be drawn:

- the balancing performed using the vector method always leads to decrease in the vibration level,
- usually only one iteration (three runs total) of the balancing is needed to obtain satisfactory reduction in the object's vibration – throughout the testing, the average unbalance after first iteration was only 27% of the initial unbalance,
- second iteration of the balancing always leads to decreasing the unbalance, however trying to perform third iteration only works around 50% of the times – third iteration should only be used if after two iterations the system's response is still far from satisfactory,
- the average unbalance after two iterations of the balancing (five runs total) was only 12% of the initial unbalance, and 52% of the unbalance after the first iteration,
- the vector method can be used for all balancing speeds and it gives good results even when balancing at the resonance speed,
- the operation speed (other than the resonance speed) of the rotating object being balanced doesn't have an impact on the balancing results – for all the speeds the unbalance reduction was approximately the same,
- the magnitude of the calibration weight used has a big impact on the final unbalance reduction – generally the lower the operational speed the higher the magnitude of the calibration weight should be,

- while calibrating at resonance speed the magnitude of the calibration weight should be considerably lower than while balancing at other speeds,
- the greatest advantage of the vector method is the instant prediction of the unbalance location – this allows to mount the calibration weights at angular location that will almost certainly lead to decreasing the unbalance; one reason this is desirable is the negligible risk of increasing the unbalance leading to excessive vibration; the other reason is that the installation of the calibration weight in the right spot might give better results than the final balance weight calculated by the system (Table 5 shows such exact behaviour for operation speeds of 2000rpm, 1500rpm and 1000rpm),
- if the response of the system changes only slightly when running with the calibration weight, the magnitude of the calibration weight should be immadiately increased – there's no point in calculating the final balance weight in such case.

Table 6 shows the balancing results obtained when the balancing system was configured to use the four runs method. The following conclusions can be drawn:

- the balancing performed using the four runs method may lead to an increase in the vibration level – there were a total of 28 balancing tests performed using the four runs method, in 3 cases the final unbalance was higher than the initial unbalance,
- the balancing using the four runs method gives poor results when balancing at the resonance speed,
- the operation speed for which the balancing is performed has a big impact on the method results – generally speaking the lower the speed the better the results,
- the magnitude of calibration weight has a big impact on the method results; increasing the magnitude of the clibration weight will usually lead to better final results, however only to a certain point; further increase in the magnitude of the calibration weight will then lead to a graduał decrease in the final balancing quality,
- the balancing using the the four runs method doesn't give any results if the calibration weight is too small – this situation occurs mostly for low operation speeds (observed for 1500rpm and 1000rpm),

- for low operation speeds the balancing requires very heavy calibration weights to produce any results – for 1000rpm the lowest effective magnitude of the calibration weights was 961gmm which is approximately 27 times higher than the lowest magnitude of the balance weights used for higher operation speeds,
- throughout the testing, the average final unbalance while using the four run method was 43% of the initial unbalance,
- the balancing using the four runs method requires the addition of the calibration weights at three equally spread angular locations; this means that for at least one of the calibration runs the vibration of the system will increase; this may lead to the rotating object failure due to excessive vibrations; such dangerous behavior was observed for run 2 (calibration weight at 0° angle) while balancing the object at operation speeds of 2833rpm (resonance) and 2750rpm.

Table 7 shows the comparison of the results obtained when the balancing system was configured to use both single plane balancing methods. The following conclusions can be drawn:

- the vector method gives much better results than the four runs method – only in one case (out of total 13 scenarios for which the balancing was performed using both methods) the final unbalance was lower for the four runs method,
- the average attenuation of the final vibration level as compared to the initial vibration was 833% for balancing using the vector method (13 total scenarios tested) and only 233% for balancing using the four runs method (28 total scenarios tested),
- the lowest final vibration of the system when balanced using the vector method was $5\mu m_{pk\text{-}pk}$ (4167% attenuation of the initial vibration) compared to $19\mu m_{pk\text{-}pk}$ (1408% attenuation of the initial vibration) when using the four runs method,
- the highest final vibration of the system when balanced using the vector method was $516\mu m_{pk\text{-}pk}$ (309% attenuation of the initial vibration) compared to $1907\mu m_{pk\text{-}pk}$ (201% gain of the initial vibration) when using the four runs method.

Table 5 – results of the balancing performed using the single plane vector method

Speed [rpm]	Run 1		Calibration weight 1		Run 2		Trim balance 1		Run 3		Calibration weight 2		Run 3 / Run 1
	Mag [um]	Phase [°]	Mag [gmm]	Phase [°]	Mag [um]	Phase [°]	Mag [gmm]	Phase [°]	Mag [um]	Phase [°]	Mag [gmm]	Phase [°]	
Res	1592	15	36	225	1021	30	87	249	955	219	36	180	59,99%
	1592	15	72	225	728	33	124	239	485	212	36	180	30,46%
	1592	15	108	225	565	44	152	239	379	201	N/A	N/A	23,81%
2750	884	194	108	180	380	318	81	197	85	202	36	202	9,62%
	884	194	202	180	346	3	143	183	138	346	36	338	15,61%
2500	346	198	108	202	124	168	152	188	42	258	36	270	12,14%
	346	198	202	202	105	10	159	205	101	104	36	90	29,19%
2000	244	181	108	180	141	193	240	196	67	175	36	180	27,46%
	244	181	202	180	81	212	275	193	51	164	36	157	20,90%
1500	238	170	108	180	194	171	579	184	66	140	135	135	27,73%
	238	170	202	180	161	163	602	166	40	209	135	202	16,81%
1000	212	174	108	180	175	183	468	215	142	174	135	180	66,98%
	212	174	202	180	179	172	1263	171	18	166	202	157	8,49%

Speed [rpm]	Run 3		Calibration weight 2		Run 4		Trim balance 2		Run 5		Final trim		Run 5 / Run 1
	Mag [um]	Phase [°]	Mag [gmm]	Phase [°]	Mag [um]	Phase [°]	Mag [gmm]	Phase [°]	Mag [um]	Phase [°]	Mag [gmm]	Phase [°]	
Res	955	219	36	180	731	31	20	181	516	32	99	239	32,41%
	485	212	36	180	527	57	17	169	355	15	131	232	22,30%
	379	201	N/A	N/A	N/A	N/A	N/A	N/A	N/A	N/A	152	239	23,81%
2750	85	202	36	202	89	310	22	239	80	328	100	206	9,05%
	138	346	36	338	201	171	15	335	24	31	129	187	2,71%
2500	42	258	36	270	24	151	28	245	15	119	171	195	4,34%
	101	104	36	90	38	222	29	106	40	336	157	194	11,56%
2000	67	175	36	180	42	168	93	196	40	286	326	189	16,39%
	51	164	36	157	20	234	37	180	27	298	305	189	8,20%
1500	66	140	135	135	31	152	249	145	14	250	788	173	5,88%
	40	209	135	202	23	245	212	235	35	132	716	172	9,66%
1000	142	174	135	180	119	172	819	170	14	181	1200	186	6,60%
	18	166	202	157	5	200	258	169	14	299	1461	169	2,36%

Speed [rpm]	Notes
Res	Resonance did not occur during the Run 3 - no further balancing needed
2750	First balancing: calibration weight 2 should be probably higher as 36 gmm almost didn't change the system response
2500	-
2000	Second balancing: Run 4 response lower than Run 5 response, therefore for final trim the cal weight 2 was used instead of trim balance 2
1500	Second balancing: Run 4 response lower than Run 5 response, therefore for final trim the cal weight 2 was used instead of trim balance 2
1000	Second balancing: Run 4 response lower than Run 5 response, therefore for final trim the cal weight 2 was used instead of trim balance 2

Legend		
	>	200%
	>	150%
	>	100%
	>	75%
	>	50%
	>	25%
	>	15%
	>	10%
	>	5%
	<	5%

Table 6 – results of the balancing performed using the single plane four runs method

Speed [rpm]	Balance weight [gmm]	Run 1 (base)	Run 2 (0 deg)	Run 3 (120 deg)	Run 4 (240 deg)	Run 5 (check)	Trim calculated		Trim added		Trim difference		Run 5 / Run 1
							Mag	Phase	Mag	Phase	Mag	Phase	
2833	36	1470	1780	1328	1663	1001	83,2	136,2	83,1	135,5	1,0	219,8	68,10%
	72	1470	1884	1556	1651	1295	123,2	164,9	122,9	164,3	1,3	240,1	88,10%
	108	1470	2009	1676	1840	1772	142,0	152,0	142,6	151,9	0,6	299,0	120,54%
2750	36	951	1130	842	876	1907	296,4	174,6	295,3	174,3	2,0	233,1	200,53%
	72	951	1362	655	836	1860	228,3	169,7	227,5	169,7	0,8	182,8	195,58%
	108	951	1595	560	778	766	205,5	173,1	204,8	172,8	1,2	233,0	80,55%
	135	951	1833	577	771	510	177,2	175,5	177,5	175,2	1,2	279,8	53,63%
	171	951	1972	1103	719	342	165,1	191,3	163,6	192,0	2,5	140,6	35,96%
	202	951	2152	1564	772	104	149,8	207,3	150,1	207,8	1,5	103,8	10,94%
2500	36	431	528	412	411	147	109,6	180,4	109,4	180,7	0,6	110,0	34,11%
	72	431	614	393	397	62	148,1	179,3	147,0	179,2	1,1	194,5	14,39%
	108	431	695	378	370	52	177,8	180,9	178,9	180,9	1,1	1,1	12,06%
	135	431	755	371	363	69	189,7	180,7	190,0	180,9	0,7	70,1	16,01%
	171	431	841	364	359	85	199,0	180,3	198,3	180,4	0,8	156,2	19,72%
	202	431	915	371	376	89	202,2	179,7	202,5	180,0	1,0	71,9	20,65%
2000	36	306	332	293	307	157	196,7	160,2	197,5	159,9	1,3	290,7	51,31%
	72	306	359	273	294	44	403,6	168,0	402,3	167,9	1,5	189,9	14,38%
	108	306	385	266	292	24	374,7	169,9	373,1	169,6	2,1	212,6	7,84%
	135	306	413	262	291	21	345,1	171,6	344,4	171,5	0,9	208,6	6,86%
	171	306	437	256	280	41	390,0	174,7	390,5	174,5	0,9	293,7	13,40%
	202	306	450	246	281	61	434,3	173,1	434,5	173,1	0,2	345,7	19,93%

Speed [rpm]	Balance weight [gmm]	Run 1 (base)	Run 2 (0 deg)	Run 3 (120 deg)	Run 4 (240 deg)	Run 5 (check)	Trim calculated		Trim added		Trim difference		Run 5 / Run 1
							Mag	Phase	Mag	Phase	Mag	Phase	
1500	36	269	278	250	259	N/A	∞	162,4	N/A	N/A	N/A	N/A	N/A
	72	269	294	254	259	71	1088,4	173,9	1088,4	173,6	4,7	264,4	26,39%
	108	269	308	241	263	35	709,4	162,9	710,5	162,9	1,1	323,5	13,01%
	135	269	313	240	259	25	843,0	167,0	845,5	167,3	4,2	40,2	9,29%
	171	269	324	229	260	55	894,5	163,7	895,3	163,8	1,2	25,3	20,45%
	202	269	338	223	260	19	783,8	164,4	785,5	164,4	1,7	336,5	7,06%
1000	36	254	254	246	250	N/A	∞	150,3	N/A	N/A	N/A	N/A	N/A
	72	254	260	245	247	N/A	∞	173,1	N/A	N/A	N/A	N/A	N/A
	108	254	261	238	245	N/A	∞	163,3	N/A	N/A	N/A	N/A	N/A
	135	254	262	237	249	N/A	∞	152,2	N/A	N/A	N/A	N/A	N/A
	171	254	270	235	242	N/A	∞	169,8	N/A	N/A	N/A	N/A	N/A
	202	254	271	229	241	N/A	∞	165,0	N/A	N/A	N/A	N/A	N/A
	472	254	297	210	219	N/A	∞	175,5	N/A	N/A	N/A	N/A	N/A
	961	254	340	189	210	48	9770,0	174,5	2114,5	180,0	7666,8	173,0	18,90%
	2114	254	482	187	249	48	2524,3	172,7	2114,5	180,0	503,4	140,7	18,90%

Table 7 – comparison of balancing results obtained by using two different methods to balance the same object

Speed [rpm]	Four runs method						Vector method						Trim difference of both methods best runs	
	Initial cal. weight [gmm]	Run 1 (base)	Run 5 (check)	Run 5 / Run 1	Final trim (four run)		Initial cal. weight [gmm]	Run 1 (base)	Best run	Run 5 / Run 1	Final trim (four run)			
					Mag [gmm]	Phase [°]					Mag [gmm]	Phase [°]	Mag [gmm]	Phase [°]
2833	36	1470	1001	68,1%	83	136	36	1592	516	32,4%	99	239	163	262
	72	1470	1295	88,1%	123	164	72	1592	355	22,3%	131	232		
	108	1470	1772	120,5%	143	152	108	1592	379	23,8%	152	239		
2750	36	951	1907	200,5%	295	174	-	-	-	-	-	-	54	85
	72	951	1860	195,6%	228	170	-	-	-	-	-	-		
	108	951	766	80,5%	205	173	108	884	80	9,0%	100	206		
	135	951	510	53,6%	178	175	-	-	-	-	-	-		
	171	951	342	36,0%	164	192	-	-	-	-	-	-		
	202	951	104	10,9%	150	208	202	884	24	2,7%	129	187		
2500	36	431	147	34,1%	109	181	-	-	-	-	-	-	44	288
	72	431	62	14,4%	147	179	-	-	-	-	-	-		
	108	431	52	12,1%	179	181	108	346	15	4,3%	171	195		
	135	431	69	16,0%	190	181	-	-	-	-	-	-		
	171	431	85	19,7%	198	180	-	-	-	-	-	-		
	202	431	89	20,6%	203	180	202	346	40	11,6%	157	194		
2000	36	306	157	51,3%	197	160	-	-	-	-	-	-	106	292
	72	306	44	14,4%	402	168	-	-	-	-	-	-		
	108	306	24	7,8%	373	170	108	244	40	16,4%	326	189		
	135	306	21	6,9%	344	171	-	-	-	-	-	-		
	171	306	41	13,4%	390	175	-	-	-	-	-	-		
	202	306	61	19,9%	434	173	202	244	20	8,2%	305	189		

Speed [rpm]	Four runs method						Vector method						Trim difference of both methods best runs	
	Initial cal. weight [gmm]	Run 1 (base)	Run 5 (check)	Run 5 / Run 1	Final trim (four run)		Initial cal. weight [gmm]	Run 1 (base)	Best run	Run 5 / Run 1	Final trim (four run)			
					Mag [gmm]	Phase [°]					Mag [gmm]	Phase [°]	Mag [gmm]	Phase [°]
1500	36	269	N/A	N/A	N/A	N/A	-	-	-	-	-	-	115	257
	72	269	71	26,4%	1088	174	-	-	-	-	-	-		
	108	269	35	13,0%	710	163	108	238	14	5,9%	788	173		
	135	269	25	9,3%	846	167	-	-	-	-	-	-		
	171	269	55	20,4%	895	164	-	-	-	-	-	-		
	202	269	19	7,1%	786	164	202	238	23	9,7%	716	172		
1000	36	254	N/A	N/A	N/A	N/A	-	-	-	-	-	-	735	22
	72	254	N/A	N/A	N/A	N/A	-	-	-	-	-	-		
	108	254	N/A	N/A	N/A	N/A	108	212	14	6,6%	1200	186		
	135	254	N/A	N/A	N/A	N/A	-	-	-	-	-	-		
	171	254	N/A	N/A	N/A	N/A	-	-	-	-	-	-		
	202	254	N/A	N/A	N/A	N/A	202	212	5	2,4%	1461	169		
	472	254	N/A	N/A	N/A	N/A	-	-	-	-	-	-		
	961	254	48	18,9%	2114	180	-	-	-	-	-	-		
	2114	254	48	18,9%	2114	180	-	-	-	-	-	-		

4. Multi plane balancing method

4.1 Introduction to the influence coefficients method

When the balancing is required for two or more axial locations along the shaft, the process of calculating the trim weights for each of these planes is called the multi plane balancing, as opposed to a single plane balancing when the calculation of the trim weight is only required for one plane. There are several methods that can be applied when performing the multi plane balancing, however the one that is used the most often if called the influence coeffienct method [86]. This method is an extension of the previously described vector method (chapter 3.1) – it uses the same approach to calculating the trim weights, however it is used in a matrix form and can be applied to any number of axial planes along the shaft. When the influence coefficient method is used for a single plane, the matrices of vectors reduce to single vectors and the equations become the exact same ones as used in the vector method.

Generally speaking, the multi plane balancing using the influence coeffiecient method consists of the following steps (Figure 35):

- perform the base run with no calibration weights; record the amplitude and phase of the unbalance at each plane,
- add calibration weight to only one plane and perform the calibration run for this particular plane; record the amplitude and phase of the unbalance at each plane; this step shall be performed for each balancing plane,
- fill the matrices in the software application within the balancing system using the collected data; the application will calculate the trim balance weights that should be added in each plane in order to attenuated the unbalance,
- apply the calculated trim balance weights and perform the check run; finish the balancing if the new unbalance is below the required limit or perform another iteration of the balancing procedure if the new unbalance is above the required limit.

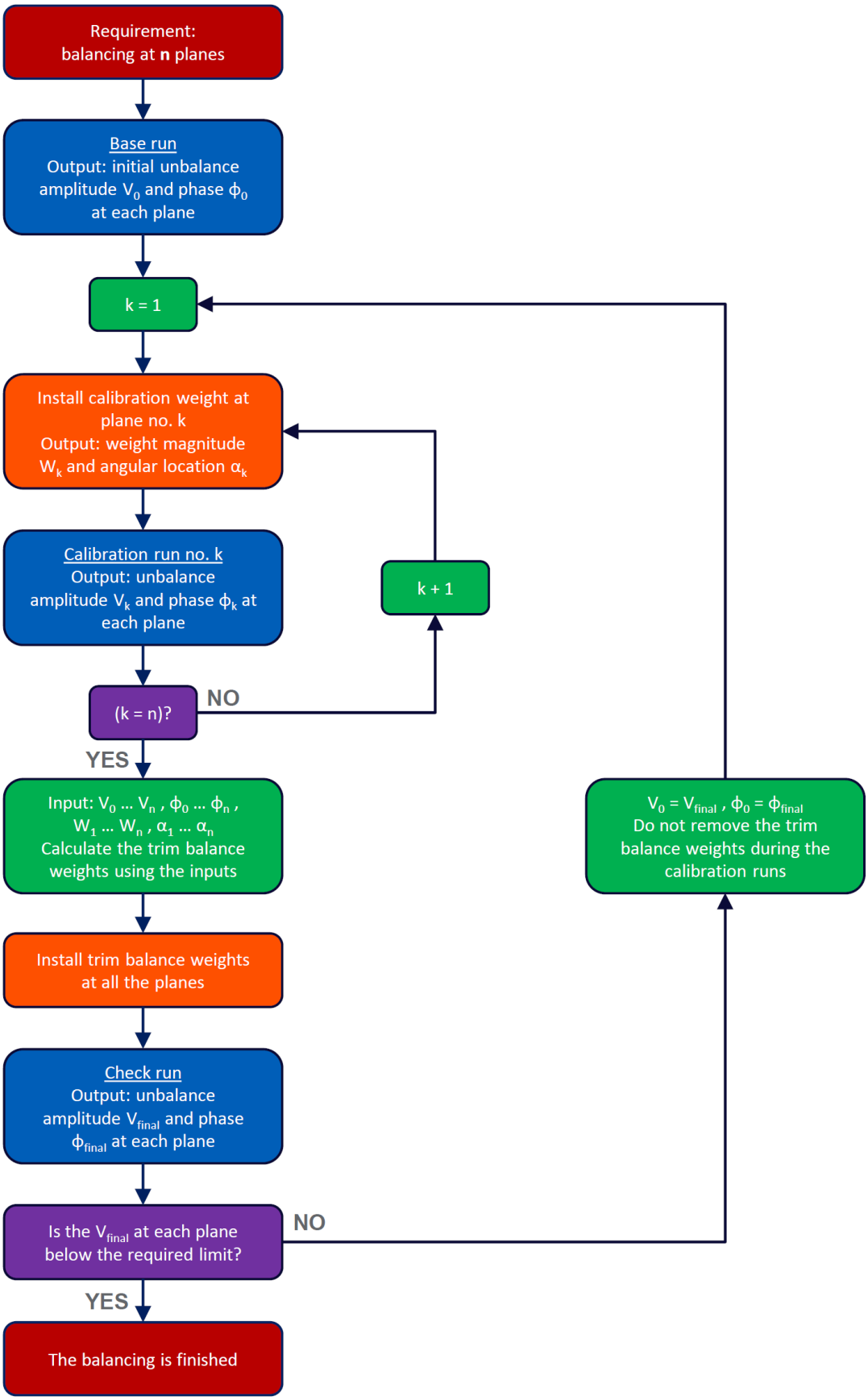

Figure 35 – the flow chart of the influence coeficient multi plane balancing method

Figure 37 shows the test stand configurations used for testing the performance of the influence coefficient method implemented within the developed balancing system. The test stand consists of a steel shaft, supported by stiff bearings at both ends and in the middle. The length of the shaft is 120cm. There is a single notch along the entire length of the shaft which serves two purposes. First, it is used by the PNP proximity probe to provide the tachometer signal. Second, it enables the steel wheels to be securely mounted on the shaft using specially shaped fittings (Figure 36). In order to simulate the balancing planes, eight steel wheels (1kg each) were used. The steel wheels were equally distributed along the shaft in four locations, each location having its dedicated analog proximity probe (shown on Figure 37).

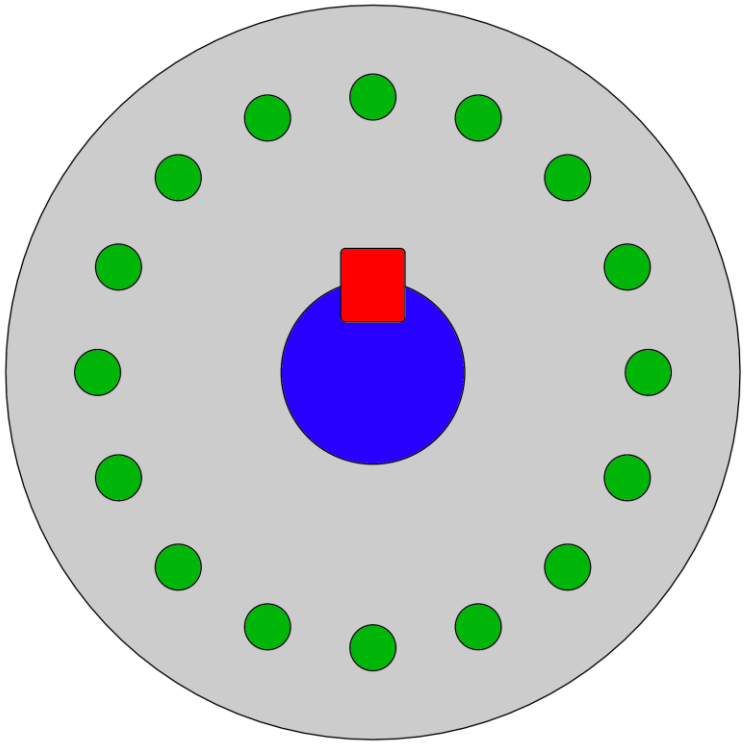

Figure 36 – cross section of the steel wheel simulating a disc shaped rotor (green – balance weights installation locations, blue – shaft, red – specially shaped fitting)

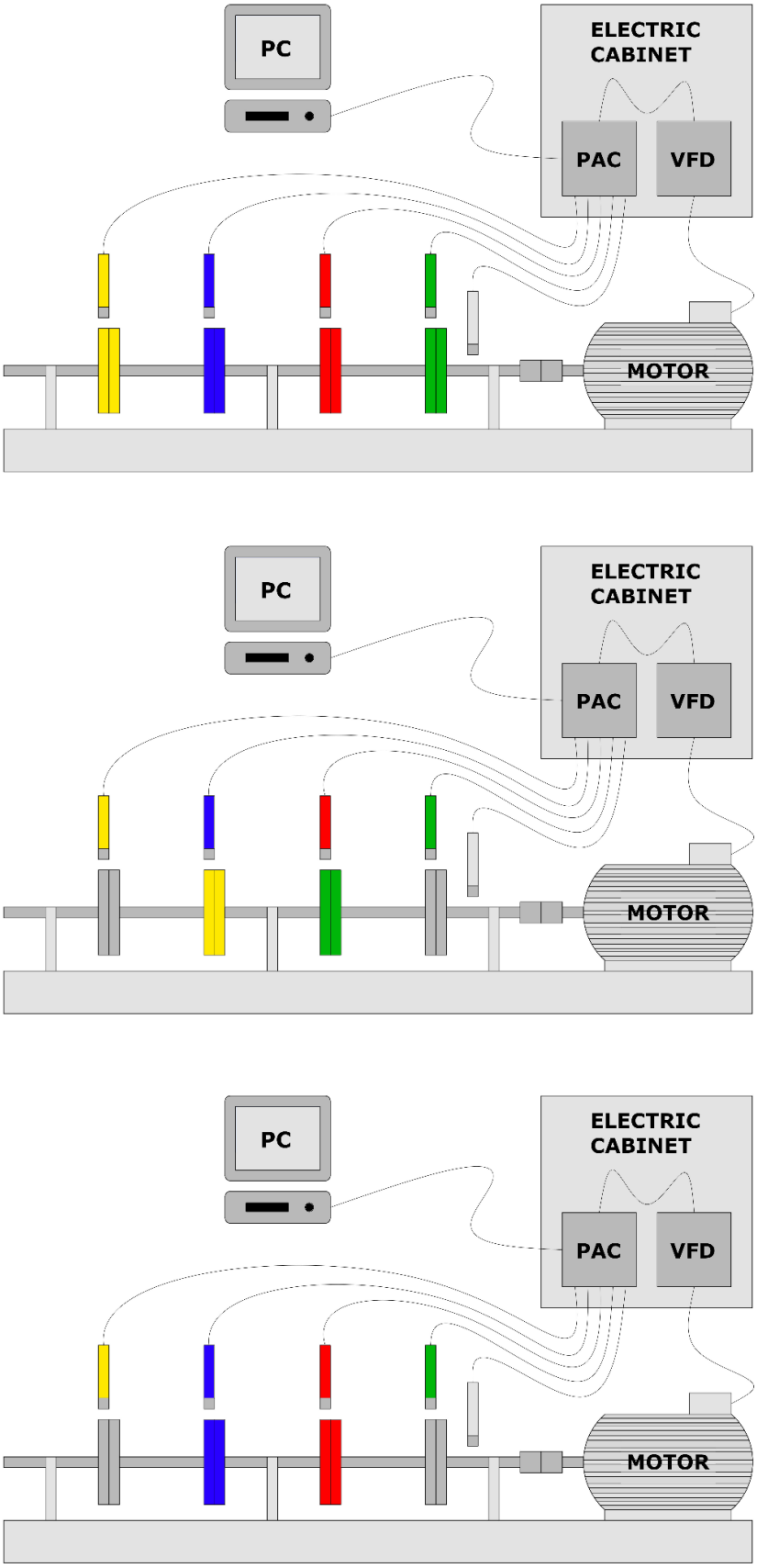

Figure 37 – the test stand configurations used to test the influence coeffiecient method implemented within the balancing system

Three configurations of the test stand were used to simulate different balancing scenarios. First configuration (Figure 37 - top) simulates the balancing at four planes, where each plane has its dedicated direct proximity analog probe (plane 1 – yellow, plane 2 – blue, plane 3 – red, plane 4 – green). Second configuration (Figure 37 - middle) simulates the balancing at two planes where each plane doesn't have its dedicated direct proximity probe. The yellow proximity probe is used as the measurement for plane 2 (yellow) and green proximity probe is used as the measurement for plane 3 (green). The blue and red proximity probes are not used for the balancing, however the data acquired by them is still stored for the balancing system performance analysis purposes. The balancing is not performed at planes 1 and 4 (grey). Third configuration (Figure 37 - bottom) simulates the balancing at two planes where each plane has its dedicated direct proximity probe (plane 2 – blue, plane 3 – red). The yellow and green proximity probes are not used for the balancing, however the data acquired by them is still stored for the balancing system performance analysis purposes. The balancing is not performed at planes 1 and 4 (grey).

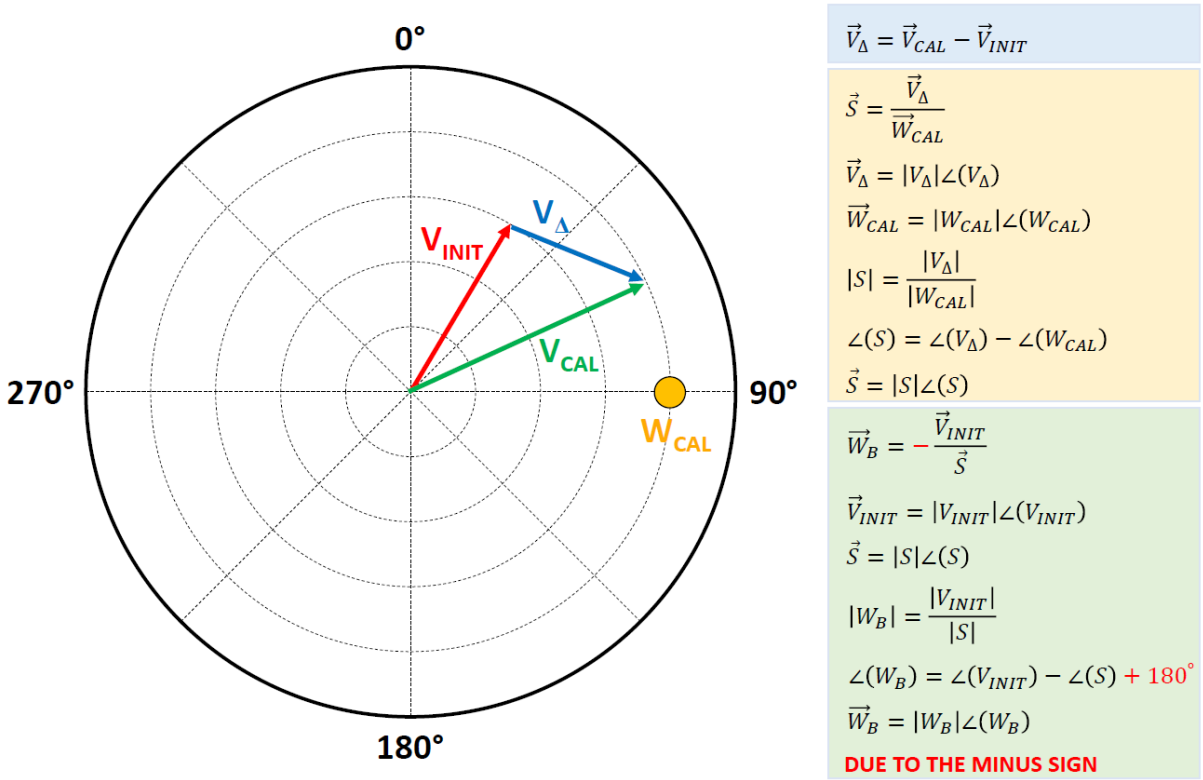

Figure 38 – the vector method overview

4.2 Calculation of the trim balance weights

Figure 38 shows the approach used in the vector method for the single plane balancing. The $\vec{V}_{\Delta}$ is a vector of the initial system response change due to the addition of the calibration weight. Having this vector calculated, we can then proceed to derive the system's sensitivity vector $\vec{S}$ which can be used to estimate the change in the reponse of the system due to any balance weight. Finally the trim balance weight is estimated by applying the calculated sensitivity to the vector opposite to the initial system's response $\vec{V}_{\mathrm{INIT}}$. Using this approach we get the final balance weight $\overrightarrow{W_B}$ which should cause the system's response change such that it will cancel out the initial response [81].

As was stated before the influence coefficients method is a mere extension of the vector method. In the vector method one single sensitivity was calculated using the magnitude and phase of the calibration weight and the magnitude and phase of the response change vector. In the case of the influence coefficients method the number of sensitivities to calculate is strictly dependant on the number of planes to balance. If we consider a system with n balancing planes, there will be n^2 sensitivities to calculate [86]. The steps required to gather all the necessary data are presented in flow chart form on the Figure 35. We start by running the system with no calibration weights added and record the magnitude and phase of the first order response at each plane at the required rotational speed. Then we proceed to install the calibration weight at plane 1, run the system again at the required rotational speed and record the first order response at each plane (this new response will be used to determine the response change at each plane due to the calibration weight installed at plane 1). We repeat the previous step for each balancing plane. The goal is to gather the necessary data to calculate all the influence coefficients (sensitivities) in the matrix. The general form of the influence coefficients matrix is shown on the Figure 39.

Response change at plane 1 due to the calibration weight at plane 1	Response change at plane 1 due to the calibration weight at plane 2	. . .	Response change at plane 1 due to the calibration weight at plane n
Response change at plane 2 due to the calibration weight at plane 1	Response change at plane 2 due to the calibration weight at plane 2	. . .	Response change at plane 2 due to the calibration weight at plane n
. . .	. . .	. . .	. . .
Response change at plane n due to the calibration weight at plane 1	Response change at plane n due to the calibration weight at plane 2	. . .	Response change at plane n due to the calibration weight at plane n

Figure 39 – the shape of the influence coefficient matrix

The trim balance weights at each plane can be calculated using the following equations [81]:

$$\vec{S}_{MATRIX} = \begin{bmatrix} \vec{S}_{(1,1)} & \vec{S}_{(1,2)} & \cdots & \vec{S}_{(1,n)} \\ \vec{S}_{(2,1)} & \vec{S}_{(2,2)} & \cdots & \vec{S}_{(2,n)} \\ \vdots & \vdots & \ddots & \vdots \\ \vec{S}_{(n,1)} & \vec{S}_{(n,2)} & \cdots & \vec{S}_{(n,n)} \end{bmatrix} \tag{16}$$

$$\vec{S}_{MATRIX} = \begin{bmatrix} \frac{\vec{V}_{CAL(1,1)} - \vec{V}_{INIT(1)}}{\vec{W}_{CAL(1)}} & \frac{\vec{V}_{CAL(1,2)} - \vec{V}_{INIT(1)}}{\vec{W}_{CAL(2)}} & \cdots & \frac{\vec{V}_{CAL(1,n)} - \vec{V}_{INIT(1)}}{\vec{W}_{CAL(n)}} \\ \frac{\vec{V}_{CAL(2,1)} - \vec{V}_{INIT(2)}}{\vec{W}_{CAL(1)}} & \frac{\vec{V}_{CAL(2,2)} - \vec{V}_{INIT(2)}}{\vec{W}_{CAL(2)}} & \cdots & \frac{\vec{V}_{CAL(2,n)} - \vec{V}_{INIT(2)}}{\vec{W}_{CAL(n)}} \\ \vdots & \vdots & \ddots & \vdots \\ \frac{\vec{V}_{CAL(n,1)} - \vec{V}_{INIT(n)}}{\vec{W}_{CAL(1)}} & \frac{\vec{V}_{CAL(n,2)} - \vec{V}_{INIT(n)}}{\vec{W}_{CAL(2)}} & \cdots & \frac{\vec{V}_{CAL(n,n)} - \vec{V}_{INIT(n)}}{\vec{W}_{CAL(n)}} \end{bmatrix} \tag{17}$$

$$\begin{bmatrix} \vec{W}_{BAL(1)} \\ \vec{W}_{BAL(2)} \\ \vdots \\ \vec{W}_{BAL(n)} \end{bmatrix} = \begin{bmatrix} \vec{S}_{(1,1)} & \vec{S}_{(1,2)} & \cdots & \vec{S}_{(1,n)} \\ \vec{S}_{(2,1)} & \vec{S}_{(2,2)} & \cdots & \vec{S}_{(2,n)} \\ \vdots & \vdots & \ddots & \vdots \\ \vec{S}_{(n,1)} & \vec{S}_{(n,2)} & \cdots & \vec{S}_{(n,n)} \end{bmatrix}^{-1} \begin{bmatrix} \vec{V}_{INIT(1)} \\ \vec{V}_{INIT(2)} \\ \vdots \\ \vec{V}_{INIT(n)} \end{bmatrix} \tag{18}$$

where:

$\vec{S}_{\mathrm{MATRIX}}$ – the influence coefficients matrix (matrix of sensitivities)

$\vec{S}_{(\mathrm{n,k})}$ – sensitivity of the plane **n** due to the calibration weight installed at plane **k**

$\vec{V}_{\mathrm{CAL(n,k)}}$ – response of the plane **n** during the run with calibration weight installed at plane **k**

$\vec{V}_{\mathrm{INIT(n)}}$ – initial response of the plane **n** (with no calibration weights installed)

$\vec{W}_{CAL(k)}$ – calibration weight installed at plane **k**

$\vec{W}_{BAL(k)}$ – calculated balance weight for plane **k**

4.3 Multi plane balancing software tool

The *Multi Plane Balancing Software Tool* available within the developed balancing system is capable of calculating the trim balance weights for a maximum of six balancing planes. However, this number was chosen arbitrary and the deciding factor was the appearance of the front panel. Addition of more balancing planes would require a scroller to move through the input data cluster which would cause part of the data to not be visible, therefore a decision has been made to limit the number of balancing planes to six. A balancing at more than six planes is almost never required and in case that such need would arise the software tool can be very easily modified to accommodate more planes. The front panel of the *Multi Plane Balancing Software Tool* (Figure 40) consists of the following items:

A) the influence coefficients method input data – lets the user input the magnitudes and phases of the calibration weights at each plane and the magnitudes and phases of the vibration recorded at each plane during all the runs (initial and calibration),

B) the trim balance weights cluster – displays the calculated trim balance weight for each of the balancing planes,

C) the single trim balance cluster – displays the magnitude and phase of the trim balance weight calculated for the plane chosen by the user in the *Plot Settings* cluster,

D) the distribution cluster – displays the magnitude and phase of the combined weights on the *Weights Plot*,

E) the difference cluster – displays the magnitude and phase of the difference between the balance weight calculated for the plane chosen by the user and the combined weights on the *Weights Plot*,

F) weights plot settings – lets the user set the rotation direction, balance plane for which the *Weights Plot* shall be used, number of possible weight locations and angle offset,

G) the application control cluster – lets the user choose the number of balancing planes, clear the data from the input cluster and stop the application,

H) weights plot – displays all the information about the weight distribution but can be also used to manually input the balance weights and to observe changes in weight distribution,

I) possible weights – lists all possible balance weights loaded from a file,

J) trim offset control – can be used to input the calculated balance weight from a previous balancing,

K) weight distribution settings – set the maximum number of allowed weight locations, load possible balance weights from a file, perform automatic balance weights distribution, abort the automatic distribution, clear all the data from weights plot, stop the application.

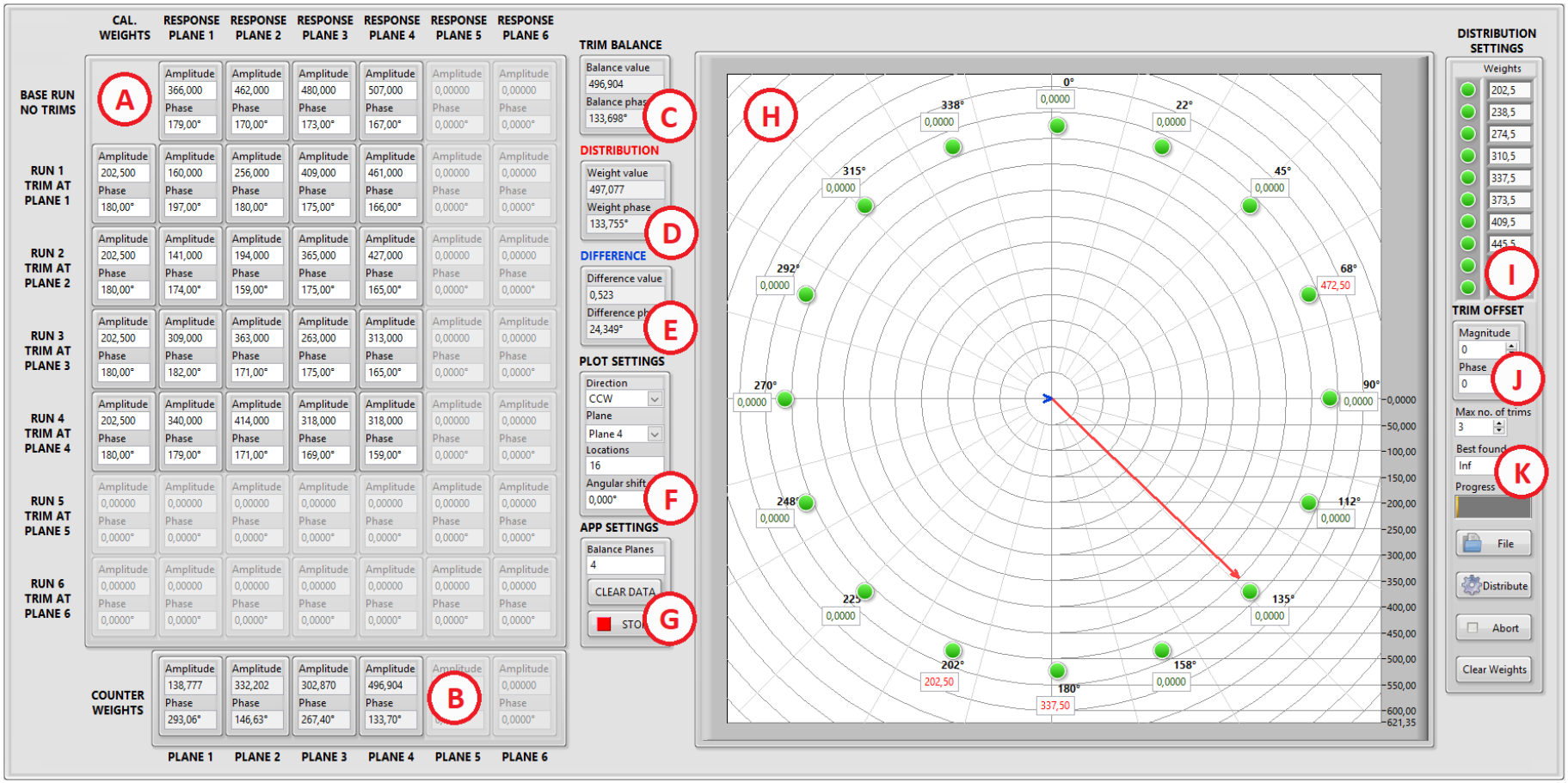

Figure 40 - the front panel of the Multi Plane Balancing Application

4.4 **Balancing results**

The following scenarios has been tested:

A) Scenario 101

Configuration no. 1 (balancing at four planes - Figure 37, top)

Balancing speed: 3000 rpm

Coarse calibration weights: 108 g-mm

Fine balancing weights: 72 g-mm

Calibration weights location: predictated angle of the unbalance

Results: Table 8

Response at different planes registered during a speed sweep: Figure 41

Combined response at all planes registered during a speed sweep: Figure 42

The coarse balancing gave satisfactory results (the combined responses at all planes has been attenuated to one third of the initial system's response). The fine balancing failed for the 3000 rpm rotational speed, however both the coarse and fine balancing responses are almost identical up to 2600 rpm. The reason for the poor results of the fine balancing was most likely the very light calibration weights used.

B) Scenario 102

Configuration no. 1 (balancing at four planes - Figure 37, top)

Balancing speed: 3000 rpm

Coarse calibration weights: 202.5 g-mm

Fine balancing weights: 135 g-mm

Calibration weights location: predictated angle of the unbalance

Results: Table 9

Response at different planes registered during a speed sweep: Figure 43

Combined response at all planes registered during a speed sweep: Figure 44

Both the coarse and fine balancing gave good results for the entire range of the speed. The final response of the system for the balancing speed was reduced by 14 times, compared to the initial response. Higher calibration weights clearly gave better results. One drawback of the fine balancing performed is that the reponse at the resonance at plane 2 (2100 rpm) was higher when compared to the unbalanced system and the system with coarse balance weights applied.

C) Scenario 103

Configuration no. 1 (balancing at four planes - Figure 37, top)

Balancing speed: 3000 rpm

Coarse and fine calibration weights: chosen to maximally attenuate the response at the calibration plane but without flipping the phase of the response

Calibration weights location: predictated angle of the unbalance

Results: Table 10

Response at different planes registered during a speed sweep: Figure 45

Combined response at all planes registered during a speed sweep: Figure 46

This was the last balancing performed for 3000 rpm speed and it was by far the most successful. The response of the system was greatly attenuated in the entire range of rotational speeds as well as at the resonance at plane 2. The effects of the balancing at speeds higher than the balancing speed unfortunately could not be observed because the 3000 rpm is the maximal operating speed of the system.

D) Scenario 104

Configuration no. 1 (balancing at four planes - Figure 37, top)

Balancing speed: 2500 rpm

Coarse calibration weights: 202.5 g-mm

Fine balancing weights: 135 g-mm

Calibration weights location: predictated angle of the unbalance

Results: Table 11

Response at different planes registered during a speed sweep: Figure 47

Combined response at all planes registered during a speed sweep: Figure 48

This was the first balancing performed for the 2500 rpm rotational speed. A relatively light calibration weights were used which didn't provide excellent results, however the final response of the system was still reduced to one sixth of the initial response. The speed sweep charts show an interesting trend for the fine balancing, which could not be observed earlier, when the system was being balanced at its maximum operating speed. The response is best attenuated at one particular speed (approximately 2650 rpm in this case) in the vicinity of the balancing speed, however the system's response gets much worse quickly after that. The fine balancing has better response than the coarse balancing up to 2850 rpm.

E) Scenario 105

Configuration no. 1 (balancing at four planes - Figure 37, top)

Balancing speed: 2500 rpm

Coarse calibration weights: 472.5 g-mm

Fine balancing weights: 108 g-mm

Calibration weights location: predictated angle of the unbalance

Results: Table 12

Response at different planes registered during a speed sweep: Figure 49

Combined response at all planes registered during a speed sweep: Figure 50

This was the best balancing performed for the 2500 rpm rotational speed – the final system's response was attenuated by 16 times, compared to the initial response. The speed sweep charts show that the applied balances are perfectly matched for the rotational speed as the fine balancing plot has its minimum exactly at the 2500 rpm. The resonance at plane 2 has also been greatly reduced. The fine balancing has better response than the coarse balancing but only up to 2600 rpm. After this speed the response of the fine balancing is very quickly rising up, even to the point that it exceeds the initial system's response at the maximum operating speed.

F) Scenarios 105÷108

Configuration no. 1 (balancing at four planes - Figure 37, top)

Balancing speed: 2500 rpm

Coarse calibration weights: 472.5 g-mm

Calibration weights location: predictated angle of the unbalance + α (sc. 105: α=0°, sc. 106: α=90°, sc. 107: α=180°, sc. 108: α=270°)

Results: Table 13

Response at different planes registered during a speed sweep: Figure 51

Combined response at all planes registered during a speed sweep: Figure 52

These 4 runs were performed to compare the calibration weight angle location impact on the balancing results. Only coarse balancing was perfomed for each scenario. Both the results and the speed sweep charts clearly indicate that placing the calibration weights at the predicted angle of the unbalance is the most effective approach. The overall system's response is very stable in the entire range of speeds. The balancing performed with calibration weights installed opposite to the predicted angle of the unbalance gave very good results for lower speeds, however it fails miserably when the higher speeds are considered. The additional advantage of installing

the calibration weights at the predicated angle of the unbalance is that it attenuates the response also during the calibration runs which is a very desirable effect. All other approaches are causing the response of the system to be higher during the calibration runs.

G) Scenario 109

Configuration no. 1 (balancing at four planes - Figure 37, top)

Balancing speed: 2500 rpm

Coarse calibration weights: 742.5 g-mm

Fine balancing weights: 135 g-mm

Calibration weights location: predictated angle of the unbalance

Results: Table 14

Response at different planes registered during a speed sweep: Figure 53

Combined response at all planes registered during a speed sweep: Figure 54

This was the last balancing run performed for the 2500 rpm at all 4 balancing planes. For coarse balancing the heaviest calibration weights were used which resulted in excellent results. However, the fine balancing didn't improve the system's response and in fact one of the calibration runs performed during the fine balancing had the best overall response. This shows that when the system's response after the coarse balancing is already very good, further balancing might not be practicable and in that situation often an experienced engineer may provide the prediction for the fine balancing weights based on the information visible on Bode and polar plots. Looking at the speed sweep charts it is apparent that the fine balancing performed by the software tool gave astonishing results but at the wrong speed – the combined system's response at approximately 2350 rpm is very close to 0, however it quickly gets worse as the speed gets higher. All the balancing runs recorded show excellent attenuation of the resonance at plane 2. This run is a best example of what the balancing for a particular rotational speed really means – it pins down the system's response causing it to have its minimum at one particular speed due to the weights added. However, after exceeding this speed the additional mass is causing the response to quickly rise up.

H) Scenario 110

Configuration no. 2 (balancing at two planes - Figure 37, middle)

Balancing speed: 2500 rpm

Coarse calibration weights: 202.5 g-mm

Fine balancing weights: 72 g-mm

Calibration weights location: predictated angle of the unbalance

Results: Table 15

Response at different planes registered during a speed sweep: Figure 55

Combined response at all planes registered during a speed sweep: Figure 56

This was the first run using a new test stand configuration. The balancing was performed only at two planes (plane no. 2 and plane no. 3), however the measurements used for balancing have not been direct, meaning that measurement at plane no. 1 was used for balancing at plane no. 2 and measurement at plane no. 4 was used for balancing at plane no. 3. The measurements at planes no. 2 and 3 were still recorded, however they haven't been used for balancing purposes. This configuration was especially designed for systems which have their balancing planes closer to the middle of the rotor, however the measurements can be only performed at the rotor ends. The tests started with relatively low calibration weights. The speed sweep charts show that the coarse and fine balancing have very similar responses. The final response of the system has been attenuated by 7 times, when only the measurements used for balancing are considered, and 8 times when all the measurements are considered. This proves that the developed balancing system works even when the test stand configuration is far from perfect.

I) Scenario 111

Configuration no. 2 (balancing at two planes - Figure 37, middle)

Balancing speed: 2500 rpm

Coarse calibration weights: 472.5 g-mm

Fine balancing weights: 135 g-mm

Calibration weights location: predictated angle of the unbalance

Results: Table 16

Response at different planes registered during a speed sweep: Figure 57

Combined response at all planes registered during a speed sweep: Figure 58

This was the second balancing performed only at two planes (plane no. 2 and plane no. 3), with the not-direct balancing measurements. The calibration weights

have been increased which had an impact especially on the fine balancing. First, the overall response has been attenuated, however only for speeds below 2450 rpm – for higher speeds the the coarse balancing shows better performance. Second, the fine balancing completely attenuated the resonance at plane no. 2, what hasn't been accomplished for any of the previous balancing. The response of the fine balancing at speeds approaching the maximum speed of the system is much worse than even the response of the unbalanced system, which again proves that after performing a balancing for a particular speed, the system should never be operated beyond that velocity.

J) Scenario 112

Configuration no. 2 (balancing at two planes - Figure 37, middle)

Balancing speed: 2500 rpm

Coarse calibration weights: 742.5 g-mm

Fine balancing weights: 202.5 g-mm

Calibration weights location: predictated angle of the unbalance

Results: Table 17

Response at different planes registered during a speed sweep: Figure 59

Combined response at all planes registered during a speed sweep: Figure 60

This was the last balancing performed only at two planes (plane no. 2 and plane no. 3), with the not-direct balancing measurements. The calibration weights have been increased further which provided excellent results. When only the measurements used for balancing are considered, the final response of the system was exceptional (attenuation by 13 times) considering that the balancing was performed with no direct measurements at the calibration planes. The complete attenuation of the resonance at plane no. 2 was again accomplished. The fine balancing proves to be superior up to the balancing speed (2500 rpm) with its response quickly rising up at higher speeds.

K) Scenario 113

Configuration no. 3 (balancing at two planes - Figure 37, bottom)

Balancing speed: 2500 rpm

Coarse calibration weights: 202.5 g-mm

Fine balancing weights: 72 g-mm

Calibration weights location: predictated angle of the unbalance

Results: Table 18

Response at different planes registered during a speed sweep: Figure 61

Combined response at all planes registered during a speed sweep: Figure 62

This was the first run using the final test stand configuration. The balancing was performed only at two planes (plane no. 2 and plane no. 3) and this time the measurements used for balancing have been direct, meaning that measurement at plane no. 2 was used for balancing at plane no. 2 and measurement at plane no. 3 was used for balancing at plane no. 3. The measurements at planes no. 1 and 4 were still recorded, however they haven't been used for balancing purposes. This configuration was tested to compare the results of the balancing with and without direct measurements at balancing planes. The tests with direct measurements again started with relatively low calibration weights, however this time the results were excellent even for the coarse balancing (attenuation by 10 times). The overall performance of the fine balancing is even better for speeds up to the balancing speed.

L) Scenario 114

Configuration no. 3 (balancing at two planes - Figure 37, bottom)

Balancing speed: 2500 rpm

Coarse calibration weights: 472.5 g-mm

Fine balancing weights: 108 g-mm

Calibration weights location: predictated angle of the unbalance

Results: Table 19

Response at different planes registered during a speed sweep: Figure 63

Combined response at all planes registered during a speed sweep: Figure 64

This was the second run using the final test stand configuration. The balancing was performed only at two planes (plane no. 2 and plane no. 3) with the direct measurements at the balancing planes. The calibration weights were increased which led to even better results. When only the measurements at the balancing planes are considered the coarse balancing reduced the unbalance by 12 times and the fine

balancing by 25 times. When all the the measurements are considered the final response of the system was attenuated by 9 times which is still a great result, considering that the measurements were taken at all four planes while the balancing was only performed at two of them. The speed sweep charts show that the fine and coarse balancing have very similar responses with the fine balancing being slightly lower but not different in shape, which is a very desirable result.

M) Scenario 115

Configuration no. 3 (balancing at two planes - Figure 37, bottom)

Balancing speed: 2500 rpm

Coarse calibration weights: 742.5 g-mm

Fine balancing weights: 202.5 g-mm

Calibration weights location: predictated angle of the unbalance

Results: Table 20

Response at different planes registered during a speed sweep: Figure 65

Combined response at all planes registered during a speed sweep: Figure 66

This was the last run using the final test stand configuration. The balancing was performed only at two planes (plane no. 2 and plane no. 3) with the direct measurements at the balancing planes. The calibration weights were increased even further which again improved the balancing results. When only the measurements at the balancing planes are considered the final response of the system was reduced by over 30 times which is an marvelous result. Overall the balancing using direct measurements at the planes gave better and more stable results.

Table 8 – balancing results (scenario 101)

Speed [rpm]	Plane	Run 1 (base)		Calibration plane 1		Run 2		Calibration plane 2		Run 3		Description
		Mag [um]	Phase [°]	Mag [gmm]	Phase [°]	Mag [um]	Phase [°]	Mag [gmm]	Phase [°]	Mag [um]	Phase [°]	
3000	1	288	159	108	158	224	159	X	X	216	157	Coarse balancing Base - Run 1 Cal. plane 1 - Run 2 Cal. plane 2 - Run 3 Cal. plane 3 - Run 4 Cal. plane 4 - Run 5
	2	273	173	X	X	228	175	108	180	206	171	
	3	444	162	X	X	393	164	X	X	364	158	
	4	493	162	X	X	460	164	X	X	429	160	
	Sum	1498	-	-	-	1305	87,12%	-	-	1215	81,11%	

Calibration plane 3		Run 4		Calibration plane 4		Run 5		Calculated balances		Combined balances		Run 6	
Mag [gmm]	Phase [°]	Mag [um]	Phase [°]	Mag [gmm]	Phase [°]	Mag [um]	Phase [°]	Mag [gmm]	Phase [°]	Mag [gmm]	Phase [°]	Mag [um]	Phase [°]
X	X	263	160	X	X	264	158	104	110	104	110	90	159
X	X	249	174	X	X	246	173	364	188	364	188	73	195
108	158	323	164	X	X	306	160	383	44	383	44	173	200
X	X	379	162	108	158	335	161	372	192	372	192	180	175
-	-	1214	81,04%	-	-	1151	76,84%	-	-	-	-	516	34,45%

Speed [rpm]	Plane	Run 6 (base)		Calibration plane 1		Run 7		Calibration plane 2		Run 8		Description
		Mag [um]	Phase [°]	Mag [gmm]	Phase [°]	Mag [um]	Phase [°]	Mag [gmm]	Phase [°]	Mag [um]	Phase [°]	
3000	1	90	159	72	158	70	161	X	X	79	145	Fine balancing Base - Run 6 Cal. plane 1 - Run 7 Cal. plane 2 - Run 8 Cal. plane 3 - Run 9 Cal. plane 4 - Run 10
	2	73	195	X	X	52	213	72	203	45	168	
	3	173	200	X	X	161	208	X	X	112	220	
	4	180	175	X	X	171	176	X	X	127	176	
	Sum	516	-	-	-	454	30,31%	-	-	363	24,23%	

Calibration plane 3		Run 9		Calibration plane 4		Run 10		Calculated balances		Combined balances		Run 11	
Mag [gmm]	Phase [°]	Mag [um]	Phase [°]	Mag [gmm]	Phase [°]	Mag [um]	Phase [°]	Mag [gmm]	Phase [°]	Mag [gmm]	Phase [°]	Mag [um]	Phase [°]
X	X	95	154	X	X	100	158	378	104	481	106	101	353
X	X	68	175	X	X	75	182	662	199	1022	195	138	356
72	203	75	217	X	X	105	230	967	337	1172	355	300	137
X	X	94	161	72	180	66	190	556	153	876	168	290	151
-	-	332	22,16%	-	-	346	23,10%	-	-	-	-	829	55,34%

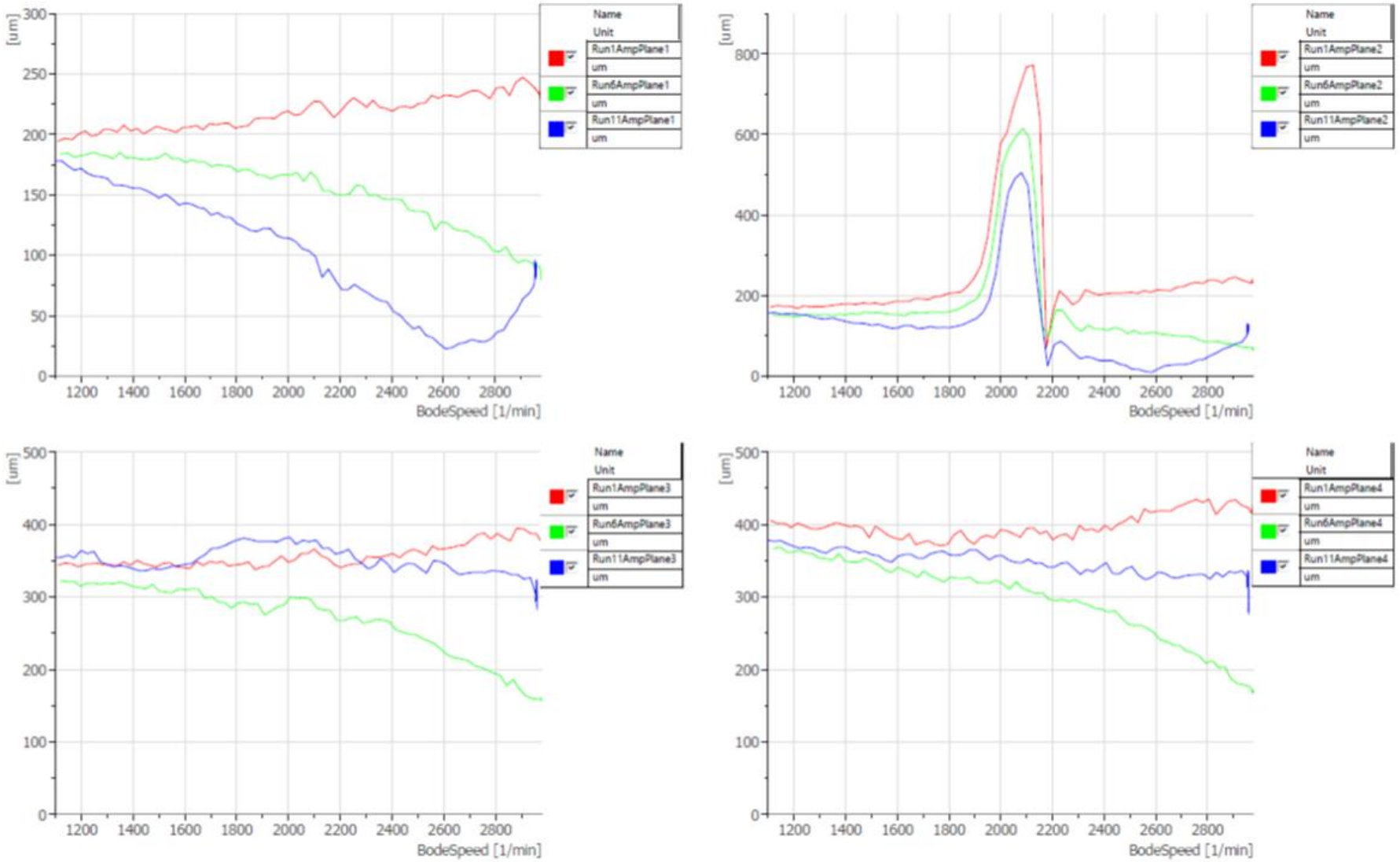

Figure 41 - the response of the system at different planes (red – initial, green – coarse balancing, blue – fine balancing, scenario 101)

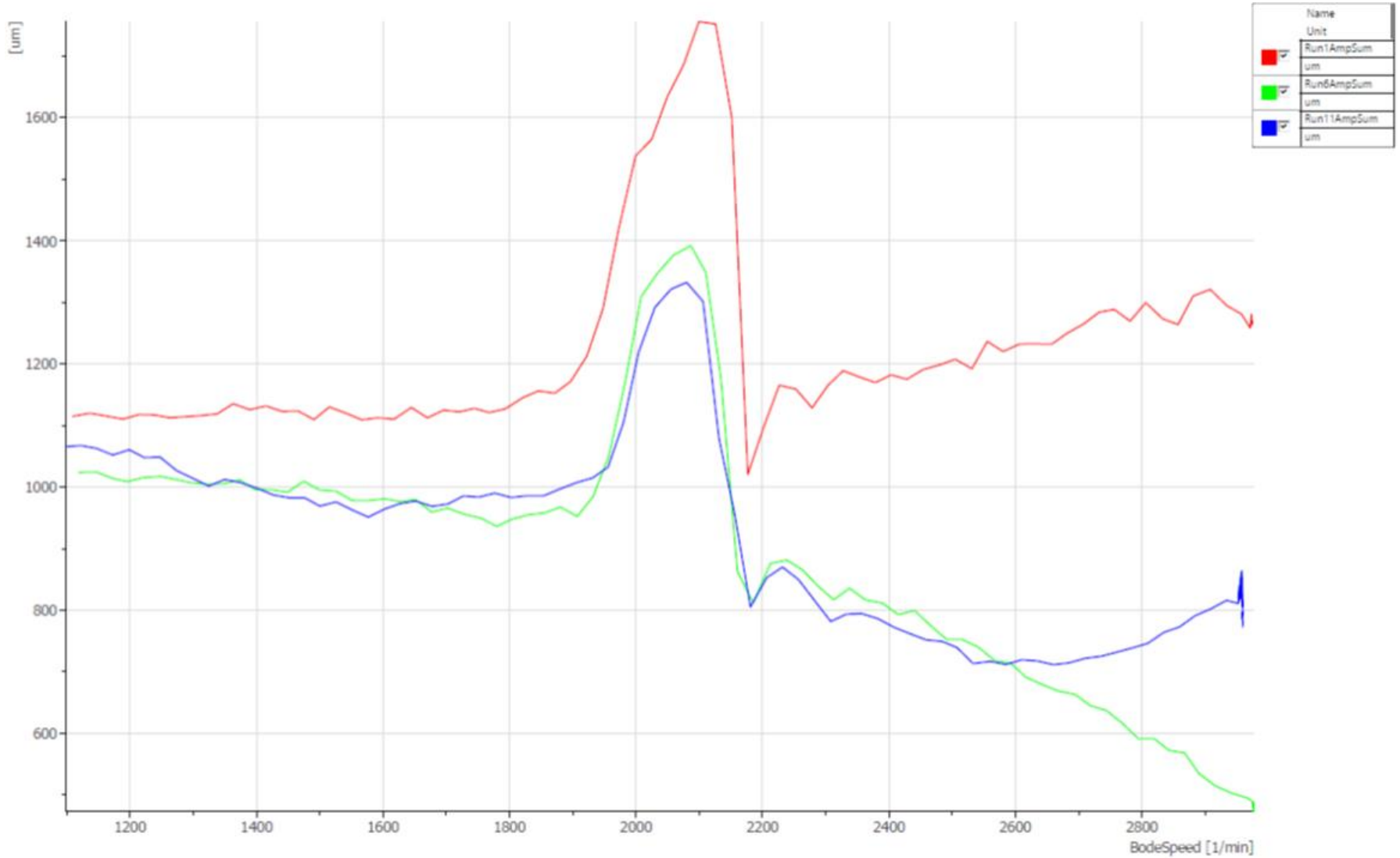

Figure 42 – the sum of responses at all the planes (red – initial, green – coarse balancing, blue – fine balancing, scenario 101)

Table 9 – balancing results (scenario 102)

Speed [rpm]	Plane	Run 1 (base)		Calibration plane 1		Run 2		Calibration plane 2		Run 3		Description
		Mag [um]	Phase [°]	Mag [gmm]	Phase [°]	Mag [um]	Phase [°]	Mag [gmm]	Phase [°]	Mag [um]	Phase [°]	
3000	1	528	168	203	180	364	153	X	X	290	148	Coarse balancing Base - Run 1 Cal. plane 1 - Run 2 Cal. plane 2 - Run 3 Cal. plane 3 - Run 4 Cal. plane 4 - Run 5
	2	504	174	X	X	345	165	203	180	235	161	
	3	1063	172	X	X	860	164	X	X	630	159	
	4	933	170	X	X	810	164	X	X	640	159	
	Sum	3028	-	-	-	2379	78,57%	-	-	1795	59,28%	

Calibration plane 3		Run 4		Calibration plane 4		Run 5		Calculated balances		Combined balances		Run 6	
Mag [gmm]	Phase [°]	Mag [um]	Phase [°]	Mag [gmm]	Phase [°]	Mag [um]	Phase [°]	Mag [gmm]	Phase [°]	Mag [gmm]	Phase [°]	Mag [um]	Phase [°]
X	X	400	153	X	X	430	156	887	88	887	88	186	178
X	X	315	162	X	X	354	163	745	251	745	251	154	168
203	180	560	155	X	X	635	155	628	19	628	19	330	193
X	X	510	153	203	180	540	150	796	164	796	164	180	203
-	-	1785	58,95%	-	-	1959	64,70%	-	-	-	-	850	28,07%

Speed [rpm]	Plane	Run 6 (base)		Calibration plane 1		Run 7		Calibration plane 2		Run 8		Description
		Mag [um]	Phase [°]	Mag [gmm]	Phase [°]	Mag [um]	Phase [°]	Mag [gmm]	Phase [°]	Mag [um]	Phase [°]	
3000	1	186	178	135	180	100	188	X	X	128	207	Fine balancing Base - Run 6 Cal. plane 1 - Run 7 Cal. plane 2 - Run 8 Cal. plane 3 - Run 9 Cal. plane 4 - Run 10
	2	154	168	X	X	116	174	135	180	92	180	
	3	330	193	X	X	406	195	X	X	388	202	
	4	180	203	X	X	269	199	X	X	265	207	
	Sum	850	-	-	-	891	29,43%	-	-	873	28,83%	

Calibration plane 3		Run 9		Calibration plane 4		Run 10		Calculated balances		Combined balances		Run 11	
Mag [gmm]	Phase [°]	Mag [um]	Phase [°]	Mag [gmm]	Phase [°]	Mag [um]	Phase [°]	Mag [gmm]	Phase [°]	Mag [gmm]	Phase [°]	Mag [um]	Phase [°]
X	X	128	171	X	X	148	183	214	220	761	100	42	189
X	X	123	164	X	X	150	175	240	138	688	232	34	152
135	203	105	286	X	X	140	184	312	237	427	352	45	270
X	X	199	316	135	203	88	305	182	45	726	151	94	291
-	-	555	18,33%	-	-	526	17,37%	-	-	-	-	215	7,10%

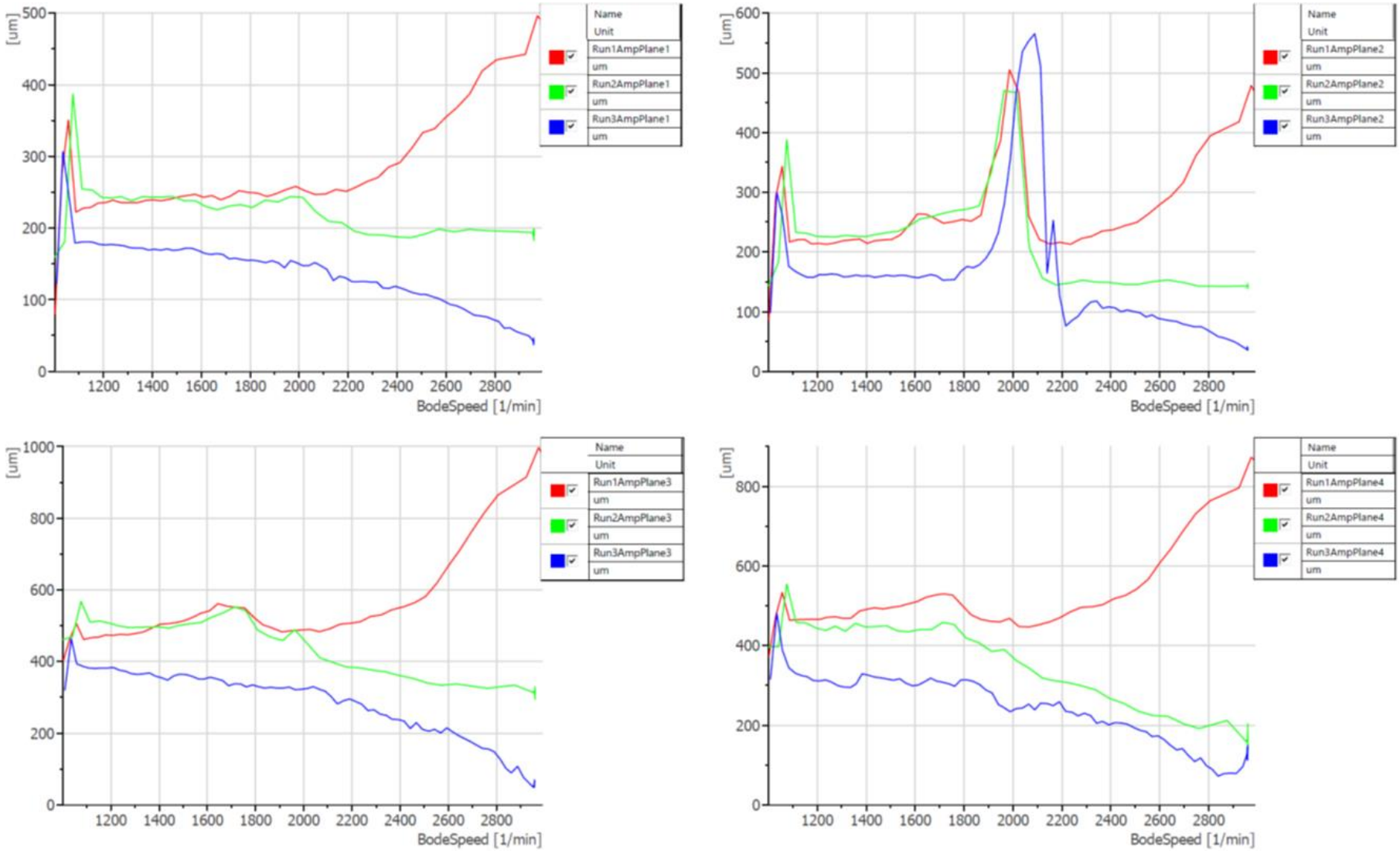

Figure 43 - the response of the system at different planes (red – initial, green – coarse balancing, blue – fine balancing, scenario 102)

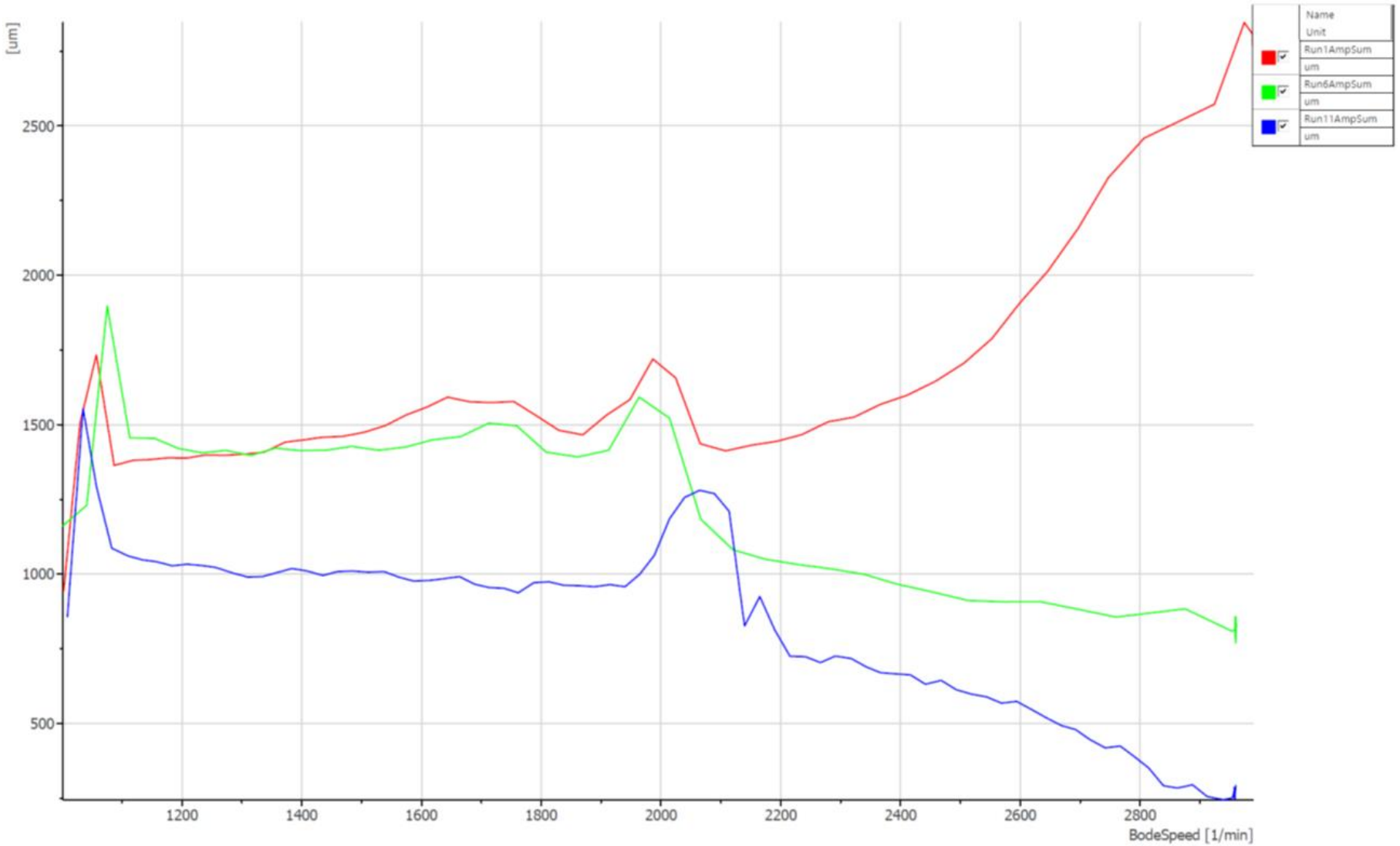

Figure 44 - the sum of responses at all the planes (red – initial, green – coarse balancing, blue – fine balancing, scenario 102)

Table 10 - balancing results (scenario 103)

Speed [rpm]	Plane	Run 1 (base)		Calibration plane 1		Run 2		Calibration plane 2		Run 3		Description
		Mag [um]	Phase [°]	Mag [gmm]	Phase [°]	Mag [um]	Phase [°]	Mag [gmm]	Phase [°]	Mag [um]	Phase [°]	
3000	1	330	164	473	158	84	150	X	X	99	127	Coarse balancing Base - Run 1 Cal. plane 1 - Run 2 Cal. plane 2 - Run 3 Cal. plane 3 - Run 4 Cal. plane 4 - Run 5
	2	326	175	X	X	102	180	473	180	74	133	
	3	550	166	X	X	315	158	X	X	206	141	
	4	565	165	X	X	410	157	X	X	333	149	
	Sum	1771	-	-	-	911	51,44%	-	-	712	40,20%	

Calibration plane 3		Run 4		Calibration plane 4		Run 5		Calculated balances		Combined balances		Run 6	
Mag [gmm]	Phase [°]	Mag [um]	Phase [°]	Mag [gmm]	Phase [°]	Mag [um]	Phase [°]	Mag [gmm]	Phase [°]	Mag [gmm]	Phase [°]	Mag [um]	Phase [°]
X	X	223	161	X	X	239	160	500	99	500	99	83	165
X	X	209	173	X	X	220	173	541	225	541	225	77	164
338	158	92	177	X	X	103	161	509	1	509	1	157	167
X	X	145	160	338	158	79	148	608	162	608	162	125	165
-	-	669	37,78%	-	-	641	36,19%	-	-	-	-	442	24,96%

Speed [rpm]	Plane	Run 6 (base)		Calibration plane 1		Run 7		Calibration plane 2		Run 8		Description
		Mag [um]	Phase [°]	Mag [gmm]	Phase [°]	Mag [um]	Phase [°]	Mag [gmm]	Phase [°]	Mag [um]	Phase [°]	
3000	1	83	165	203	158	17	182	X	X	34	174	Fine balancing Base - Run 6 Cal. plane 1 - Run 7 Cal. plane 2 - Run 8 Cal. plane 3 - Run 9 Cal. plane 4 - Run 10
	2	77	164	X	X	16	180	171	158	21	178	
	3	157	167	X	X	112	201	X	X	88	218	
	4	125	165	X	X	112	204	X	X	73	200	
	Sum	442	-	-	-	257	14,51%	-	-	216	12,20%	

Calibration plane 3		Run 9		Calibration plane 4		Run 10		Calculated balances		Combined balances		Run 11	
Mag [gmm]	Phase [°]	Mag [um]	Phase [°]	Mag [gmm]	Phase [°]	Mag [um]	Phase [°]	Mag [gmm]	Phase [°]	Mag [gmm]	Phase [°]	Mag [um]	Phase [°]
X	X	91	161	X	X	98	167	396	178	695	133	25	55
X	X	76	160	X	X	88	169	148	18	415	234	25	32
99	158	55	212	X	X	101	180	72	208	446	357	34	87
X	X	45	141	72	158	52	220	50	234	626	166	35	61
-	-	267	15,08%	-	-	339	19,14%	-	-	-	-	119	6,72%

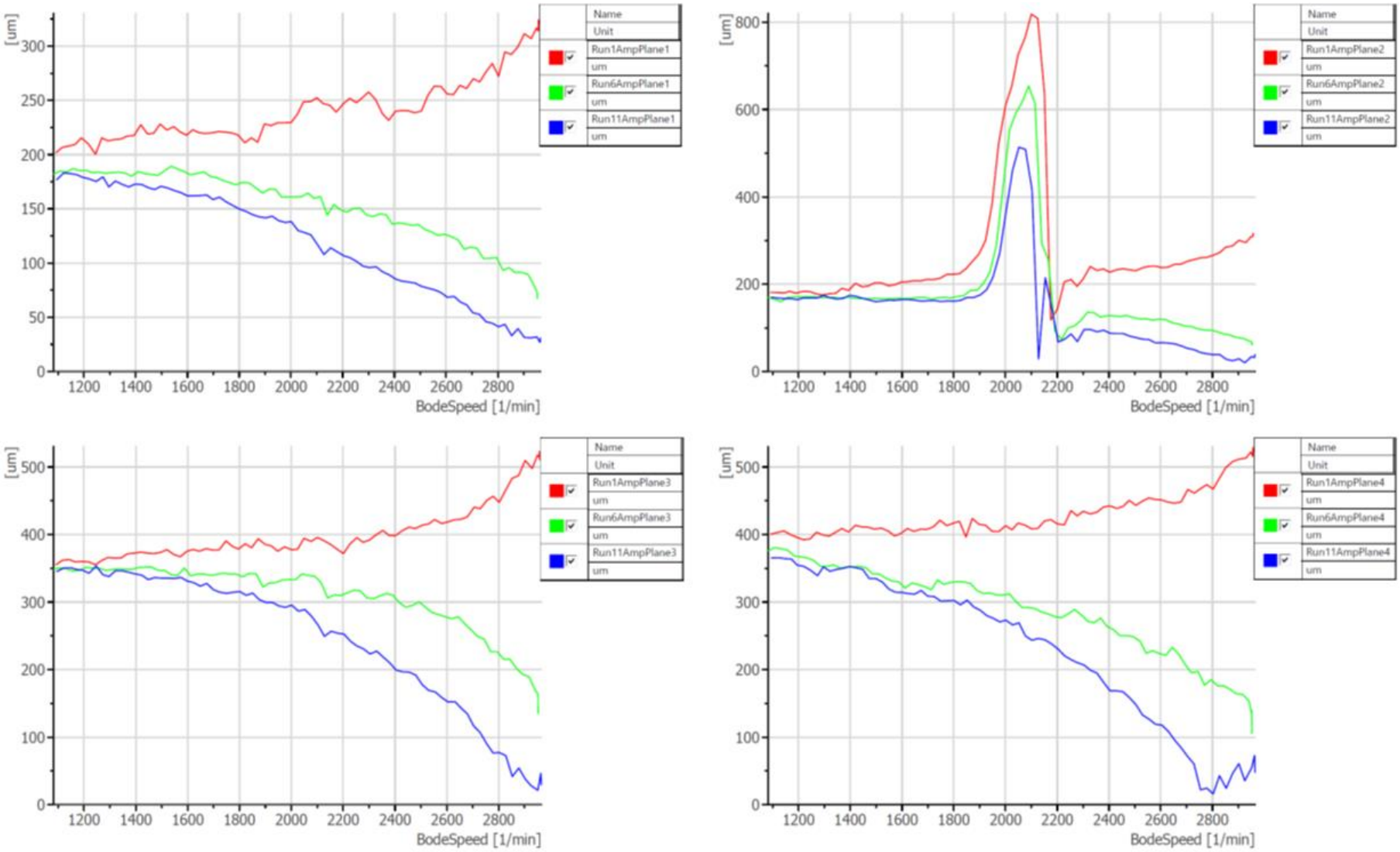

Figure 45 - the response of the system at different planes (red – initial, green – coarse balancing, blue – fine balancing, scenario 103)

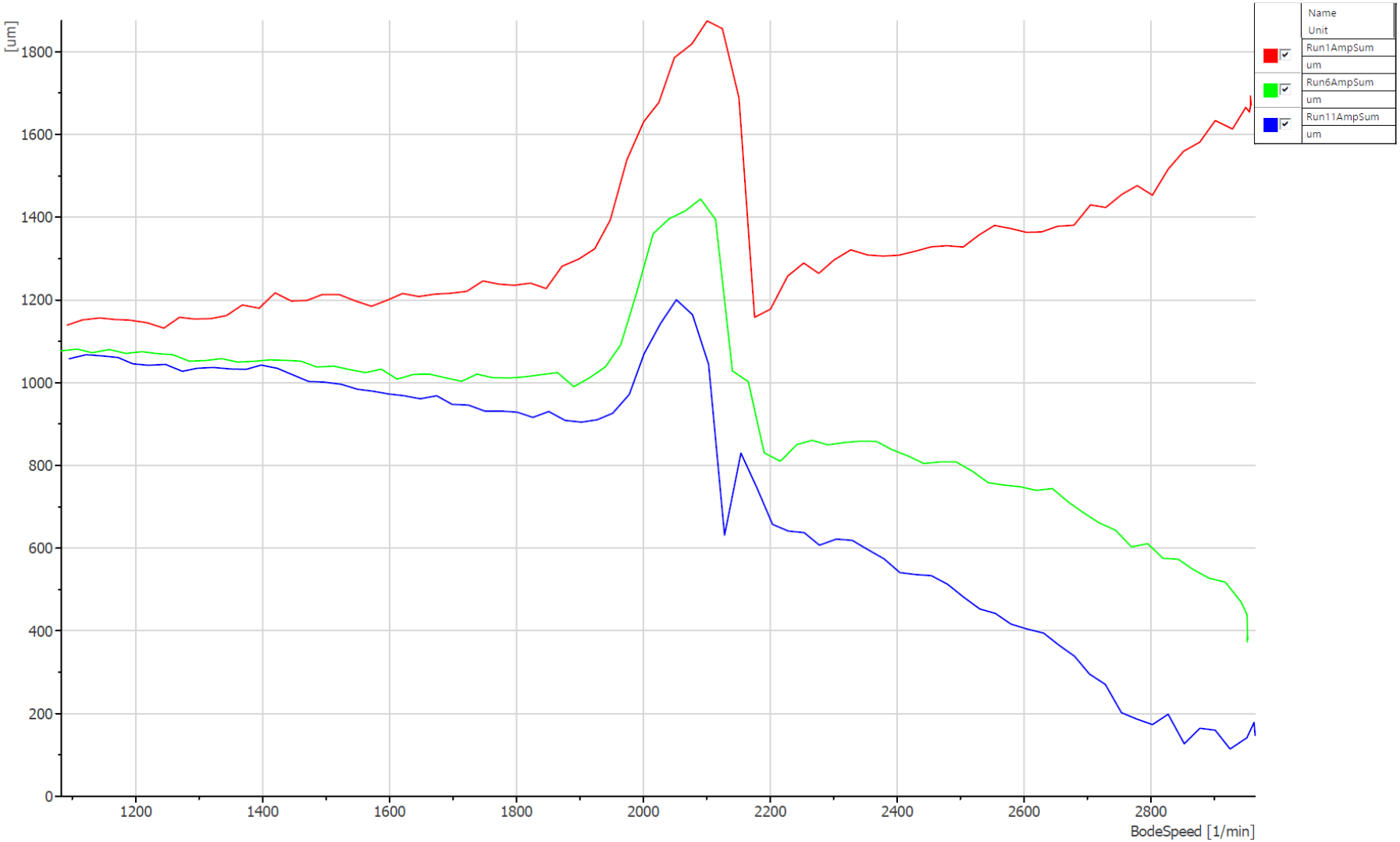

Figure 46 - the sum of responses at all the planes (red – initial, green – coarse balancing, blue – fine balancing, scenario 103)

Table 11 – balancing results (scenario 104)

Speed [rpm]	Plane	Run 1 (base)		Calibration plane 1		Run 2		Calibration plane 2		Run 3		Description
		Mag [um]	Phase [°]	Mag [gmm]	Phase [°]	Mag [um]	Phase [°]	Mag [gmm]	Phase [°]	Mag [um]	Phase [°]	
2500	1	274	160	203	158	197	160	X	X	195	156	Coarse balancing Base - Run 1 Cal. plane 1 - Run 2 Cal. plane 2 - Run 3 Cal. plane 3 - Run 4 Cal. plane 4 - Run 5
	2	278	176	X	X	214	181	203	180	190	176	
	3	467	154	X	X	391	156	X	X	360	151	
	4	481	156	X	X	435	158	X	X	411	157	
	Sum	1500	-	-	-	1237	82,47%	-	-	1156	77,07%	

Calibration plane 3		Run 4		Calibration plane 4		Run 5		Calculated balances		Combined balances		Run 6	
Mag [gmm]	Phase [°]	Mag [um]	Phase [°]	Mag [gmm]	Phase [°]	Mag [um]	Phase [°]	Mag [gmm]	Phase [°]	Mag [gmm]	Phase [°]	Mag [um]	Phase [°]
X	X	228	162	X	X	239	161	625	62	625	62	119	166
X	X	231	181	X	X	243	179	1028	219	1028	219	80	171
203	158	273	161	X	X	286	158	808	65	808	65	170	152
X	X	314	163	203	158	287	164	752	224	752	224	242	145
-	-	1046	69,73%	-	-	1055	70,33%	-	-	-	-	611	40,73%

Speed [rpm]	Plane	Run 6 (base)		Calibration plane 1		Run 7		Calibration plane 2		Run 8		Description
		Mag [um]	Phase [°]	Mag [gmm]	Phase [°]	Mag [um]	Phase [°]	Mag [gmm]	Phase [°]	Mag [um]	Phase [°]	
2500	1	119	166	135	158	93	167	X	X	98	167	Fine balancing Base - Run 6 Cal. plane 1 - Run 7 Cal. plane 2 - Run 8 Cal. plane 3 - Run 9 Cal. plane 4 - Run 10
	2	80	171	X	X	59	174	135	180	53	169	
	3	170	152	X	X	138	149	X	X	105	145	
	4	242	145	X	X	211	150	X	X	180	149	
	Sum	611	-	-	-	501	47,90%	-	-	436	41,68%	

Calibration plane 3		Run 9		Calibration plane 4		Run 10		Calculated balances		Combined balances		Run 11	
Mag [gmm]	Phase [°]	Mag [um]	Phase [°]	Mag [gmm]	Phase [°]	Mag [um]	Phase [°]	Mag [gmm]	Phase [°]	Mag [gmm]	Phase [°]	Mag [um]	Phase [°]
X	X	119	166	X	X	119	166	1128	152	1293	123	19	169
X	X	80	169	X	X	84	171	635	325	1039	255	53	141
135	158	79	149	X	X	103	166	804	72	1608	69	78	157
X	X	138	147	135	135	140	161	726	228	1477	226	100	122
-	-	416	27,73%	-	-	446	29,73%	-	-	-	-	250	16,67%

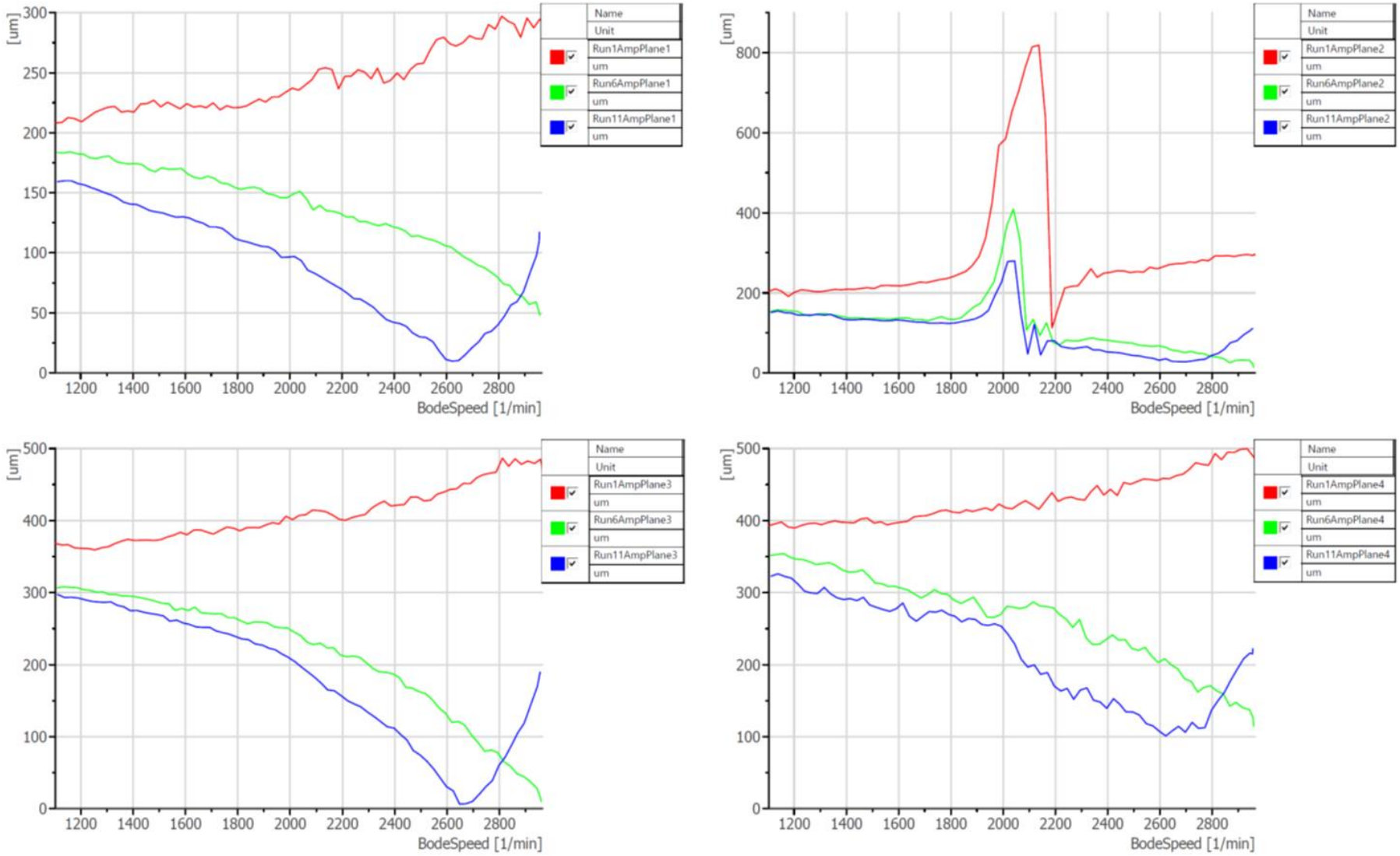

Figure 47 - the response of the system at different planes (red – initial, green – coarse balancing, blue – fine balancing, scenario 104)

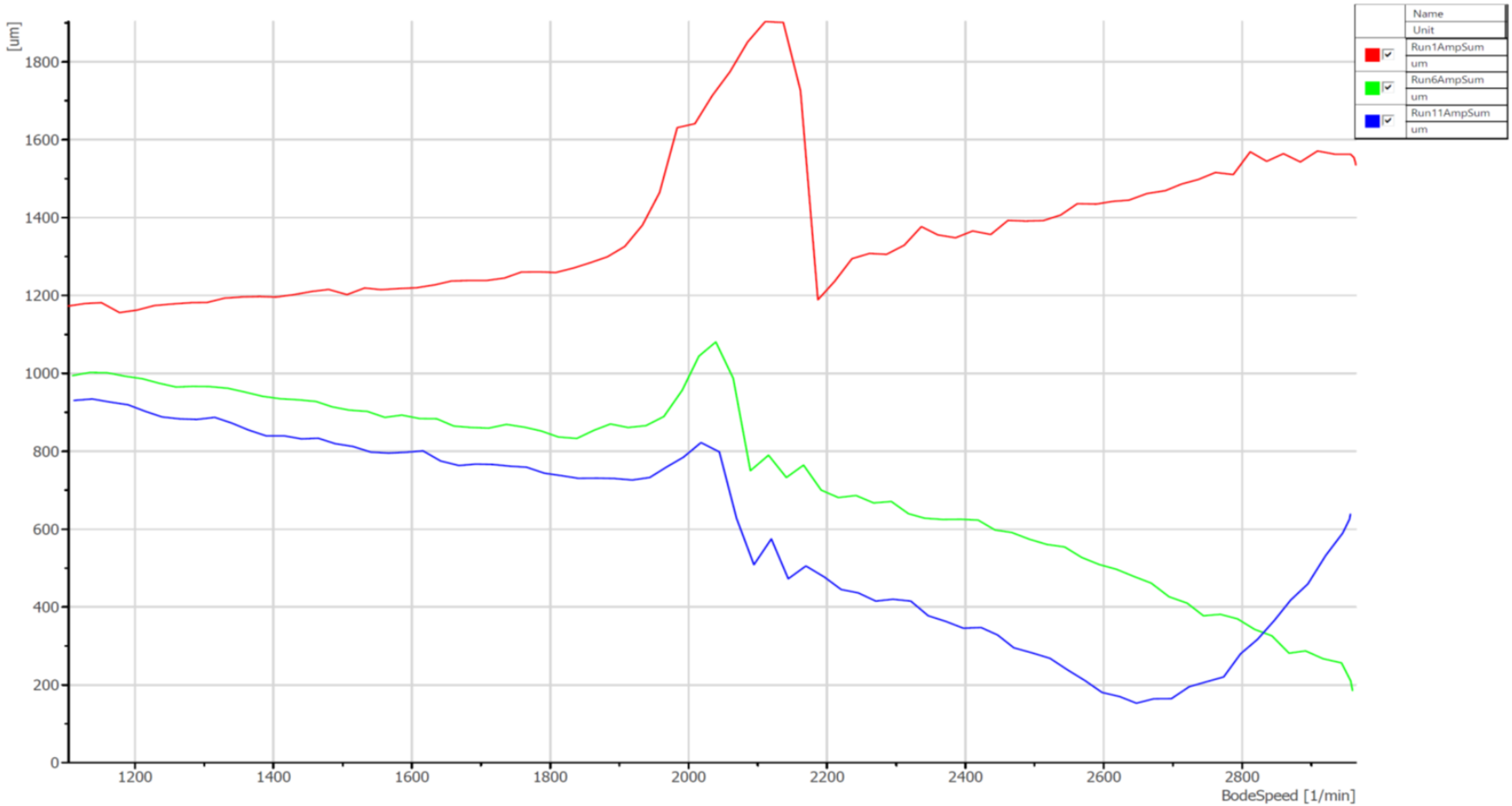

Figure 48 - the sum of responses at all the planes (red – initial, green – coarse balancing, blue – fine balancing, scenario 104)

Table 12 – balancing results (scenario 105)

Speed [rpm]	Plane	Run 1 (base)		Calibration plane 1		Run 2		Calibration plane 2		Run 3		Description
		Mag [um]	Phase [°]	Mag [gmm]	Phase [°]	Mag [um]	Phase [°]	Mag [gmm]	Phase [°]	Mag [um]	Phase [°]	
2500	1	394	162	473	158	174	161	X	X	148	148	Coarse balancing Base - Run 1 Cal. plane 1 - Run 2 Cal. plane 2 - Run 3 Cal. plane 3 - Run 4 Cal. plane 4 - Run 5
	2	396	175	X	X	193	179	473	180	125	160	
	3	695	160	X	X	458	158	X	X	315	144	
	4	652	160	X	X	499	161	X	X	399	150	
	Sum	2137	-	-	-	1324	61,96%	-	-	987	46,19%	

Calibration plane 3		Run 4		Calibration plane 4		Run 5		Calculated balances		Combined balances		Run 6	
Mag [gmm]	Phase [°]	Mag [um]	Phase [°]	Mag [gmm]	Phase [°]	Mag [um]	Phase [°]	Mag [gmm]	Phase [°]	Mag [gmm]	Phase [°]	Mag [um]	Phase [°]
X	X	236	164	X	X	288	162	779	133	779	133	106	166
X	X	206	177	X	X	261	175	450	273	450	273	87	162
473	158	158	169	X	X	284	157	602	58	602	58	94	180
X	X	208	161	473	158	230	160	834	193	834	193	61	180
-	-	808	37,81%	-	-	1063	49,74%	-	-	-	-	348	16,28%

Speed [rpm]	Plane	Run 6 (base)		Calibration plane 1		Run 7		Calibration plane 2		Run 8		Description
		Mag [um]	Phase [°]	Mag [gmm]	Phase [°]	Mag [um]	Phase [°]	Mag [gmm]	Phase [°]	Mag [um]	Phase [°]	
2500	1	106	166	203	180	52	148	X	X	58	160	Fine balancing Base - Run 6 Cal. plane 1 - Run 7 Cal. plane 2 - Run 8 Cal. plane 3 - Run 9 Cal. plane 4 - Run 10
	2	87	162	X	X	61	137	203	158	48	150	
	3	94	180	X	X	48	159	X	X	64	158	
	4	61	180	X	X	20	197	X	X	46	146	
	Sum	348	-	-	-	181	8,47%	-	-	216	10,11%	

Calibration plane 3		Run 9		Calibration plane 4		Run 10		Calculated balances		Combined balances		Run 11	
Mag [gmm]	Phase [°]	Mag [um]	Phase [°]	Mag [gmm]	Phase [°]	Mag [um]	Phase [°]	Mag [gmm]	Phase [°]	Mag [gmm]	Phase [°]	Mag [um]	Phase [°]
X	X	95	164	X	X	97	170	65	289	720	135	30	173
X	X	87	152	X	X	111	173	458	152	447	212	10	106
135	180	42	146	X	X	82	155	176	76	772	62	50	355
X	X	22	60	108	180	68	135	68	184	901	192	58	49
-	-	246	11,51%	-	-	358	16,75%	-	-	-	-	148	6,93%

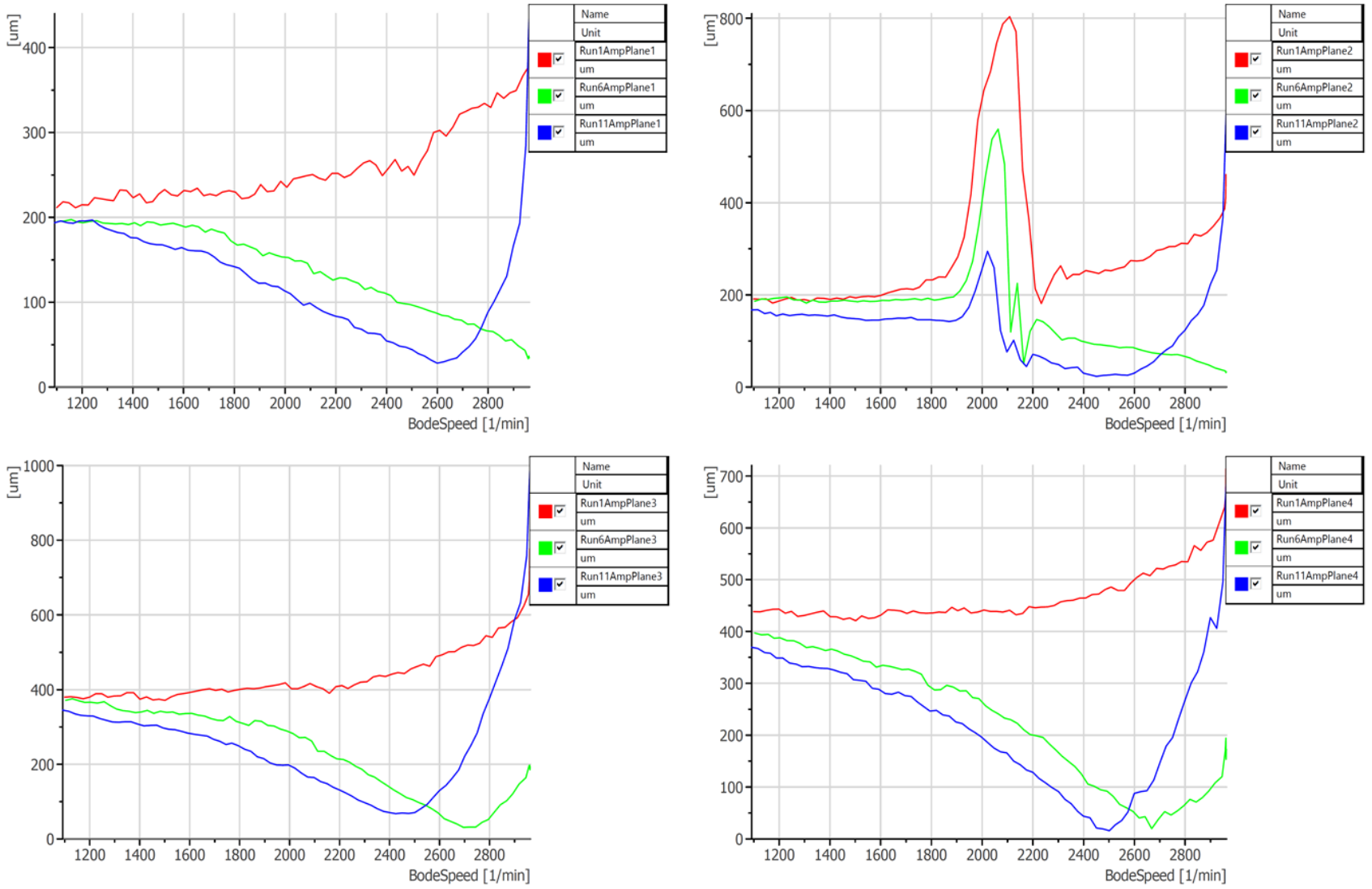

Figure 49 - the response of the system at different planes (red – initial, green – coarse balancing, blue – fine balancing, scenario 105)

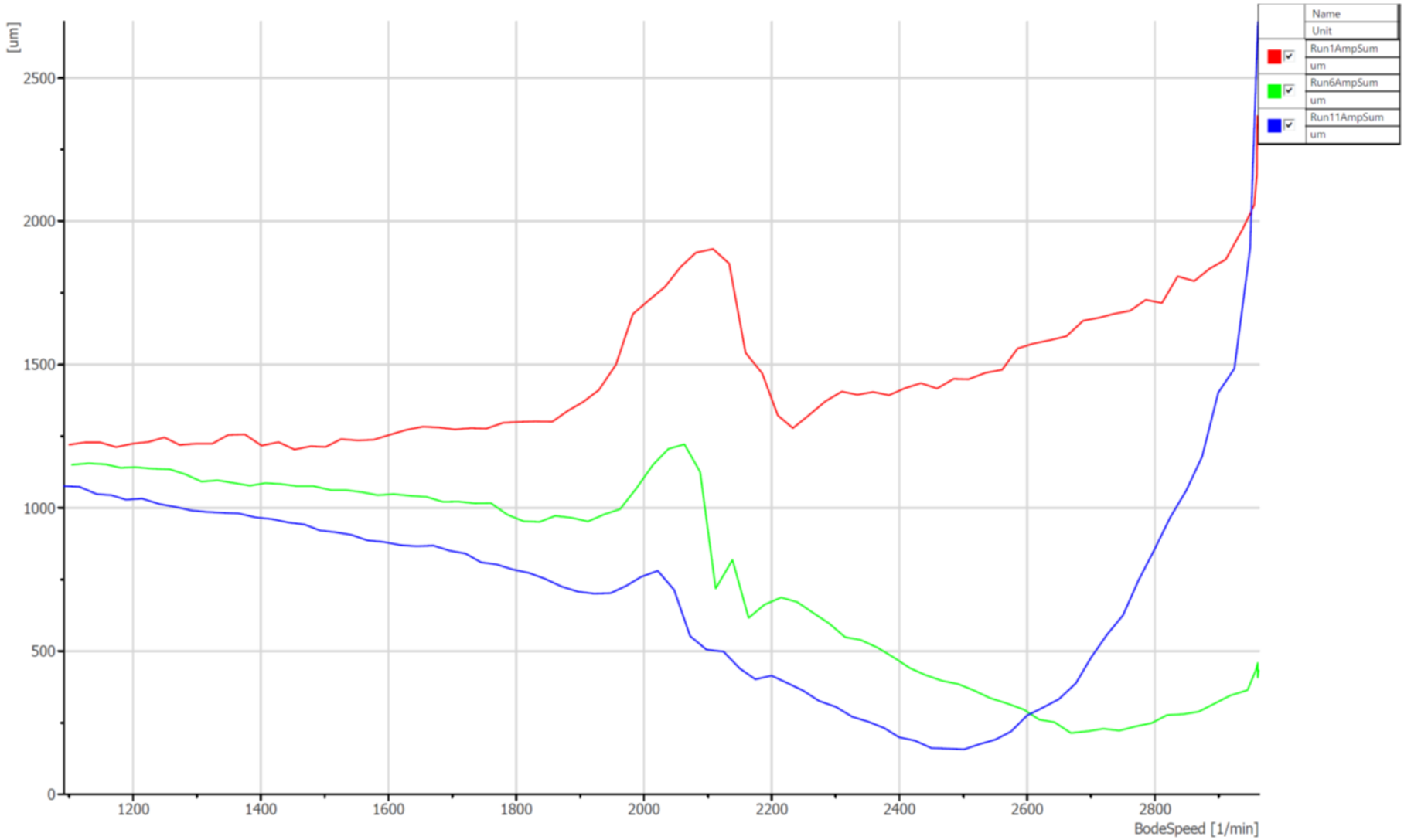

Figure 50 - the sum of responses at all the planes (red – initial, green – coarse balancing, blue – fine balancing, scenario 105)

Table 13 – balancing results (just coarse balancing, scenarios 105÷108)

Speed [rpm]	Plane	Run 1 (base)		Calibration plane 1		Run 2		Calibration plane 2		Run 3		Description
		Mag [um]	Phase [°]	Mag [gmm]	Phase [°]	Mag [um]	Phase [°]	Mag [gmm]	Phase [°]	Mag [um]	Phase [°]	
2500	1	394	162	473	158	174	161	X	X	148	148	Coarse balancing: scenario 105 Calibration weights installed at the predicted angle of the unbalance Base - Run 1 Cal. plane 1 - Run 2 Cal. plane 2 - Run 3 Cal. plane 3 - Run 4 Cal. plane 4 - Run 5
	2	396	175	X	X	193	179	473	180	125	160	
	3	695	160	X	X	458	158	X	X	315	144	
	4	652	160	X	X	499	161	X	X	399	150	
	Sum	2137	-	-	-	1324	61,96%	-	-	987	46,19%	
Calibration plane 3		**Run 4**		**Calibration plane 4**		**Run 5**		**Calculated balances**		**Run 6**		
Mag [gmm]	**Phase [°]**	**Mag [um]**	**Phase [°]**	**Mag [gmm]**	**Phase [°]**	**Mag [um]**	**Phase [°]**	**Mag [gmm]**	**Phase [°]**	**Mag [um]**	**Phase [°]**	
X	X	236	164	X	X	288	162	779	133	106	166	
X	X	206	177	X	X	261	175	450	273	87	162	
473	158	158	169	X	X	284	157	602	58	94	180	
X	X	208	161	473	158	230	160	834	193	61	180	
-	-	808	37,81%	-	-	1063	49,74%	-	-	348	16,28%	

Speed [rpm]	Plane	Run 1 (base)		Calibration plane 1		Run 2		Calibration plane 2		Run 3		Description
		Mag [um]	Phase [°]	Mag [gmm]	Phase [°]	Mag [um]	Phase [°]	Mag [gmm]	Phase [°]	Mag [um]	Phase [°]	
2500	1	394	162	473	248	396	136	X	X	452	137	Coarse balancing: scenario 106 Calibration weights installed at the predicted angle of the unbalance Base - Run 1 Cal. plane 1 - Run 2 Cal. plane 2 - Run 3 Cal. plane 3 - Run 4 Cal. plane 4 - Run 5
	2	396	175	X	X	362	150	473	270	427	145	
	3	695	160	X	X	655	139	X	X	753	134	
	4	652	160	X	X	616	145	X	X	672	140	
	Sum	2137	-	-	-	2029	94,95%	-	-	2304	107,81%	
Calibration plane 3		**Run 4**		**Calibration plane 4**		**Run 5**		**Calculated balances**		**Run 6**		
Mag [gmm]	**Phase [°]**	**Mag [um]**	**Phase [°]**	**Mag [gmm]**	**Phase [°]**	**Mag [um]**	**Phase [°]**	**Mag [gmm]**	**Phase [°]**	**Mag [um]**	**Phase [°]**	
X	X	380	149	X	X	374	154	1560	110	45	95	
X	X	379	158	X	X	370	165	1381	252	95	100	
473	248	724	125	X	X	690	131	728	349	382	107	
X	X	658	129	473	248	674	129	960	159	271	125	
-	-	2141	100,19%	-	-	2108	98,64%	-	-	793	37,11%	

Speed [rpm]	Plane	Run 1 (base)		Calibration plane 1		Run 2		Calibration plane 2		Run 3		Description
		Mag [um]	Phase [°]	Mag [gmm]	Phase [°]	Mag [um]	Phase [°]	Mag [gmm]	Phase [°]	Mag [um]	Phase [°]	
2500	1	394	162	473	338	583	161	X	X	558	161	Coarse balancing: scenario 107 Calibration weights installed at the predicted angle of the unbalance Base - Run 1 Cal. plane 1 - Run 2 Cal. plane 2 - Run 3 Cal. plane 3 - Run 4 Cal. plane 4 - Run 5
	2	396	175	X	X	572	171	473	0	562	174	
	3	695	160	X	X	809	156	X	X	832	159	
	4	652	160	X	X	713	156	X	X	731	157	
	Sum	2137	-	-	-	2677	125,27%	-	-	2683	125,55%	
Calibration plane 3		**Run 4**		**Calibration plane 4**		**Run 5**		**Calculated balances**		**Run 6**		
Mag [gmm]	**Phase [°]**	**Mag [um]**	**Phase [°]**	**Mag [gmm]**	**Phase [°]**	**Mag [um]**	**Phase [°]**	**Mag [gmm]**	**Phase [°]**	**Mag [um]**	**Phase [°]**	
X	X	454	156	X	X	448	158	453	260	64	110	
X	X	473	171	X	X	456	173	991	143	55	67	
473	338	931	152	X	X	894	154	439	272	385	24	
X	X	861	152	473	338	888	155	1013	163	312	25	
-	-	2719	127,23%	-	-	2686	125,69%	-	-	816	38,18%	

Speed [rpm]	Plane	Run 1 (base)		Calibration plane 1		Run 2		Calibration plane 2		Run 3		Description
		Mag [um]	Phase [°]	Mag [gmm]	Phase [°]	Mag [um]	Phase [°]	Mag [gmm]	Phase [°]	Mag [um]	Phase [°]	
2500	1	394	162	473	68	477	179	X	X	424	182	Coarse balancing: scenario 108 Calibration weights installed at the predicted angle of the unbalance Base - Run 1 Cal. plane 1 - Run 2 Cal. plane 2 - Run 3 Cal. plane 3 - Run 4 Cal. plane 4 - Run 5
	2	396	175	X	X	494	192	473	90	434	199	
	3	695	160	X	X	767	170	X	X	712	179	
	4	652	160	X	X	691	165	X	X	646	171	
	Sum	2137	-	-	-	2429	113,66%	-	-	2216	103,70%	
Calibration plane 3		**Run 4**		**Calibration plane 4**		**Run 5**		**Calculated balances**		**Run 6**		
Mag [gmm]	**Phase [°]**	**Mag [um]**	**Phase [°]**	**Mag [gmm]**	**Phase [°]**	**Mag [um]**	**Phase [°]**	**Mag [gmm]**	**Phase [°]**	**Mag [um]**	**Phase [°]**	
X	X	498	172	X	X	481	170	2395	176	10	242	
X	X	503	189	X	X	482	186	2320	327	35	269	
473	68	895	183	X	X	848	182	1235	111	200	235	
X	X	783	180	473	68	783	184	1049	211	170	231	
-	-	2679	125,36%	-	-	2594	121,39%	-	-	415	19,42%	

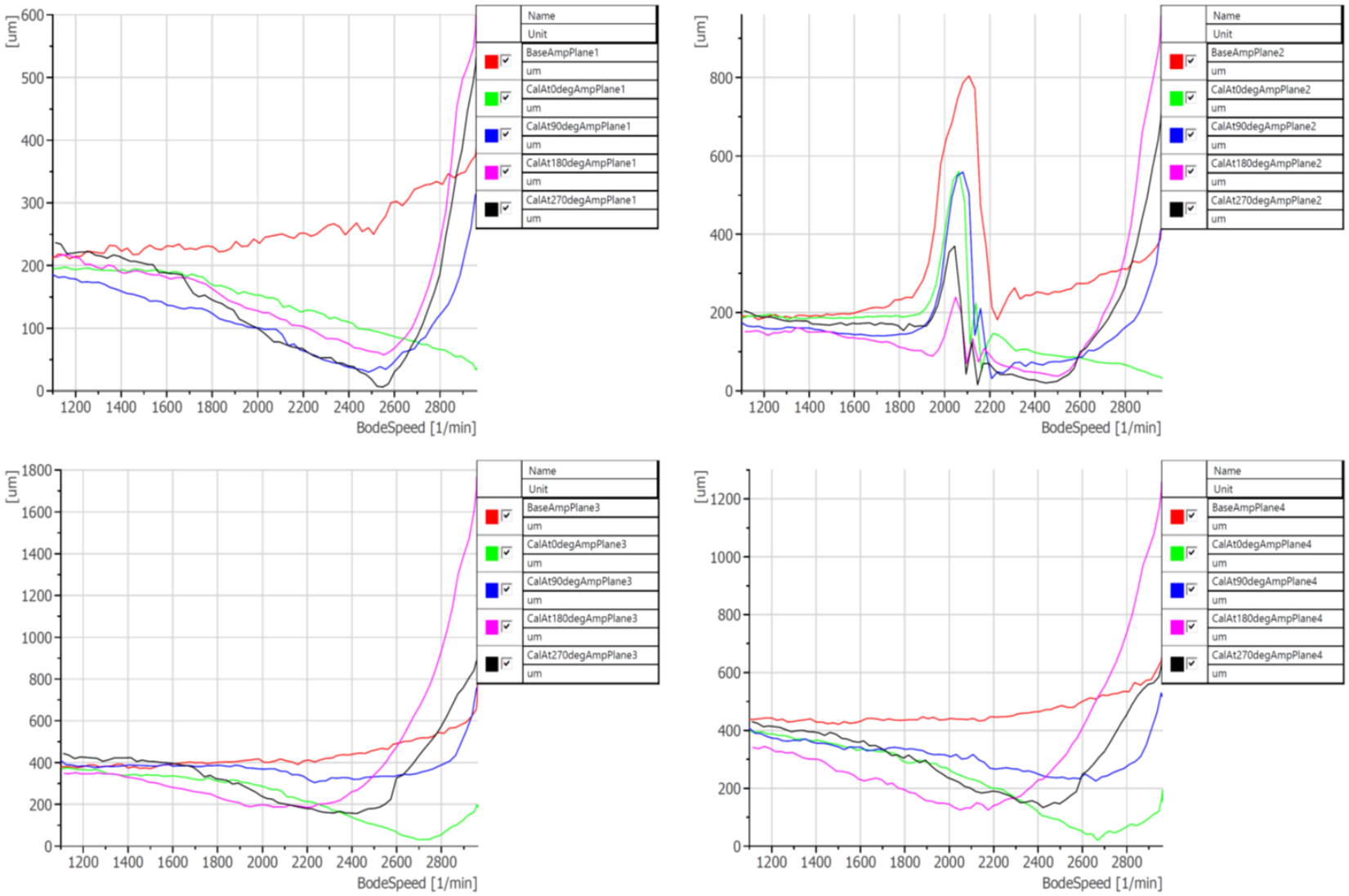

Figure 51 - the response at different planes (red – initial, green – scenario 105, blue – scenario 106, magenta – scenario 107, black – scenario 108)

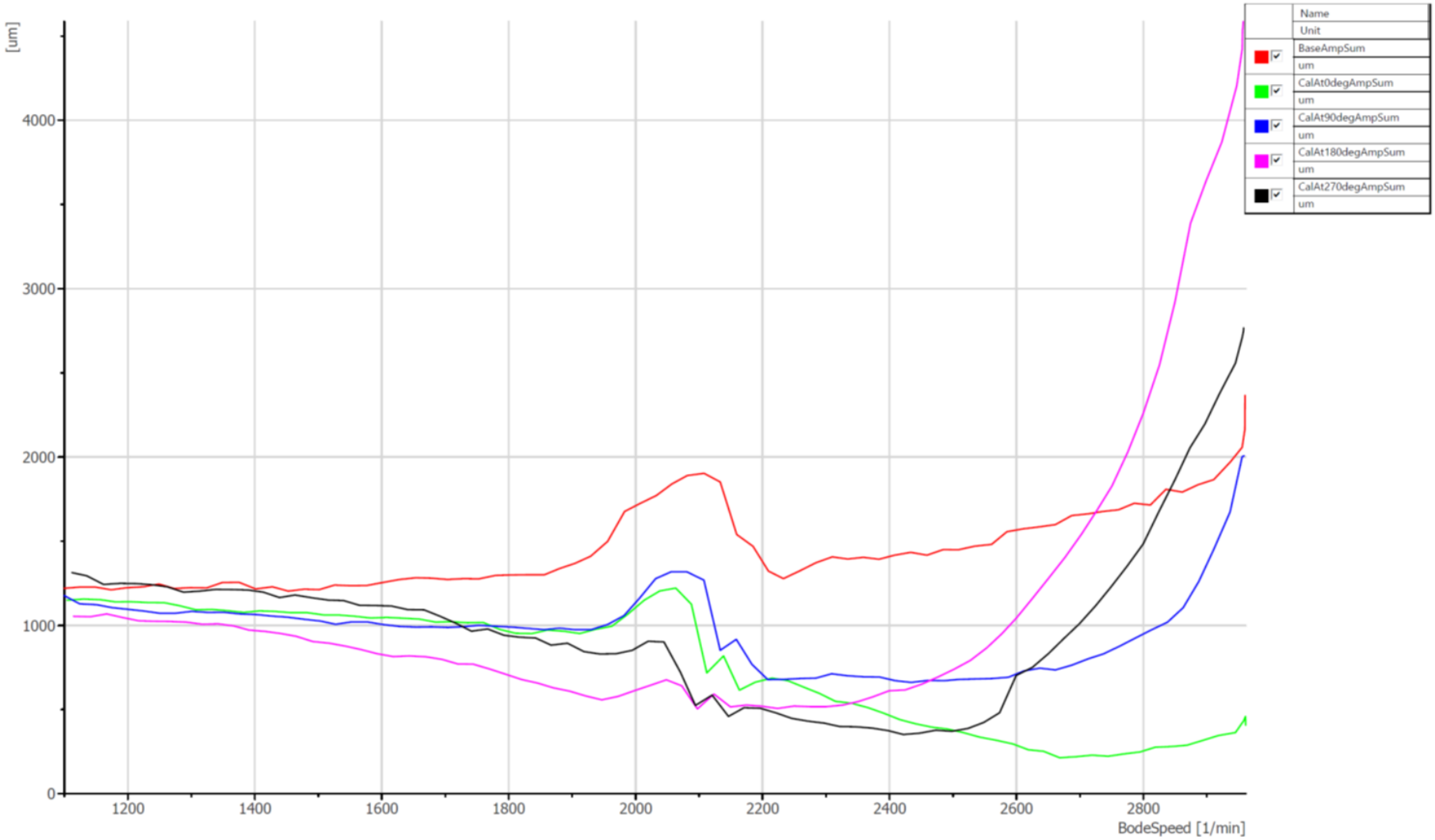

Figure 52 – the sum of the responses (red – initial, green – scenario 105, blue – scenario 106, magenta – scenario 107, black – scenario 108)

Table 14 - balancing results (scenario 109)

Speed [rpm]	Plane	Run 1 (base)		Calibration plane 1		Run 2		Calibration plane 2		Run 3		Description
		Mag [um]	Phase [°]	Mag [gmm]	Phase [°]	Mag [um]	Phase [°]	Mag [gmm]	Phase [°]	Mag [um]	Phase [°]	
2500	1	424	162	743	158	116	166	X	X	100	136	Coarse balancing Base - Run 1 Cal. plane 1 - Run 2 Cal. plane 2 - Run 3 Cal. plane 3 - Run 4 Cal. plane 4 - Run 5
	2	432	176	X	X	162	190	743	180	63	140	
	3	730	159	X	X	455	164	X	X	241	139	
	4	676	158	X	X	500	162	X	X	353	149	
	Sum	2262	-	-	-	1233	54,51%	-	-	757	33,47%	

Calibration plane 3		Run 4		Calibration plane 4		Run 5		Calculated balances		Combined balances		Run 6	
Mag [gmm]	Phase [°]	Mag [um]	Phase [°]	Mag [gmm]	Phase [°]	Mag [um]	Phase [°]	Mag [gmm]	Phase [°]	Mag [gmm]	Phase [°]	Mag [um]	Phase [°]
X	X	215	169	X	X	338	303	732	152	732	152	44	127
X	X	178	183	X	X	303	179	161	215	161	215	40	115
743	158	26	215	X	X	280	177	84	300	84	300	84	46
X	X	71	204	743	158	164	184	708	160	708	160	46	40
-	-	490	21,66%	-	-	1085	47,97%	-	-	-	-	214	9,46%

Speed [rpm]	Plane	Run 6 (base)		Calibration plane 1		Run 7		Calibration plane 2		Run 8		Description
		Mag [um]	Phase [°]	Mag [gmm]	Phase [°]	Mag [um]	Phase [°]	Mag [gmm]	Phase [°]	Mag [um]	Phase [°]	
2500	1	44	127	72	135	33	126	X	X	36	153	Fine balancing Base - Run 6 Cal. plane 1 - Run 7 Cal. plane 2 - Run 8 Cal. plane 3 - Run 9 Cal. plane 4 - Run 10
	2	40	115	X	X	28	108	72	112	22	167	
	3	84	46	X	X	77	41	X	X	44	44	
	4	46	40	X	X	44	38	X	X	32	51	
	Sum	214	-	-	-	182	8,05%	-	-	134	5,92%	

Calibration plane 3		Run 9		Calibration plane 4		Run 10		Calculated balances		Combined balances		Run 11	
Mag [gmm]	Phase [°]	Mag [um]	Phase [°]	Mag [gmm]	Phase [°]	Mag [um]	Phase [°]	Mag [gmm]	Phase [°]	Mag [gmm]	Phase [°]	Mag [um]	Phase [°]
X	X	48	141	X	X	49	137	555	146	1286	150	46	320
X	X	33	136	X	X	32	129	184	357	113	297	30	302
72	45	40	78	X	X	42	137	137	107	58	88	110	300
X	X	27	112	72	45	18	100	55	311	660	162	23	31
-	-	148	6,54%	-	-	141	6,23%	-	-	-	-	209	9,24%

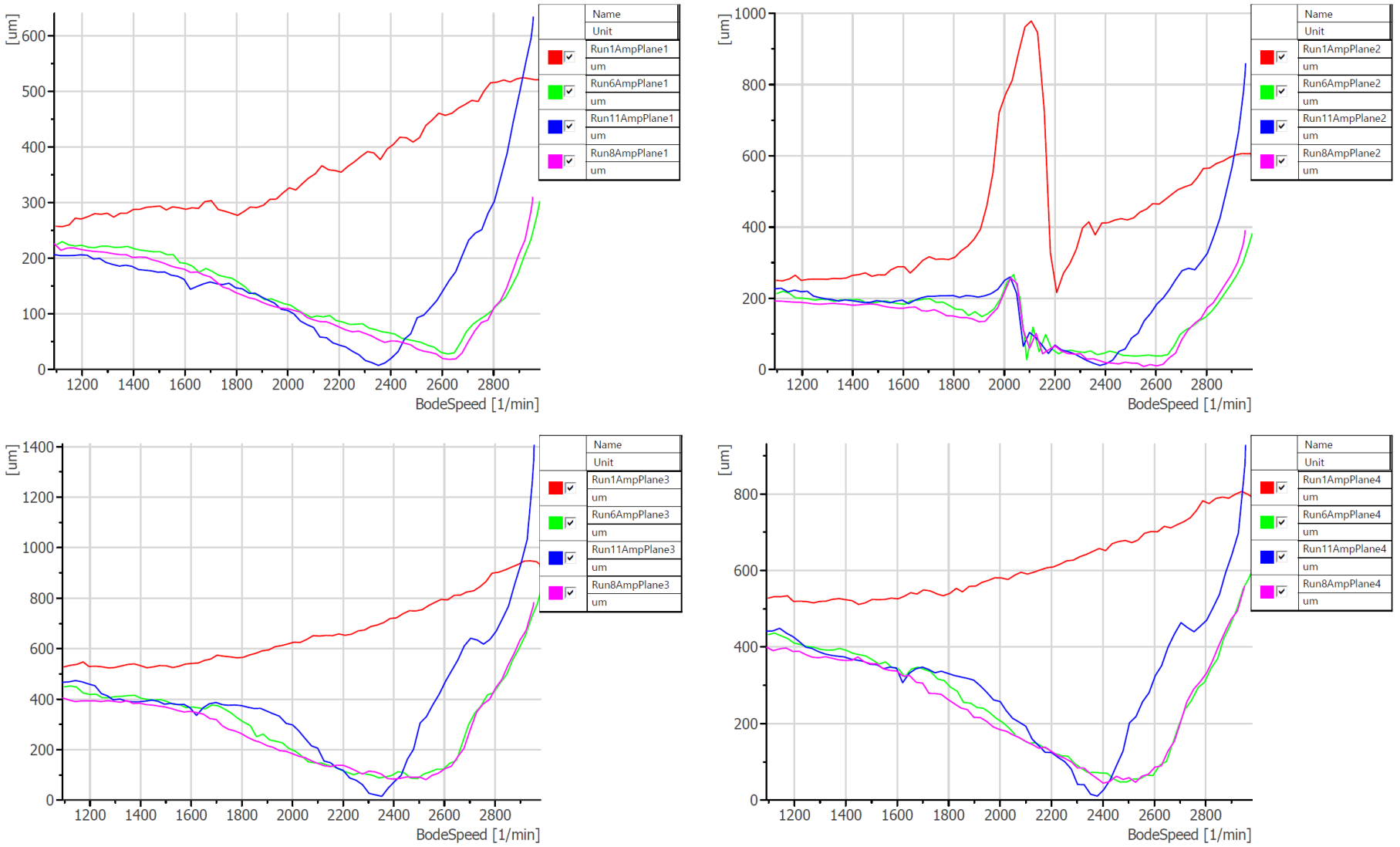

Figure 53 - the response at different planes (red – initial, green – coarse balancing, blue – fine balancing, magenta – best fine calibration result, scenario 109)

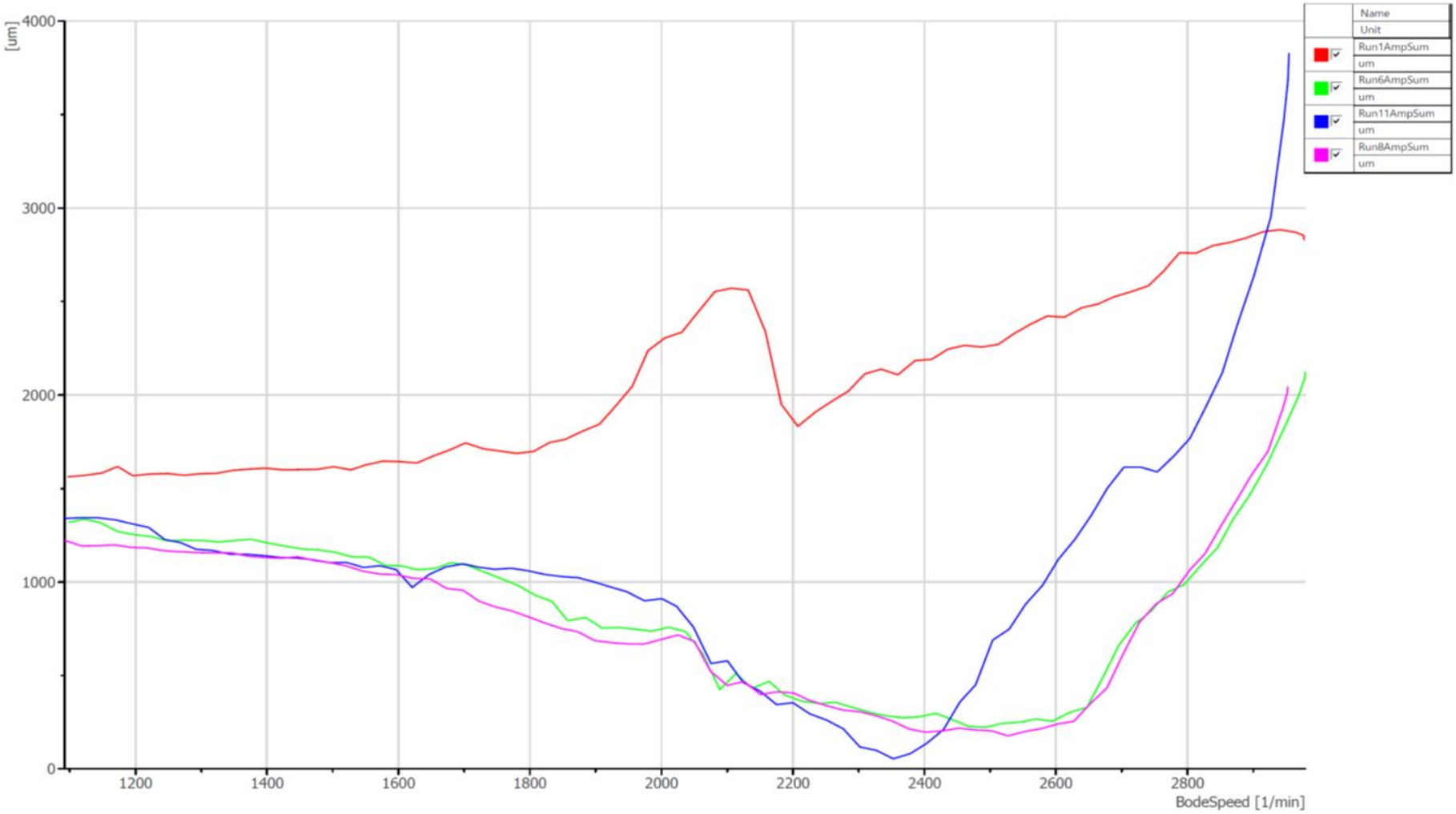

Figure 54 - the sum of responses (red – initial, green – coarse balancing, blue – fine balancing, magenta – best fine calibration result, scenario 109)

Table 15 - balancing results (scenario 110)

Speed [rpm]	Plane	Run 1 (base)		Calibration plane 2		Run 2		Calibration plane 3		Run 3	
		Mag [um]	Phase [°]	Mag [gmm]	Phase [°]	Mag [um]	Phase [°]	Mag [gmm]	Phase [°]	Mag [um]	Phase [°]
2500	1	402	160	X	X	293	157	X	X	349	163
	2	410	173	203	180	269	169	X	X	334	176
	3	725	155	X	X	605	151	203	158	542	162
	4	670	156	X	X	600	153	X	X	535	158
	Used	1072	-	-	-	893	83,30%	-	-	884	82,46%
	All	2207	-	-	-	1767	80,06%	-	-	1760	79,75%

Speed [rpm]	Plane	Calculated balances		Combined balances		Run 4		Description
		Mag [gmm]	Phase [°]	Mag [gmm]	Phase [°]	Mag [um]	Phase [°]	
2500	1	X	X	X	X	124	150	Coarse balancing at 2 planes. Calibration weight (202.5 gmm) installed at the predicted angle of the unbalance. Measurement at plane 1 used as the balancing measurement for plane 2. Measurement at plane 4 used as the balancing measurement for plane 3.
	2	361	196	361	196	87	148	
	3	847	156	847	156	146	344	
	4	X	X	X	X	44	323	
	Used	-	-	-	-	168	15,67%	
	All	-	-	-	-	401	18,17%	

Speed [rpm]	Plane	Run 4 (base)		Calibration plane 2		Run 5		Calibration plane 3		Run 6	
		Mag [um]	Phase [°]	Mag [gmm]	Phase [°]	Mag [um]	Phase [°]	Mag [gmm]	Phase [°]	Mag [um]	Phase [°]
2500	1	124	150	X	X	109	146	X	X	126	148
	2	87	148	72	158	60	143	X	X	94	151
	3	146	344	X	X	161	342	72	315	102	331
	4	44	323	X	X	58	326	X	X	18	331
	Used	168	-	-	-	167	15,58%	-	-	144	13,43%
	All	401	-	-	-	388	17,58%	-	-	340	15,41%

Speed [rpm]	Plane	Calculated balances		Combined balances		Run 7		Description
		Mag [gmm]	Phase [°]	Mag [gmm]	Phase [°]	Mag [um]	Phase [°]	
2500	1	X	X	X	X	64	190	Fine balancing at 2 planes. Calibration weight (72 gmm) installed at the predicted angle of the unbalance. Measurement at plane 1 used as the balancing measurement for plane 2. Measurement at plane 4 used as the balancing measurement for plane 3.
	2	556	119	729	148	38	254	
	3	413	302	556	181	94	338	
	4	X	X	X	X	88	110	
	Meas.	-	-	-	-	152	14,18%	
	All	-	-	-	-	284	12,87%	

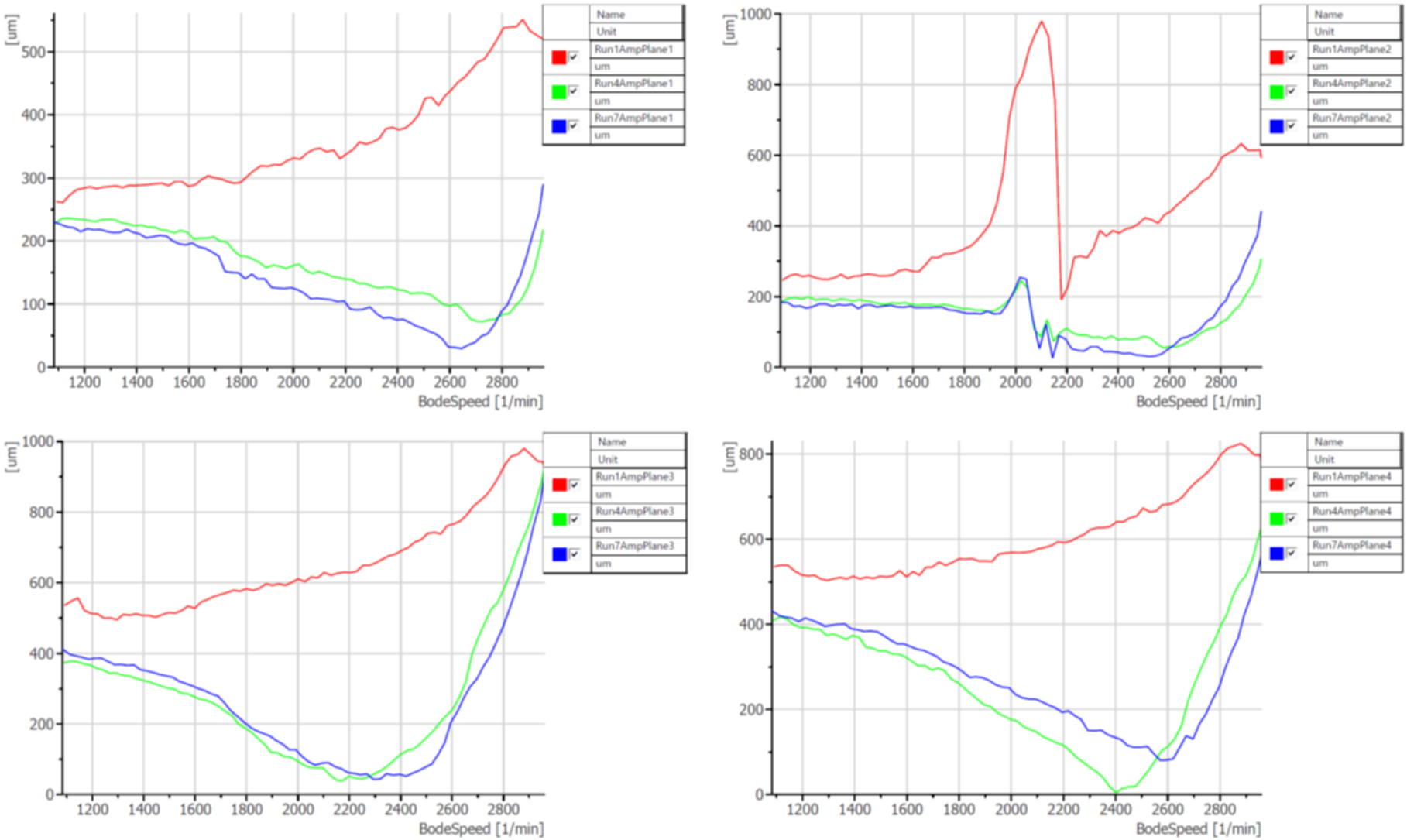

Figure 55 - the response of the system at different planes (red – initial, green – coarse balancing, blue – fine balancing, scenario 110)

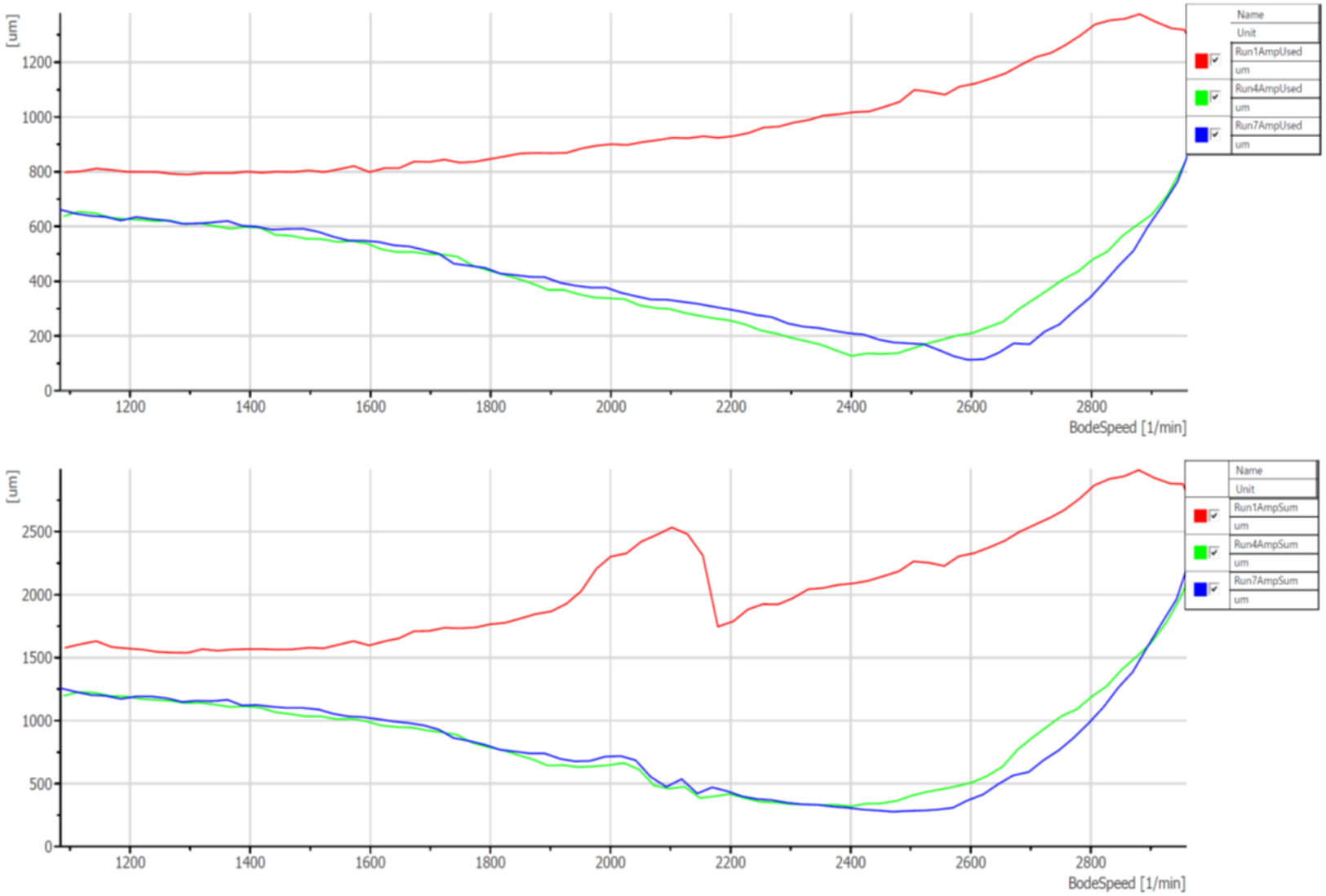

Figure 56 - the sum of responses (top – 2 balancing measurements, bottom – all, red – initial, green – coarse balancing, blue – fine balancing, scenario 110)

Table 16 - balancing results (scenario 111)

Speed [rpm]	Plane	Run 1 (base)		Calibration plane 2		Run 2		Calibration plane 3		Run 3	
		Mag [um]	Phase [°]	Mag [gmm]	Phase [°]	Mag [um]	Phase [°]	Mag [gmm]	Phase [°]	Mag [um]	Phase [°]
2500	1	422	162	X	X	181	168	X	X	304	167
	2	431	176	473	158	161	187	X	X	264	181
	3	746	158	X	X	426	160	473	158	315	171
	4	685	158	X	X	472	158	X	X	316	164
	Used	1107	-	-	-	653	58,99%	-	-	620	56,01%
	All	2284	-	-	-	1240	54,29%	-	-	1199	52,50%

Speed [rpm]	Plane	Calculated balances		Combined balances		Run 4		Description
		Mag [gmm]	Phase [°]	Mag [gmm]	Phase [°]	Mag [um]	Phase [°]	
2500	1	X	X	X	X	87	159	Coarse balancing at 2 planes. Calibration weight (472.5 gmm) installed at the predicted angle of the unbalance. Measurement at plane 1 used as the balancing measurement for plane 2. Measurement at plane 4 used as the balancing measurement for plane 3.
	2	550	169	550	169	40	179	
	3	565	156	565	156	57	303	
	4	X	X	X	X	60	175	
	Used	-	-	-	-	147	13,28%	
	All	-	-	-	-	244	10,68%	

Speed [rpm]	Plane	Run 4 (base)		Calibration plane 2		Run 5		Calibration plane 3		Run 6	
		Mag [um]	Phase [°]	Mag [gmm]	Phase [°]	Mag [um]	Phase [°]	Mag [gmm]	Phase [°]	Mag [um]	Phase [°]
2500	1	87	159	X	X	60	162	X	X	80	160
	2	40	179	135	158	11	310	X	X	31	168
	3	57	303	X	X	100	312	135	180	124	331
	4	60	175	X	X	39	188	X	X	17	311
	Used	147	-	-	-	99	8,94%	-	-	97	8,76%
	All	244	-	-	-	210	9,19%	-	-	252	11,03%

Speed [rpm]	Plane	Calculated balances		Combined balances		Run 7		Description
		Mag [gmm]	Phase [°]	Mag [gmm]	Phase [°]	Mag [um]	Phase [°]	
2500	1	X	X	X	X	36	358	Fine balancing at 2 planes. Calibration weight (135 gmm) installed at the predicted angle of the unbalance. Measurement at plane 1 used as the balancing measurement for plane 2. Measurement at plane 4 used as the balancing measurement for plane 3.
	2	437	163	986	166	114	352	
	3	47	311	522	158	286	330	
	4	X	X	X	X	100	332	
	Used	-	-	-	-	136	12,29%	
	All	-	-	-	-	536	23,47%	

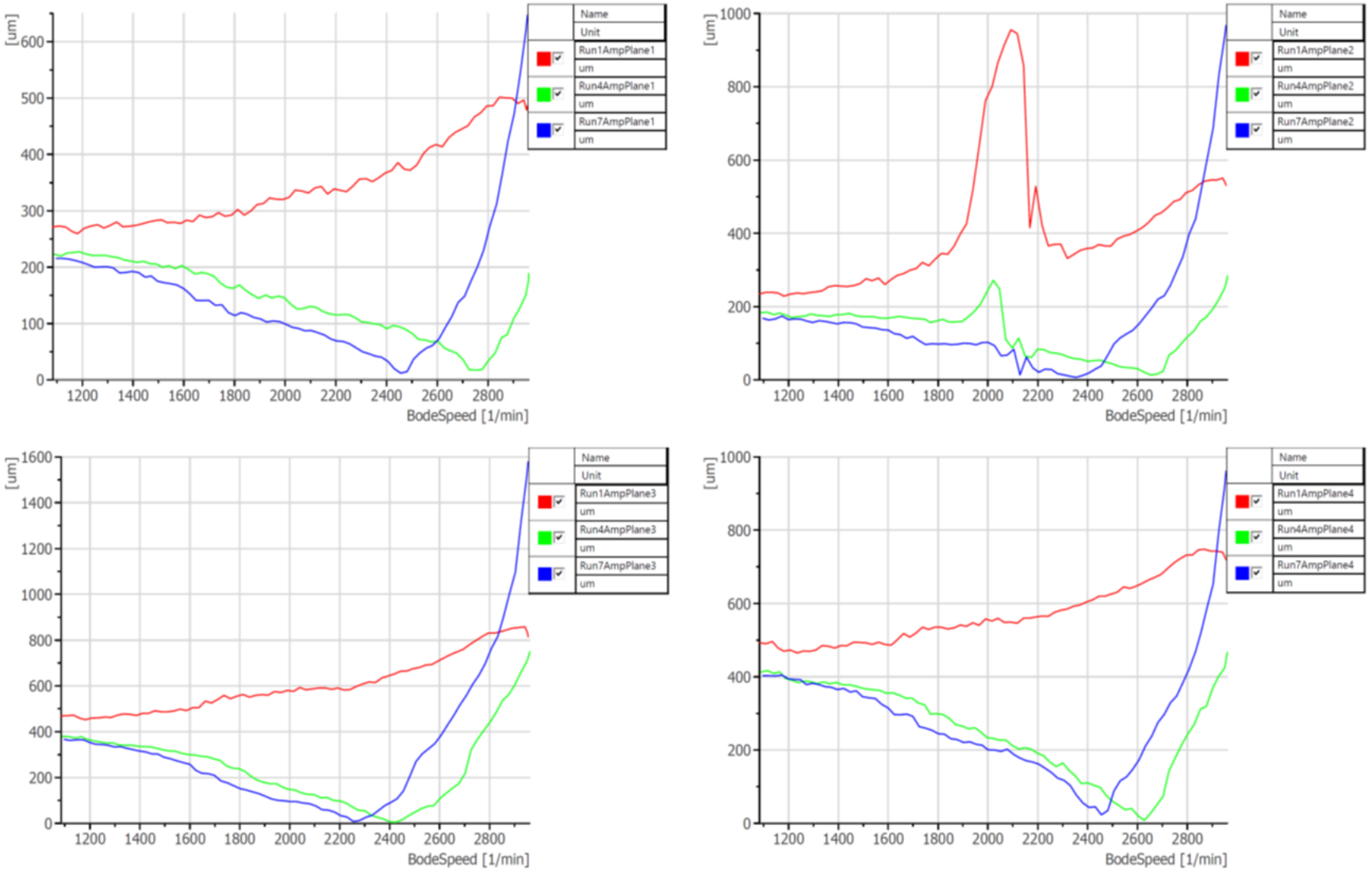

Figure 57 - the response of the system at different planes (red – initial, green – coarse balancing, blue – fine balancing, scenario 111)

Figure 58 - the sum of responses (top – 2 balancing measurements, bottom – all, red – initial, green – coarse balancing, blue – fine balancing, scenario 111)

Table 17 – balancing results (scenario 112)

Speed [rpm]	Plane	Run 1 (base)		Calibration plane 2		Run 2		Calibration plane 3		Run 3	
		Mag [um]	Phase [°]	Mag [gmm]	Phase [°]	Mag [um]	Phase [°]	Mag [gmm]	Phase [°]	Mag [um]	Phase [°]
2500	1	439	162	X	X	86	166	X	X	214	166
	2	442	176	743	158	51	208	X	X	169	182
	3	774	159	X	X	208	170	743	158	42	272
	4	704	160	X	X	326	158	X	X	64	206
	Used	1143	-	-	-	412	36,05%	-	-	278	24,32%
	All	2359	-	-	-	671	28,44%	-	-	489	20,73%

Speed [rpm]	Plane	Calculated balances		Combined balances		Run 4		Description
		Mag [gmm]	Phase [°]	Mag [gmm]	Phase [°]	Mag [um]	Phase [°]	
2500	1	X	X	X	X	79	171	Coarse balancing at 2 planes. Calibration weight (742.5 gmm) installed at the predicted angle of the unbalance. Measurement at plane 1 used as the balancing measurement for plane 2. Measurement at plane 4 used as the balancing measurement for plane 3.
	2	657	160	657	160	39	213	
	3	417	158	417	158	71	262	
	4	X	X	X	X	96	171	
	Used	-	-	-	-	175	15,31%	
	All	-	-	-	-	285	12,08%	

Speed [rpm]	Plane	Run 4 (base)		Calibration plane 2		Run 5		Calibration plane 3		Run 6	
		Mag [um]	Phase [°]	Mag [gmm]	Phase [°]	Mag [um]	Phase [°]	Mag [gmm]	Phase [°]	Mag [um]	Phase [°]
2500	1	79	171	X	X	34	165	X	X	61	174
	2	39	213	203	180	26	317	X	X	23	237
	3	71	262	X	X	104	301	203	180	161	319
	4	96	171	X	X	59	178	X	X	25	324
	Used	175	-	-	-	93	8,14%	-	-	86	7,52%
	All	285	-	-	-	223	9,45%	-	-	270	11,45%

Speed [rpm]	Plane	Calculated balances		Combined balances		Run 7		Description
		Mag [gmm]	Phase [°]	Mag [gmm]	Phase [°]	Mag [um]	Phase [°]	
2500	1	X	X	X	X	24	356	Fine balancing at 2 planes. Calibration weight (202,5 gmm) installed at the predicted angle of the unbalance. Measurement at plane 1 used as the balancing measurement for plane 2. Measurement at plane 4 used as the balancing measurement for plane 3.
	2	326	174	977	165	96	348	
	3	71	211	463	165	247	331	
	4	X	X	X	X	67	342	
	Used	-	-	-	-	91	7,96%	
	All	-	-	-	-	434	18,40%	

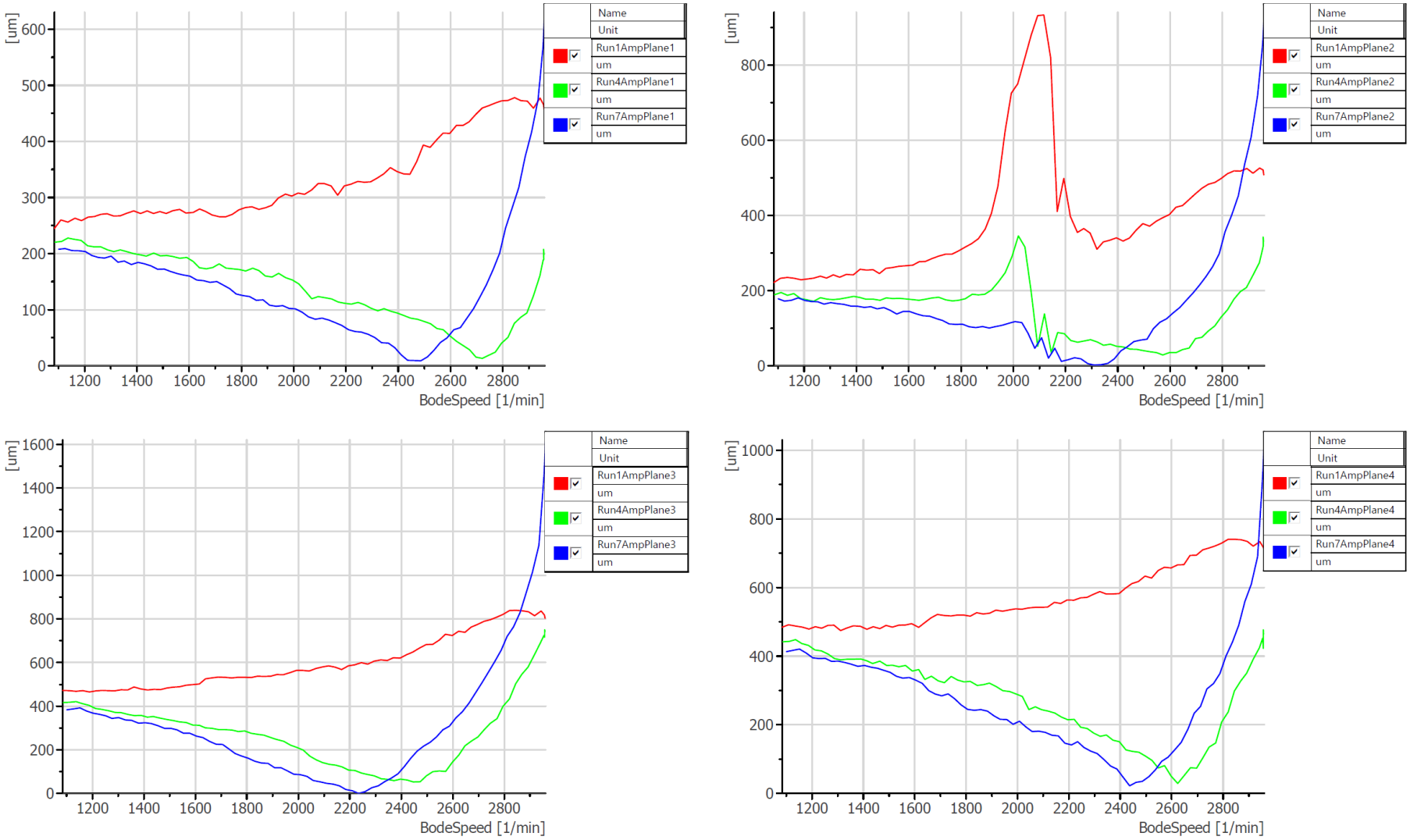

Figure 59 - the response of the system at different planes (red – initial, green – coarse balancing, blue – fine balancing, scenario 112)

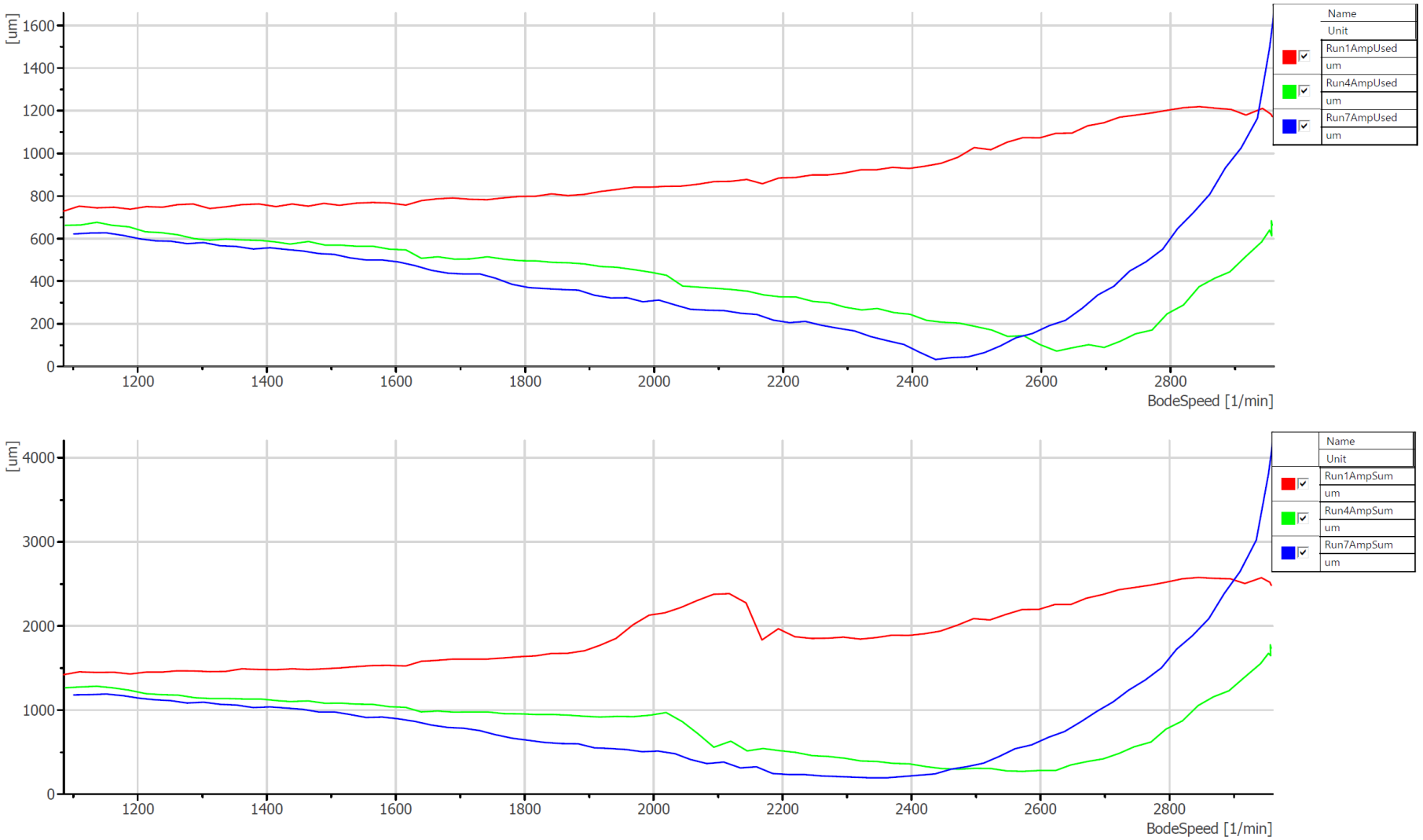

Figure 60 - the sum of responses (top – 2 balancing measurements, bottom – all, red – initial, green – coarse balancing, blue – fine balancing, scenario 112)

Table 18 – balancing results (scenario 113)

Speed [rpm]	Plane	Run 1 (base)		Calibration plane 2		Run 2		Calibration plane 3		Run 3	
		Mag [um]	Phase [°]	Mag [gmm]	Phase [°]	Mag [um]	Phase [°]	Mag [gmm]	Phase [°]	Mag [um]	Phase [°]
2500	1	413	161	X	X	301	157	X	X	371	163
	2	405	176	203	180	271	170	X	X	346	176
	3	720	158	X	X	598	152	203	158	558	164
	4	664	159	X	X	588	155	X	X	541	161
	Used	1125	-	-	-	869	77,24%	-	-	904	80,36%
	All	2202	-	-	-	1758	79,84%	-	-	1816	82,47%

Speed [rpm]	Plane	Calculated balances		Combined balances		Run 4		Description
		Mag [gmm]	Phase [°]	Mag [gmm]	Phase [°]	Mag [um]	Phase [°]	
2500	1	X	X	X	X	125	163	Coarse balancing at 2 planes. Calibration weight (202.5 gmm) installed at the predicted angle of the unbalance. Measurement at plane 2 used as the balancing measurement for plane 2. Measurement at plane 3 used as the balancing measurement for plane 3.
	2	382	158	382	158	83	178	
	3	529	174	529	174	29	10	
	4	X	X	X	X	108	125	
	Used	-	-	-	-	112	9,96%	
	All	-	-	-	-	345	15,67%	

Speed [rpm]	Plane	Run 4 (base)		Calibration plane 2		Run 5		Calibration plane 3		Run 6	
		Mag [um]	Phase [°]	Mag [gmm]	Phase [°]	Mag [um]	Phase [°]	Mag [gmm]	Phase [°]	Mag [um]	Phase [°]
2500	1	125	163	X	X	110	161	X	X	131	163
	2	83	178	72	180	66	174	X	X	91	179
	3	29	10	X	X	41	8	72	0	41	152
	4	108	125	X	X	103	122	X	X	151	138
	Used	112	-	-	-	107	9,51%	-	-	132	11,73%
	All	345	-	-	-	320	14,53%	-	-	414	18,80%

Speed [rpm]	Plane	Calculated balances		Combined balances		Run 7		Description
		Mag [gmm]	Phase [°]	Mag [gmm]	Phase [°]	Mag [um]	Phase [°]	
2500	1	X	X	X	X	54	163	Fine balancing at 2 planes. Calibration weight (72 gmm) installed at the predicted angle of the unbalance. Measurement at plane 2 used as the balancing measurement for plane 2. Measurement at plane 3 used as the balancing measurement for plane 3.
	2	379	167	759	163	16	252	
	3	99	9	441	159	77	290	
	4	X	X	X	X	74	165	
	Used	-	-	-	-	93	8,27%	
	All	-	-	-	-	221	10,04%	

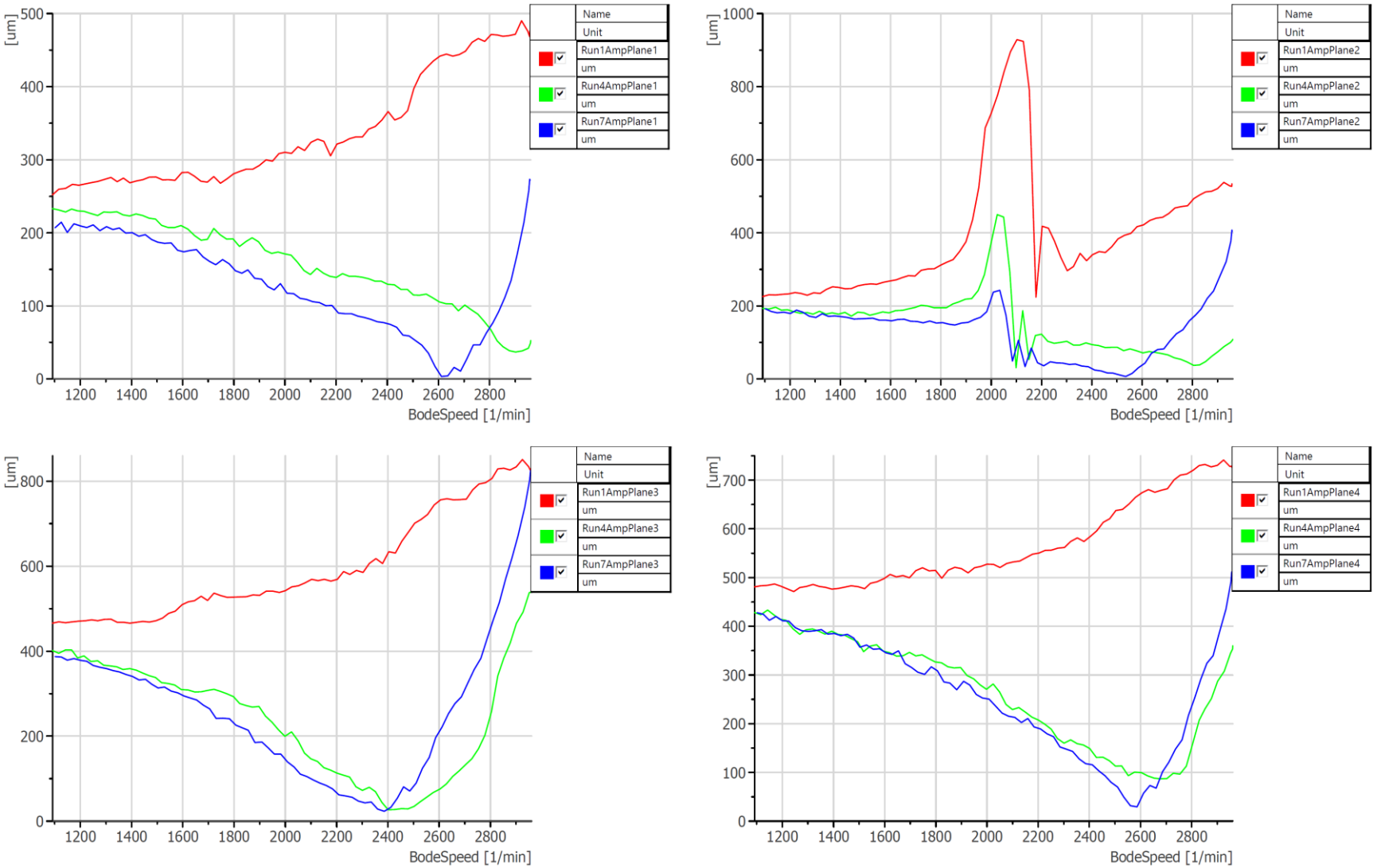

Figure 61 - the response of the system at different planes (red – initial, green – coarse balancing, blue – fine balancing, scenario 113)

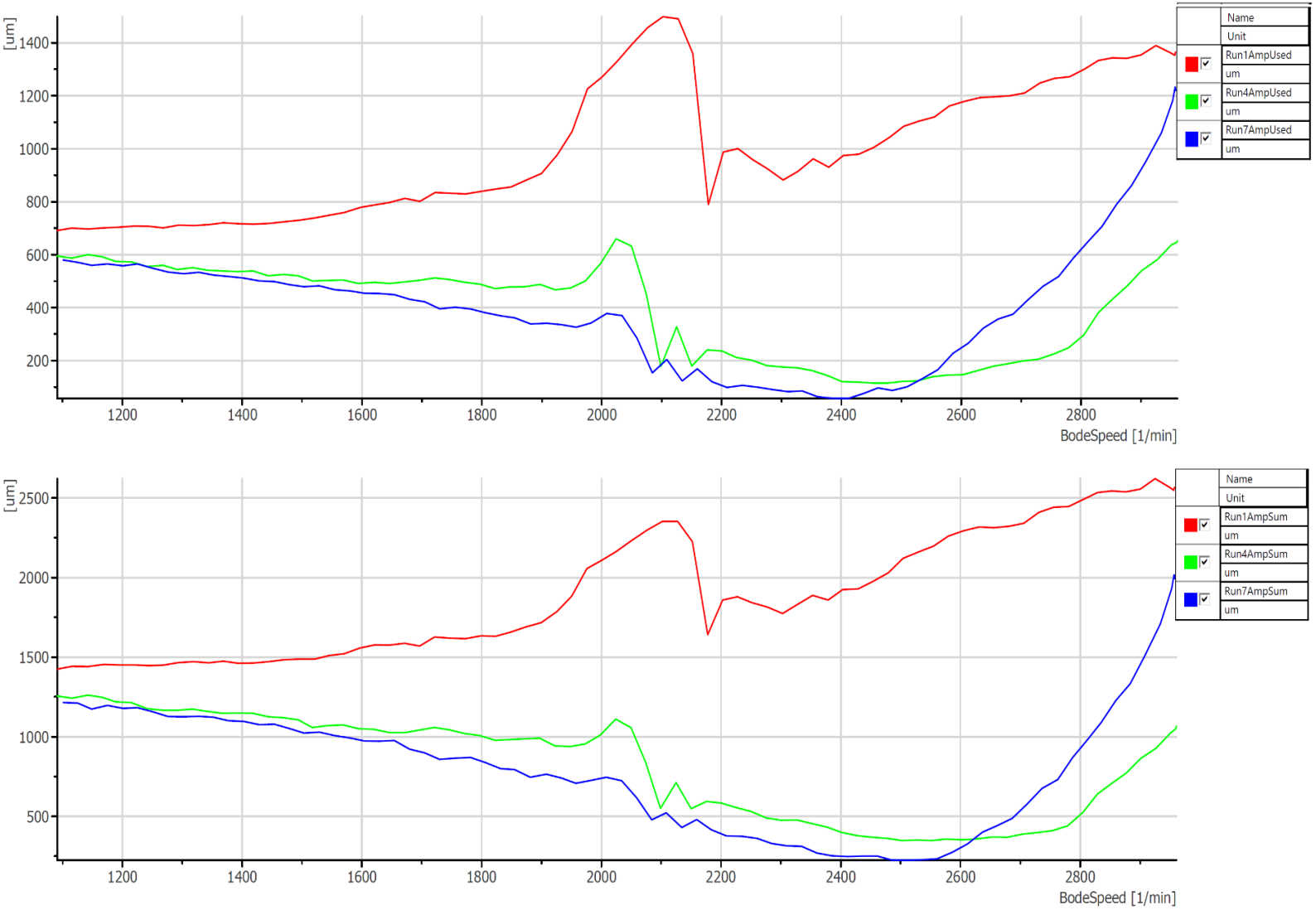

Figure 62 - the sum of responses (top – 2 balancing measurements, bottom – all, red – initial, green – coarse balancing, blue – fine balancing, scenario 113)

Table 19 – balancing results (scenario 114)

Speed [rpm]	Plane	Run 1 (base)		Calibration plane 2		Run 2		Calibration plane 3		Run 3	
		Mag [um]	Phase [°]	Mag [gmm]	Phase [°]	Mag [um]	Phase [°]	Mag [gmm]	Phase [°]	Mag [um]	Phase [°]
2500	1	414	162	X	X	194	153	X	X	300	169
	2	**410**	**177**	**473**	**180**	**167**	**165**	**X**	**X**	**254**	**185**
	3	**725**	**160**	**X**	**X**	**448**	**151**	**473**	**158**	**288**	**179**
	4	674	160	X	X	486	155	X	X	280	173
	Used	1135	-	-	-	615	54,19%	-	-	542	47,75%
	All	2223	-	-	-	1295	58,25%	-	-	1122	50,47%

Speed [rpm]	Plane	Calculated balances		Combined balances		Run 4		Description
		Mag [gmm]	Phase [°]	Mag [gmm]	Phase [°]	Mag [um]	Phase [°]	
2500	1	X	X	X	X	107	152	Coarse balancing at 2 planes. Calibration weight (472.5 gmm) installed at the predicted angle of the unbalance. Measurement at plane 2 used as the balancing measurement for plane 2. Measurement at plane 3 used as the balancing measurement for plane 3.
	2	**498**	**177**	**498**	**177**	**67**	**161**	
	3	**437**	**161**	**437**	**161**	**27**	**158**	
	4	X	X	X	X	108	159	
	Used	-	-	-	-	94	8,28%	
	All	-	-	-	-	309	13,90%	

Speed [rpm]	Plane	Run 4 (base)		Calibration plane 2		Run 5		Calibration plane 3		Run 6	
		Mag [um]	Phase [°]	Mag [gmm]	Phase [°]	Mag [um]	Phase [°]	Mag [gmm]	Phase [°]	Mag [um]	Phase [°]
2500	1	107	152	X	X	79	151	X	X	100	153
	2	**67**	**161**	**135**	**158**	**31**	**163**	**X**	**X**	**60**	**157**
	3	**27**	**158**	**X**	**X**	**32**	**291**	**135**	**158**	**60**	**326**
	4	108	159	X	X	86	164	X	X	40	180
	Used	94	-	-	-	63	5,55%	-	-	120	10,57%
	All	309	-	-	-	228	10,26%	-	-	260	11,70%

Speed [rpm]	Plane	Calculated balances		Combined balances		Run 7		Description
		Mag [gmm]	Phase [°]	Mag [gmm]	Phase [°]	Mag [um]	Phase [°]	
2500	1	X	X	X	X	68	152	Fine balancing at 2 planes. Calibration weight (135 gmm) installed at the predicted angle of the unbalance. Measurement at plane 2 used as the balancing measurement for plane 2. Measurement at plane 3 used as the balancing measurement for plane 3.
	2	**283**	**160**	**773**	**171**	**23**	**127**	
	3	**139**	**316**	**316**	**172**	**23**	**207**	
	4	X	X	X	X	137	142	
	Used	-	-	-	-	46	4,05%	
	All	-	-	-	-	251	11,29%	

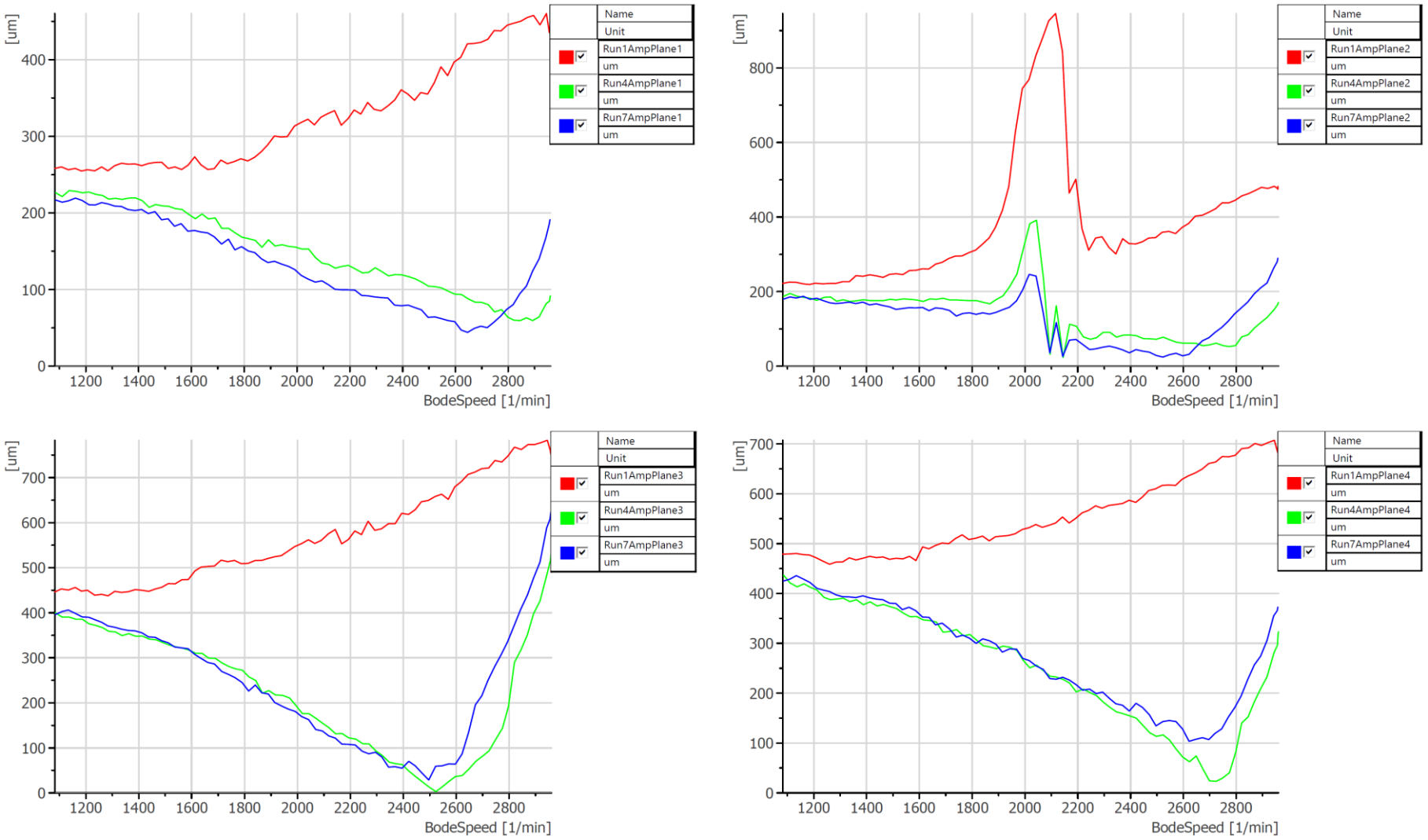

Figure 63 - the response of the system at different planes (red – initial, green – coarse balancing, blue – fine balancing, scenario 114)

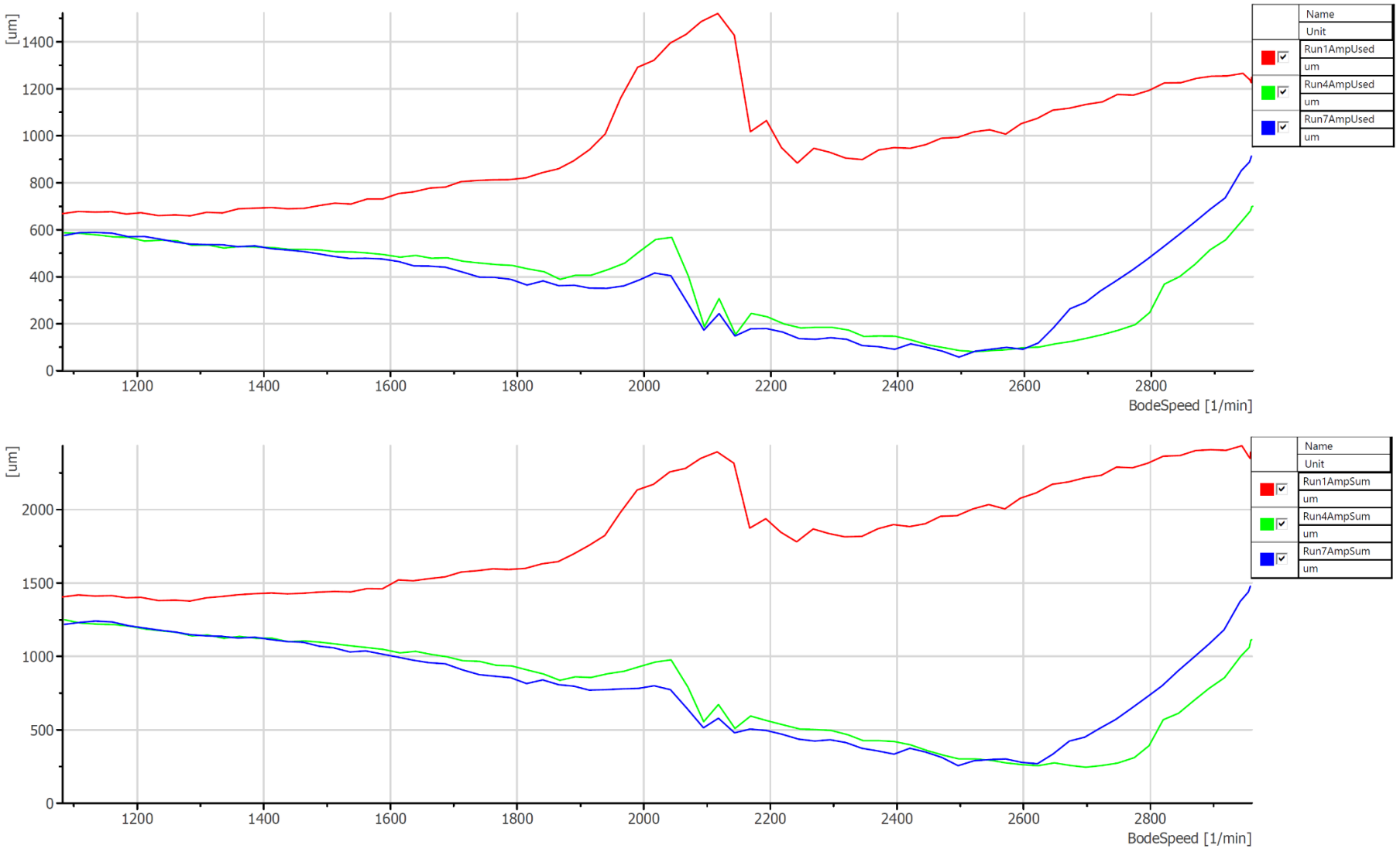

Figure 64 - the sum of responses (top – 2 balancing measurements, bottom – all, red – initial, green – coarse balancing, blue – fine balancing, scenario 114)

Table 20 – balancing results (scenatio 115)

Speed [rpm]	Plane	Run 1 (base)		Calibration plane 2		Run 2		Calibration plane 3		Run 3	
		Mag [um]	Phase [°]	Mag [gmm]	Phase [°]	Mag [um]	Phase [°]	Mag [gmm]	Phase [°]	Mag [um]	Phase [°]
2500	1	399	162	X	X	101	137	X	X	219	167
	2	**385**	**177**	**743**	**180**	**60**	**141**	**X**	**X**	**168**	**183**
	3	**692**	**159**	**X**	**X**	**222**	**147**	**743**	**158**	**53**	**271**
	4	648	159	X	X	335	152	X	X	61	219
	Used	1077	-	-	-	282	26,18%	-	-	221	20,52%
	All	2124	-	-	-	718	33,80%	-	-	501	23,59%

Speed [rpm]	Plane	Calculated balances		Combined balances		Run 4		Description
		Mag [gmm]	Phase [°]	Mag [gmm]	Phase [°]	Mag [um]	Phase [°]	
2500	1	X	X	X	X	88	147	Coarse balancing at 2 planes. Calibration weight (742.5 gmm) installed at the predicted angle of the unbalance. Measurement at plane 2 used as the balancing measurement for plane 2. Measurement at plane 3 used as the balancing measurement for plane 3.
	2	**668**	**174**	**668**	**174**	**42**	**152**	
	3	**273**	**162**	**273**	**162**	**53**	**164**	
	4	X	X	X	X	176	150	
	Used	-	-	-	-	95	8,82%	
	All	-	-	-	-	359	16,90%	

Speed [rpm]	Plane	Run 4 (base)		Calibration plane 2		Run 5		Calibration plane 3		Run 6	
		Mag [um]	Phase [°]	Mag [gmm]	Phase [°]	Mag [um]	Phase [°]	Mag [gmm]	Phase [°]	Mag [um]	Phase [°]
2500	1	88	147	X	X	47	136	X	X	70	145
	2	**42**	**152**	**203**	**158**	**17**	**26**	**X**	**X**	**19**	**139**
	3	**53**	**164**	**X**	**X**	**26**	**261**	**203**	**158**	**66**	**314**
	4	176	150	X	X	133	150	X	X	59	154
	Used	95	-	-	-	43	3,99%	-	-	85	7,89%
	All	359	-	-	-	223	10,50%	-	-	214	10,08%

Speed [rpm]	Plane	Calculated balances		Combined balances		Run 7		Description
		Mag [gmm]	Phase [°]	Mag [gmm]	Phase [°]	Mag [um]	Phase [°]	
2500	1	X	X	X	X	63	152	Fine balancing at 2 planes. Calibration weight (202,5 gmm) installed at the predicted angle of the unbalance. Measurement at plane 2 used as the balancing measurement for plane 2. Measurement at plane 3 used as the balancing measurement for plane 3.
	2	**160**	**130**	**791**	**166**	**15**	**146**	
	3	**79**	**233**	**308**	**176**	**17**	**117**	
	4	X	X	X	X	143	142	
	Used	-	-	-	-	32	2,97%	
	All	-	-	-	-	238	11,21%	

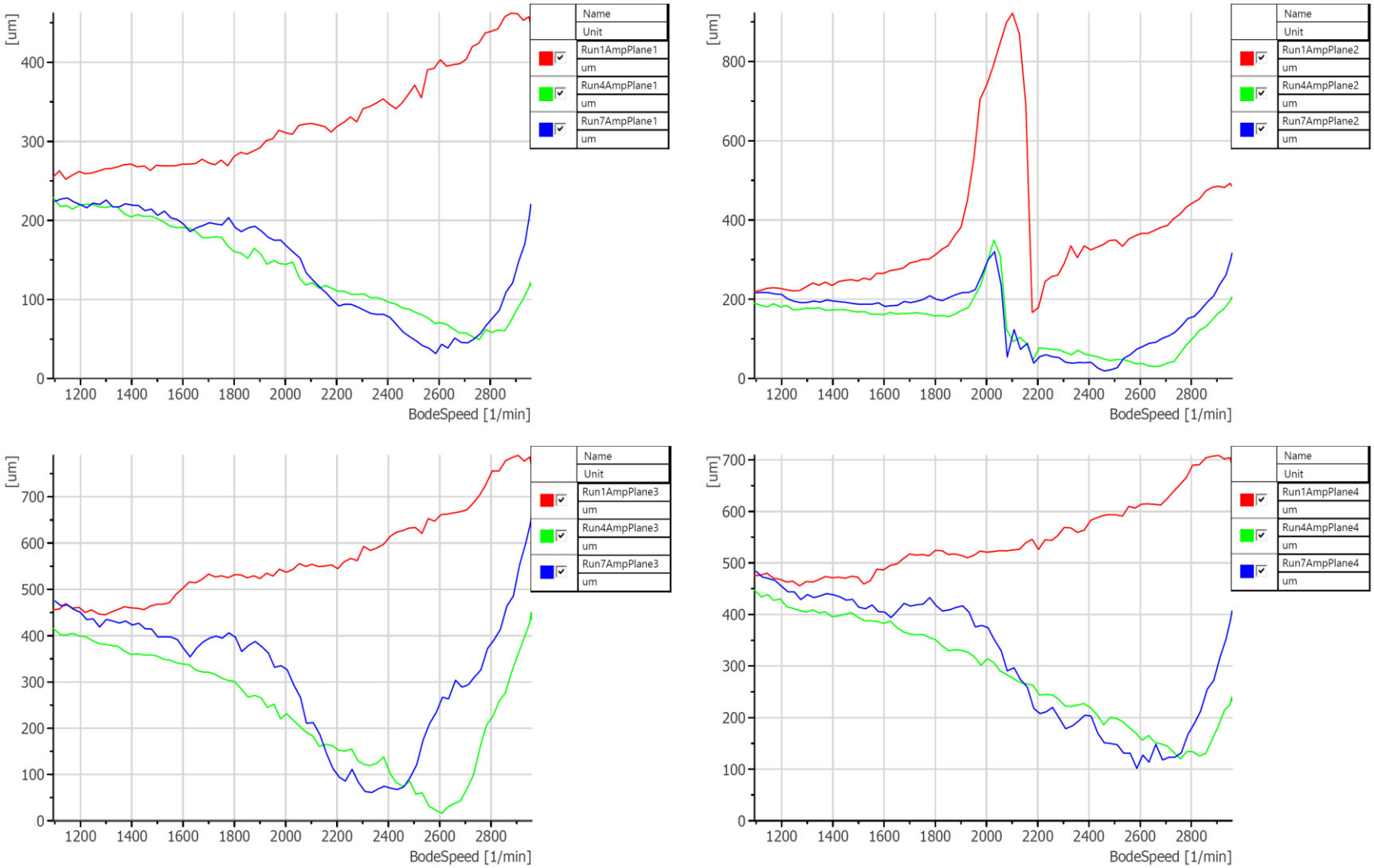

Figure 65 - the response of the system at different planes (red – initial, green – coarse balancing, blue – fine balancing, scenario 115)

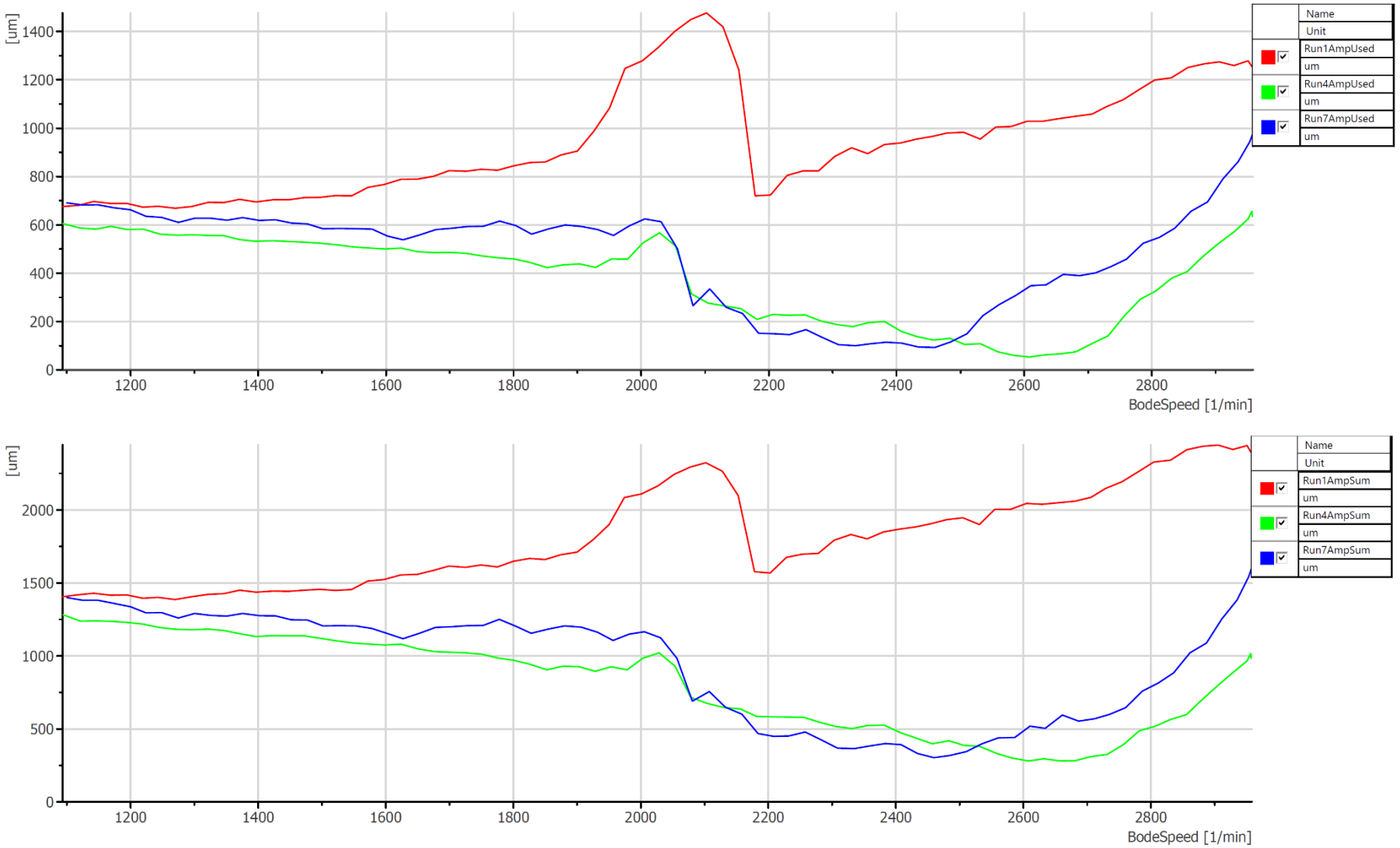

Figure 66 - the sum of responses (top – 2 balancing measurements, bottom – all, red – initial, green – coarse balancing, blue – fine balancing, scenario 115)

4.5 **Conclusions**

Through analysis of the data obtained while performing the balancing using the influence coefficients method within the developed balancing system, the following conclusions can be drawn:

- by following the proposed optimum balancing procedure, the balancing performed using the influence coefficient method always leads to decrease in the vibration level (the worse result obtained was the final vibration approximately 35% of the initial response, which is still a satisfactory result),
- the modified differential evolution (MDE) algorithm always finds the best balance weight distribution in no more than 15 seconds with error below 0.5g-mm,
- the number of runs required to perform one iteration of the balancing is dependent on the number of planes to balance ($n + 1$ runs are required, where n equals the number of planes and the check run is not considered),
- usually only one iteration of the balancing is needed to obtain satisfactory reduction in the object's vibration – throughout the testing, the average unbalance after first iteration was only 23% of the initial unbalance,
- the average unbalance after two iterations of the balancing was only 16% of the initial unbalance, and 69% of the unbalance after the first iteration, however it is always recommended to try to perform the fine balancing – even if the results are worse, still the coarse balance weights can be used,
- second iteration of the balancing almost always leads to decreasing of the unbalance for the balancing speed, however in every case the fine balancing is causing the response of the system to quickly rise for higher speeds,
- when a system is balanced for a particular speed it should never be operated for higher speeds,
- the less planes to balance the better the results,
- direct measurements at the balancing planes help to achieve better balancing results when compared to situation when the probes must be installed at different parts of the rotor,
- the magnitude of the calibration weight used has a big impact on the final unbalance reduction – generally the lower the operational speed the higher the magnitude of the calibration weight should be,

- the best results of the balancing can be observed when the calibration weights have a big impact on the change in the response of the system,
- if too small calibration weight is used the balancing system will over-estimate the trim weights required which, in the worst case scenario, may cause the increase in the rotor's unbalance,
- the calibration weights should always be installed at the predicted angle of the unbalance for a given plane – it not only gives the best results but is also the safest approach as even during the calibration runs the overall response of the system should decrease, therefore there is a much lower risk of causing a damaging vibration.

5. Summary

5.1 Overview

In this thesis a comprehensive study of rotor balancing techniques has been conducted. The need for improvement to the already existing balancing systems was identified during preparation to one of the certification tests of turbofan jet engine at Łukasiewicz Research Network – Institute of Aviation. The available balancing tools (like the VibroDAQ system [87]) have proven to be insufficient to reliably and accurately balance a jet engine fan, therefore the existing balancing data was used to develop a more suitable balancing system. Additionally a dedicated test stand has been build for the sole purpose of tests and development of the balancing system. The findings and results of the development process and conducted experiments are presented is this thesis. The developed balancing system has delivered better balancing results than any of the existing balancing systems tested. Throughout the entire research and development conducted during thesis preparation the following tasks have been accomplished:

- identifying the problems and required solutions for balancing of rotors in industrial and testing facilities,
- design and assembly of a versitile test stand capable of running a range of single-plane and multi-plane balancing simulations,
- design and implementation of a complete balancing system capable of controlling the test stand, acquiring high sampling rate data and performing a real-time order analysis (Bode plots and polar plot updated during the balancing runs),
- design and assembly of a modal analysis test stand,
- identifying the steps required to obtain the optimum balancing results,
- development of original and modern weight distribution algorithm (modified differential evolution),
- using the developed balancing system for balancing of turbomachinery in several testing facilities,
- implementation of a non-contact single-plane balancing vector method in the developed balancing system,

- implementation of a non-contact single-plane four runs method in the developed balancing system,
- implementation of a non-contact multi-plane influence coefficient method in the developed balancing system,
- analysis and testing of the signal processing tools that can best fulfill the task of extracting useful data (in terms of balancing) from the raw data acquired by the balancing system,
- design and testing of the balancing data analysis tool,
- design and testing of the balance weight calculator tool,
- design and testing of the balance weights distribution tool,
- extensive testing of the developed balancing system using wide range of different test stand configurations,
- analysis and comparison of the test results,
- drawing conclusions from all the performed tasks.
- literature overview with special emphasis on methods that can be used for balancing of rotors in their own bearings.

The balancing of rotors is an extensively researched field and there are many papers and books available on the topic. The most noteworthy amongst them had been described in more details in the literature overview part of the thesis (chapter 1.4). In comparison to the available knowledge in the rotor balancing field, the developed system is an original project solution to the unbalance problem in the following scope:

- the developed balancing system can be used to balance a rotor in virtually any conditions (in the rotor's own bearings, after the rotor is disassembled from the machine or any other situation imaginable) – as long as the rotor can be spun and there's a room available to install the sensors, it can be balanced,
- the balancing can be performed using any kind of sensor capable of acquiring the rotor vibration in any form (accelerometers, proximity probes, strain gages and so on) – this enables one of the greatest advantage of the proposed methods, their capability of balancing using non-contact probes,
- the angular location of the final balance weight can be predicted (using the developed data analysis tools) after the base run and before the calibration

weight is added, therefore the risk of extensive vibration during the calibration runs is mitigated,

- the best distribution of the final balance weight in the available angular locations using the available weights can be automatically calculated by the system – a tool which uses an original optimization technique (modified differential evolution) has been developed for this purpose,
- the optimum balancing results can be obtained by following the recommended balancing procedure, which includes the implementation of electromagnetic interference mitigation techniques, the checks of the probes' brackets modal response, the calibration of the probes, the guidelines concerning the probes installation and finally the balancing itself using the developed system.

The research and development presented in this thesis are planned to be continued. There are possible improvements to be tested and some new areas to be explored. The plans include the following topics:

- determine which type of sensor (accelerometers, proximity probes or straing gages) leads to the best vibration attenuation in different balancing scenarios – research can be performed by balancing of the same rotor using different types of sensors and by comparing the final results,
- develop similar balancing system capable of attenuating not only the radial, but also the axial and torsional vibration,
- extend the proposed balancing system to be able to balance rotating fans and bladed rotors using data acquired by proximity probes mounted in the plane of rotating blades,
- research the impact of the accuracy, resolution and sampling rate of the data acquisition part of the balancing system on the final balancing results,
- test the probes' brackets vibration impact on the balancing results and develop the problem mitigation techniques,
- develop additional optimization techniques for trim weight distribution.

5.2 **Conducted experiments**

Several experiments have been conducted in order to prove the effectiveness of the developed balancing system. In all the performed experiments, the results obtained showed an improvent over the balancing systems described and tested throughtout this dissertation. The most noteworthy of the conducted experiments were:

- partial fan of the GE9X turbofan engine at the Łukasiewicz Research Network – Institute of Aviation – this type of test article has been balanced on several occasions, in different configurations, for the purpose of conducting tests like the large bird ingestion test or the overspeed test; details concerning the test article and the balancing process could not be shared due to proprietary reasons; Figure 67 shows the high speed shaft on which the test article is mounted during the test,
- the GE9X turbogan engine RSR (Rear Stages Rig) testing at the Polonia Aero testing facility in Zielonka - tested vehicle was mounted on a cantilevered shaft of the bearing cartridge presented on the Figure 68; test article pictures from proprietary aspect stand point could not be shared; bearing cartridge is a spindle type of device, spinning up to 5000rpm, bearing support in two locations and oil damper in one location; first balancing plane was present outside of the bearing cartridge housing (on a rotor) and second balancing plane was present at the test article; balancing mas was added as a bolt, nuts and spacers; the whole rotor system has been balanced within a four days using the system (balancing is introduction to whole turbine testing campaign and a lot of details must be put on this effort to make it success); Polonia Aero is planning to acquire license to use the balancing system as it proved to be working extremely well and allows to balance the whole rotordynamic system in multiple planes,
- the moving ground system in the wind tunnel (Figure 69) at the Łukasiewicz Research Network – Institute of Aviation – the main part of the system is the conveyor belt stretched on two rollers and driven by one of them; the rollers can rotate up to 6000rpm; the balancing system developed by the author was used to balance the rollers, each one in two planes (balancing planes were located on the opposite ends of the rollers); balancing was extremely successful, allowing the system to be accelerated to its maximum operating speed without any issues coused by vibrations.

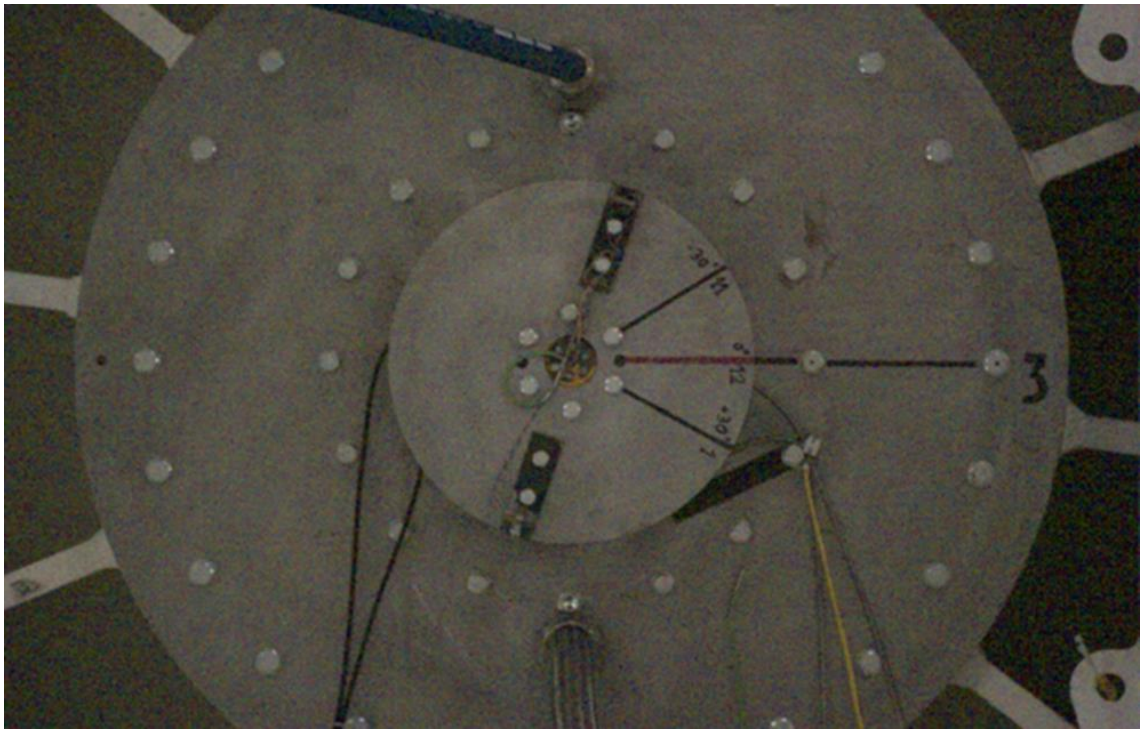

Figure 67 – the high speed shaft of the FBO Whirligig Test Laboratory (photo courtesy of Łukasiewicz Research Network – Institute of Aviation)

Figure 68 – bearing cartridge used during the GE9X tests (photo courtesy of Polonia Aero)

Figure 69 – the moving ground system in the wind tunel (photo courtesy of Łukasiewicz Research Network – Institute of Aviation)

6. Bibliography

[1] Md. Abdul Saleem, G. Diwakar, Dr. M.R.S. Satyanarayana, „Detection of Unbalance in Rotating Machines Using Shaft Deflection Measurement during Its Operation", IOSR Journal of Mechanical and Civil Engineering (ISSN: 2278-1684), Volume 3, Issue 3 (Sep-Oct. 2012), PP 08-20

[2] Phuoc Vinh Dang, Le Hung Toan Do, Nhu Thanh Vo, Thanh Nghi Ngo, Hoai Nam Le, „Identification of Unbalance in Rotating Machinery Using Vibration Analyse Solution", 4th International Conference on Mechatronics and Electrical Systems, IOP Publishing, 2019

[3] Stefan Heindel, Fabian Becker, Stephan Rinderknecht, „Unbalance and resonance elimination with active bearings on a Jeffcott Rotor", Mechanical Systems and Signal Processing, issue 85 (2017), pages 339–353

[4] Mark S. Darlow, "Balancing of High-Speed Machinery", Springer Verlag, 1989

[5] Ahmed A. Ibraheem, Nouby M. Ghazaly, G. T. Abd el- Jaber, „Review of Rotor Balancing Techniques", American Journal of Industrial Engineering, 2019, Vol. 6, No. 1, 19-25

[6] Benniu Zhang, Junqian Zhang, Kaihong Zhang, Zhixiang Zhou, "A non-contact proximity sensor with low frequency electromagnetic field", Sensors and Actuators A Physical, March 2007, 162-167

[7] A. G. Parkinson, „Balancing of Rotating Machinery", Proceedings of the Institution of Mechanical Engineers, Part C: Mechanical Engineering Science, 1991, 205(1), 53-66

[8] W. C. Foiles, P. E. Allaire, E. J. Gunter, "Review: Rotor balancing", Shock and Vibration, 1998, Volume 5, 325-336

[9] International Organization of Standardization, „Mechanical vibration - Rotor balancing - Part 2: Vocabulary", ISO 21940-2, 2017

[10] Charles T. Hatch, "Fundamentals of Rotating Machinery Diagnostics", Bently Nevada Press, 2002

[11] Ramakrishnan Ambur, Stephan Rinderknecht, "Unbalance detection in rotor systems with active bearings using self-sensing piezoelectric actuators", Mechanical Systems and Signal Processing, Volume 102, 2018, Pages 72-86

[12] Yi Yang, Jiaying Wang, Xurong Wang, Yiping Dai, "A general method to predict unbalance responses of geared rigid rotor systems", Journal of Sound and Vibration, 2016, Volume 381, pp 246-263

[13] Zengwei Wang, Ping Zhu, "Response prediction for modified mechanical systems based on in-situ frequency response functions: Theoretical and numerical studies", Journal of Sound and Vibration, 2017, Volume 400, pp 417-441.

[14] G. B. Karelitz, "Field balancing rotors at operating speed", Power, 1928, Volume 67, pp 286–289

[15] F. Ribary, "The balancing of masses in rotating bodies", Brown Boveri Review, 1936, Volume 23, pp 186–192

[16] I. J. Somervaille, "Balancing a rotating disc, simple graphical construction", Engineering, 1954, pp 241–242

[17] C. Jackson, "The Practical Vibration Primer", Gulf Publishing Company, 1979

[18] Louis J. Everett, "Two-Plane Balancing of a Rotor System Without Phase Response Measurements", Journal of Vibration, Acoustics, Stress and Reliability in Design, 1987, Volume 109, pp 162–167

[19] E.J. Gunter, H. Springer, R.R. Humphris, "Balancing of multimass flexible rotor bearing system without phase measurements", 11th Biennial Conference on Mechanical Vibration and Noise, Boston, MA, September 1982

[20] Sabah. M. Jamil Ali, "Analytical And Experimental Study Of Three Test-Run Balancing Method", Al-Rafidain Engineering, April 2009

[21] W.C. Foiles, D.E. Bently, "Balancing With Phase Only (Single-Plane and Multiplane)", Journal of Vibration, Acoustics, Stress and Reliability in Design, 1988, Volume 110, pp 151-157

[22] L. J. Everett, "Optimal Two-plane Balance of Rigid Rotors", Journal of Sound and Vibration, 1997, Volume 208, pp 656–663

[23] M. Chouksey, J. K. Dutt, S. V. Modak, "Model updating of rotors supported on ball bearings and its application in response prediction and balancing", Journal of Measurement, 2013, Volume 46, pp 4261-4273

[24] C. C. Ozoegwu, C. C. Nwangwu, C. F. Uzoh, A. V. Ogunoh, "Pure Analytical Approach to Rotational Balancing", Journal of Safety Engineering, 2012, Volume 1, pp 50-56

[25] V. N. Carvalho, et al., "Robust Balancing Approach for Rotating Machines Based on Fuzzy Logic", Journal of Vibration and Acoustic, 2018, Volume 140

[26] C. D. Untaroiu, P. E. Allaire, W. C. Foiles, "Balancing of Flexible Rotors Using Convex Optimization Techniques: Optimum Min-Max LMI Influence Coefficient Balancing", Journal of Vibration and Acoustics, 2008, Volume 130, pp 111–120

[27] B. Xu, L. Qu, R. Sun, "The optimization technique-based balancing of flexible rotors without test runs", Journal of Sound and Vibration, 2000, Volume 238, pp 877-892

[28] M. V. Saldarriaga, V. Steffen, J. Der Hagopian, J. Mahfoud, "On the balancing of flexible rotating machines by using an inverse problem approach", Journal of Vibration and Control, 2010, Vilume 17, pp 1021-1033

[29] L. Li, S. Cao, J. Li, R. Nie, L. Hou, "Review of Rotor Balancing Methods, Machines, 2021, 9(5):89

[30] J.R. Lindsey, "Significant Developments in Methods for Balancing High-Speed Rotors", ASME Vibration Conference, No. 69-Vibr-53, Philadelphia, 1969

[31] I. Bucher, D. J. Ewins, "Modal analysis and testing of rotating structures", Philosophical Transactions of The Royal Society B Biological Sciences, 2001, Volume 359, pp 61-96

[32] H. D. Ju, "Generalized modal balancing for non-isotropic rotor systems", Mechanical Systems and Signal Processing, 2007, Volume 21, pp 2137–2160

[33] M. B. Deepthikumar, A. S. Sekhar, M. R. Srikanthan, "Modal balancing of flexible rotors with bow and distributed unbalance", Journal of Sound and Vibration, 2013, Volume 332, pp 6216–6233

[34] P. Nauclér, T. Söderström, "Unbalance estimation using linear and nonlinear regression", Automatica, 2010, Volume 46, pp 1752–1761

[35] Shachar Tresser, Amit Dolev and Izhak Bucher, "Dynamic balancing of super-critical rotating structures using slow-speed data via parametric excitation", Dynamics Laboratory, Israel, 2017

[36] R. Tiwari, V. Chakravarthy, "Simultaneous identification of residual unbalances and bearing dynamic parameters from impulse responses of rotor–bearing systems", Mechanical Systems and Signal Processing, 2006, Volume 20, pp 1590–1614

[37] Cong Yue, Xingmin Ren, Yongfeng Yang, Wangqun Deng, „Unbalance Identification of Speed-Variant Rotary Machinery without Phase Angle Measurement”, Shock and Vibration, Volume 2015, Article ID 934231

[38] Peter Avitabile, “Single Plane Balancing Notes”, University of Massachusetts Lowell, 2001

[39] Jaafar Alsalaet, “Dynamic Balancing and Shaft Alignment”, College of Engineering - University of Basrah, 2015

[40] Rieger N.F. (1988) „Principles of Balancing and of Balancing Machines”, In: Rieger N.F. (ed.) *Rotordynamics 2*, Springer, Vienna

[41] Swith Claude Burgos Alconz, Grover Zurita V., "Designing and Development of a Dynamic Vibration Balancing Machine for Industrial Applications", Investigación & Desarrollo, 2019, No. 1, 73-93

[42] Joe Kimbrell, "Fundamentals of Industrial Encoder Sensing Technologies, Motion Detection Theory and Methods, and Signal Output Styles", AutomationDirect, 2013

[43] Jacek Pieniążek, Paulina Ryba, „Eddy-current sensor for a tachometer”, Transactions of the Institute of Aviation, 2017, No. 2, 57-68

[44] Łukasz Kędzierski, Rafał Sikorski, „Rotating machinery single plane balancing non-contact method”, Przegląd Elektrotechniczny, 2020, No. 4, 162-167

[45] Stéphane Leleu, Thierry Coorevits, Olivier Gibaru, "Calibration of capacitive sensors and electronic levels for the straightness measurements using multiprobe method", 2011

[46] “Grounding Considerations - Intermediate Analog Concepts”, National Instruments, 2021

[47] “Modal Analysis in LabVIEW”, National Instruments, 2020

[48] Barlian Henryranu Prasetio, Dahnial Syauqy, Rizal Maulana, Gembong Edhi Setyawan, "Study of voice data communication using network streams on dataflow programming", MATEC Web of Conferences 154, 2018

[49] „The LabVIEW RIO Architecture: A Foundation for Innovation”, National Instruments, 2020

[50] A. Viana, O.R. Polo, P. Parra, "Increasing the Determinism in Real-Time Operating Systems for ERC32 Architecture", Proceedings of the 5th WSEAS Int. Conf. on Software Engineering, Parallel and Distributed Systems, Madrid, Spain, February 15-17, 2006, pp 110-116

[51] „Introduction to NI Linux Real-Time”, National Instruments, 2020

[52] Macdara MacCamhaoil, “Static and Dynamic Balancing of Rigid Rotors”, Brüel & Kjær, 2016

[53] Giancarlo Genta, “Dynamics of Rotating Systems”, Springer, 2005

[54] Yuhe Liao, Peng Zhang, "Unbalance related rotor precession behavior analysis and modification to the holobalancing method", Mechanism and Machine Theory, vol. 45, 2010, 601-610

[55] Edgar J. Gunter, "Understanding Amplitude and Phase in Rotating Machinery", Vibration Institute 33rd Annual Meeting, Harrisburg, June 2009

[56] Sena Jeong, Eojin Kim, Kyungho Jeong, "Effects of Residual Imbalance on the Rotordynamic Performance of Variable-Speed Turbo Blower", International Symposium on Transport Phenomena and Dynamics of Rotating Machinery, Hawaii, Honolulu, 2016

[57] Steven W. Smith, “The Scientist and Engineer’s Guide to Digital Signal Processing”, Butterworth Heinemann, 2001

[58] Michael Cerna, Audrey F. Harvey, "The Fundamentals of FFT-Based Signal Analysis and Measurement", National Instruments, Application Note 041, July 2000

[59] Mehmet Akar, "Detection of a static eccentricity fault in a closed loop driven induction motor by using the angular domain order tracking analysis method", Mechanical Systems and Signal Processing, vol. 34, 2013, 173-182

[60] “Order Analysis Toolkit User Manual”, National Instruments, 2005

[61] Dejan Asic, „Rotational Analysis in the Angular Domain”, New England NoiseCon-16, Providence, June 2016

[62] P.N. Saavedra, C.G. Rodriguez, "Accurate assessment of computed order tracking", Shock and Vibration, vol. 13, 2016, 13-32

[63] Ignacio Santamaria-Caballero, et al., "Improved procedures for estimating amplitudes and phases of harmonics with application to vibration analysis", IEEE Transactions on Instrumentation and Measurement, vol. 47.1, 1998, 209-214

[64] Anders Brandt, et al., "Main Principles and Limitations of Current Order Tracking Methods", Sound and Vibration, March 2005, 19-22

[65] Zlatan Racic, Marin Racic, "Interpretation of Dynamic Data Plots for Troubleshooting and Resolving Vibration in Large Rotating Machinery", Proceedings of the 10th International Conference on Rotor Dynamics, 2019

[66] Jeremy Daniel Van Dam, Anthony Kaminsky, Blake Weldon Wilson, „Method and Apparatus for Balancing a Rotor”, United States Patent, **US 8 051 710 B2**, Nov. 8 2011

[67] Gary K. Grim, John W. Haidler, Bruce J. Mitchell, “The Basics of Balancing”, Balance Technology Inc., 2014

[68] Ababneh Mohammad, et al., "Occurrences Algorithm for String Searching Based on Brute-force Algorithm", Journal of Computer Science, January 2016, 82-85

[69] Charles M. Grinstead, Laurie J. Snell, “Introduction to Probability”, American Mathematical Society, 1997

[70] Anand Jayant Kulkarni, et al., "Cohort Intelligence: A Socio-inspired Optimization Method", Springer, 2017

[71] Ming-Hua Lin, et al., "A Review of Deterministic Optimization Methods in Engineering and Management", Mathematical Problems in Engineering, Volume 2012, Article ID 756023

[72] Xin-She Yang, "Nature-Inspired Optimization Algorithms", Elsevier, 2014

[73] M. Nazari-Heris, et al., "A comprehensive review of heuristic optimization algorithms for optimal combined heat and power dispatch from economic and environmental perspectives", Renewable and Sustainable Energy Reviews 81, 2018, 2128–2143

[74] Franco Busetti, "Genetic Algorithms Overview", May 2001

[75] M. A. El-Shorbagy, Aboul Ella Hassanien, "Particle Swarm Optimization from Theory to Applications", International Journal of Rough Sets and Data Analysis, Volume 5, Issue 2, 2018

[76] Swagatam Das, et al., "Recent Advances in Differential Evolution – An Updated Survey", Swarm and Evolutionary Computation, February 2016

[77] Shan He, Jon Richard Saunders, "Group Search Optimizer: An Optimization Algorithm Inspired by Animal Searching Behavior", IEEE Transactions on Evolutionary Computation, November 2009, 973-990

[78] Omkar Kulkarni, et al., "Cuckoo Search Optimization- A Review", Materials Today: Proceedings 4, 2017, 7262-7269

[79] "Global Optimization VI", National Instruments, March 2018, Available: https://zone.ni.com/reference/en-XX/help/371361R-01/gmath/global_optimization/

[80] Kamalkishor Uke, Surendra Kumar, "In-situ Single Plane Balancing in Vertical Circulating Water Pump-Motor System", International Journal of Mechanical and Production Engineering Research and Development, June 2018, pages 452-458

[81] Stanley R. Bognatz, "Rotor Balancing & Influence Coefficient Analysis", M&B Engineered Solutions Inc., 2017

[82] William C. Foiles, P. E. Allaire, "Single Plane and Multi-Plane Rotor Balancing Using Only Amplitude", 7th IFToMM-Conference on Rotor Dynamics, Vienna, Austria, 25-28 September 2006

[83] "2D Compass Plot Helper VI", National Instrument, March 2018, Available: https://zone.ni.com/reference/en-XX/help/371361R-01/lvpict/2d_compass_plot_vi

[84] Ron Larson, "Trigonometry", Cengage Learning, 2017

[85] Troy Feese, "Examples of Balancing Method: Four-run and Least-squares Influence Coefficients", Engineering Dynamics Inc., 2014

[86] Ray D. Kelm, "Advanced Field Balancing Techniques", Kelm Engineering, 2008

[87] Jarosław Doliński, "VibroDAQ and VibroDAQ portable – balancing systems made in Poland", Elektronika Praktyczna, 2016, No. 11, 86-90